THE HORIZONTAL REDISTRIBUTION OF ANOMALOUS VERTICAL HEAT FLUXES AT TROPICAL LATITUDES

A Dissertation

presented to

the Faculty of the Graduate School

at the University of Missouri-Columbia

In Partial Fulfillment

of the Requirements for the Degree

Ph.D. Natural Resources

---

by

EVAN KUTTA

Dissertation Co-advisors: Jason A. Hubbart, Ph.D. and Anthony Lupo, Ph.D.

May 2017

The undersigned, appointed by the dean of the Graduate School, have examined the dissertation entitled

The Horizontal Redistribution of Anomalous Vertical Heat Fluxes at Tropical Latitudes

Presented by Evan Kutta,

a candidate for the degree of Ph.D. Natural Resources

and hereby certify that, in their opinion, it is worthy of acceptance.

_____

Dr. Jason A. Hubbart

_____

Dr. Anthony Lupo

_____

Dr. Bohumil Svoma

_____

Dr. Christopher Wikle

_____

Dr. Timothy Eichler,

Unofficial Committee Member

ACKNOWLEDGEMENTS

I would like to thank Dr. Jason Hubbart for his dedication of time, expertise, and resources to ensure my successful completion of this major professional milestone. His high professional standards and timely constructive criticisms undoubtedly enhanced the quality of my writing and research skills and in particular this dissertation.

I would like to thank each of my family members for encouraging (enduring) my passion for everything weather and my parents in particular whose tireless efforts have enabled countless opportunities culminating in this dissertation.

I would like to thank my co-advisor Dr. Anthony Lupo and additional committee members Dr. Bohumil Svoma, Dr. Timothy Eichler, and Dr. Christopher Wikle for always having an open door and the willingness to share their expertise and guidance.

TABLE OF CONTENTS

LIST OF FIGURES

Figure Page

LIST OF TABLES

Table Page

The Horizontal Redistribution of Anomalous Vertical Heat Fluxes at Tropical Latitudes

Evan Kutta

Dissertation Co-advisors: Jason A. Hubbart and Anthony Lupo

ABSTRACT

A study was conducted to improve quantitative understanding of how anomalous vertical heat fluxes associated with the El Niño-Southern Oscillation (ENSO) are transported poleward to maintain climate equilibrium. State-of-the-art atmospheric reanalysis output was used to quantify anomalous horizontal, tropospheric mean fluxes of sensible and latent heat monthly over a global domain during all ENSO events that occurred between January 1979 and June 2016. Results showed coherent spatial patterns ($p < 0.05$) of horizontal fluxes of latent heat connecting ENSO and Pacific North American (PNA) pattern regions implying potential to quantify the interrelationship between ENSO and PNA patterns. Spatial patterns of anomalous sensible heat fluxes showed anomalous circulation dipoles consistent with PNA and North Atlantic Oscillation (NAO) patterns. Results indicated a linear relationship between ENSO, PNA, and NAO patterns that was most apparent for the PNA (NAO) pattern during January (November). Strong ENSO forcing produced a more temporally consistent linear relationship between ENSO, PNA, and NAO patterns, but was shown to transition to a non-linear relationship during January of weak ENSO forcing. Results suggested the most substantial climate impacts occurred across North America during strong El Niño and weak La Niña events when the anomalous circulations were closest to the west coast of North America. Finally, the methods presented in this work provide a mechanism for monitoring ENSO related climate impacts for North America and Western Europe in near real-time.

CHAPTER 1

INTRODUCTION

Background

The El Niño-Southern Oscillation (ENSO) represents the dominant quasi-oscillatory mode of inter-annual climate variability in the coupled ocean-atmosphere climate system (e.g. Wolter and Timlin 2011; Graf and Zanchettin 2012) and is mechanistically responsible for a cascade of global climate impacts that remain only partially understood (Brönnimann 2007). Global climate impacts include both extreme precipitation and temperature patterns in distant locations (McPhaden 1999; McPhaden et al. 2006) that can have human and societal impacts including agricultural losses, damaged property, and loss of life (e.g. Dilley and Heyman 1995; Kovats et al. 2003; Zebiak et al. 2015). For example, in mountainous regions, snow water equivalent of the snowpack is a key factor influencing human water resources, ecosystem health, and the occurrence of agricultural or hydrologic drought (e.g. Minder 2010; Svoma 2011). Numerous metropolitan areas, including many in the western United States, have increased demand for water during the warm season and are dependent on reservoirs filled by high elevation snow melt (Svoma 2011). Snowfall is characterized by generally slower hydrologic cycling than rainfall due to storage in the snowpack reducing runoff rates (Williams et al. 2009) such that both seasonal accumulation and timing of melt have important implications for available water resources (e.g. Svoma 2011; Hubbart et al. 2015).

Atmospheric rivers are responsible for approximately 90% of the poleward water vapor transport over just 10% of the of Earth's zonal circumference (Zhu and Newell 1998; Neiman et al. 2008) and have been shown to be more frequent along the California coast during El Niño rather than La Niña events (Guan et al. 2013; Kim and Alexander 2015). Atmospheric rivers are a boon for precipitation, but they are also associated with elevated melting levels reducing basin average snow water equivalent as well as enhancing risk for rain on snow events that can lead to flooding and associated property damage (Guan et al. 2016). Therefore, societal impacts associated with ENSO stem from changes to regional precipitation patterns, including elevated melting levels during El Niño that reduce basin average snow water equivalents, increase runoff and the risk of flooding due to more frequent rain on snow precipitation events.

Studies have repeatedly and conclusively shown that anomalous fluxes of sensible and latent heat from the Pacific Ocean into the troposphere are partially responsible for the cascade of global climate impacts (e.g. Ropelewski and Halpert 1986; Trenberth et al. 1998). Anomalous vertical heat fluxes connecting the hydrosphere to the atmosphere are forced by sea surface temperature anomalies (SSTAs) associated with ENSO (Peixoto and Oort 1992). SSTAs within the Niño 3.4 region (5ºN - 5ºS; 170ºW- 120ºW) are characterized by maximum magnitude and temporal variability during December (Okumura and Deser 2010). Therefore, quantification of ENSO event magnitude, duration, and associated atmospheric response is possible through analyses of SSTAs within the Niño 3.4 region of the central Pacific Ocean (Trenberth 1997). The Climate Prediction Center (CPC; Kirtman et al. 2014) monitors and forecasts the occurrence of El Niño (La Niña) events using an operational definition of five or more consecutive tri-monthly averages of SSTAs within the Niño 3.4 region above (below) 0.5ºC (-0.5ºC; Harrison and Chiodi 2017).

El Niño and La Niña events represent the warm and cool phases of the ENSO phenomena and despite great advancements in monitoring and prediction of ENSO events substantial challenges remain (e.g. Trenberth et al. 1998; Larson and Kirtman 2016). Progress has been made in monitoring and numerically modeling the ENSO phenomena (Trenberth et al. 1998) that has continued through the use of fully coupled Earth System Models (Bellenger et al. 2014). However, operational predictions of ENSO event evolution are still limited by initial condition errors, systematic modelling errors, and noise-driven errors (Larson and Kirtman 2016). In particular, modelling errors have caused failures in recent forecasts of ENSO event evolution (McPhaden 2015) and subsequent extratropical impacts (Jacox et al. 2016) including minimal recovery from a multi-year drought and reduced impacts to ecosystem productivity of the California Current System. Errors in initial conditions have been reduced through advanced data assimilation schemes (Larson and Kirtman 2016) that have also been used to perform atmospheric reanalysis projects that have provided tremendous value to atmospheric and climate monitoring and research (22,000+ citations; Kalnay et al. 1996). Ongoing advancements to data assimilation schemes that incorporate satellite and in-situ observations (4D-Variability; Simmons et al. 2007) achieved atmospheric reanalyses far superior to first generation reanalyses (Saha et al. 2010). Therefore, state-of-the-art atmospheric reanalyses with high spatiotemporal resolution, such as the ERA-Interim reanalysis project (Dee et al. 2011), have implied potential to greatly advance understanding of the ENSO phenomena and its interrelationship with a variety of patterns of internal climate variability (Liu and Alexander 2007).

ENSO events force distinct mid-latitude patterns that alter the probability of occurrence for each phase of the North Atlantic Oscillation (NAO) and Pacific North American (PNA) patterns of internal, intra-annual climate variability (e.g. Straus and Shukla 2002; Hurrell and

Deser 2010). NAO and PNA influence regional temperature and precipitation patterns across Europe and North America (e.g. Leathers et al. 1991; Seager et al. 2010), but the sub-seasonal influence of ENSO events on NAO and PNA patterns is not fully understood (e.g. Brönnimann 2007; Kim and Alexander 2015). Hurrell and Deser (2010) described the NAO pattern as a single north-south dipole (NSD) characterized by simultaneously out-of-phase anomalous circulation features between temperature and high-latitude locations such that NAO representative coordinates (single-point correlation) are 65ºN 30ºW. The PNA pattern is characterized by a pair of simultaneously out-of-phase NSDs across the northeast Pacific Ocean and North America with representative coordinates of 45ºN 165ºW (Hurrell and Deser 2010). Representative locations for PNA and NAO patterns were located east of the climatologic position the Aleutian and Icelandic lows consistent with observed results during El Niño events indicating an interrelationship between ENSO, PNA, and NAO patterns (Müller and Roeckner 2008). Hurrell and Deser (2010) concluded that ENSO, PNA, and NAO patterns are driven by alternate atmospheric dynamics, but a linear relationship between ENSO and PNA patterns is favored (Straus and Shukla 2002) whereas both linear (e.g. Wu and Hsieh 2004) and non-linear (e.g. Brönnimann 2007) relationships between ENSO and NAO patterns have been proposed. However, Meehl and Teng (2007) noted generally more consistent changes of teleconnection patterns associated with increased ENSO magnitude. Therefore, an interrelationship between ENSO, PNA, and NAO patterns exists, but the relative influence of either phase of ENSO is not fully understood especially for ENSO events of various magnitudes.

The magnitude and duration of SSTAs within the central Pacific Ocean associated with an ENSO event are not perfectly symmetric (e.g. An and Jin 2004, Okumura and Deser 2010, Choi et al. 2013) such that the atmospheric response to SSTAs also has an asymmetric

component (e.g. Wu and Hsieh 2004; Cai et al. 2012; Zhang et al. 2014; Feng et al. 2016). Zhang et al. (2014) identified climatologically relevant impacts to surface temperature and precipitation anomaly patterns across North America associated with the asymmetric component of the atmospheric response to ENSO forcing. Kang and Kug (2002) identified nonlinear dynamics (surface wind stress anomalies) responsible for the asymmetric distribution of SSTAs and used an idealized general circulation model forced by SSTAs of equal amplitude and opposite sign to show the nonlinear tropical atmosphere response (convection anomalies). Despite ENSO being an inherently nonlinear phenomena with a corresponding nonlinear atmospheric response, linear techniques are widely used for studying ENSO and its atmospheric response (Okumura and Deser 2010; Choi et al. 2013; Zhang et al. 2014; Kim and Alexander 2015). Additionally, despite ENSO representing anomalous vertical fluxes of heat into the troposphere, few studies were designed to quantitatively characterize the anomalous horizontal fluxes of heat associated with the cascade of extratropical climate impacts during ENSO events (Kim and Alexander 2015). Therefore, nonlinearities in the interrelationship between ENSO, PNA, and NAO patterns need to be quantified to improve understanding and prediction of associated climate impacts.

The overall scope of this work was to analyze the anomalous horizontal, tropospheric-mean redistribution of heat from anomalous vertical heat fluxes at the ocean-atmosphere interface associated with ENSO events. This analysis required three tracks of work that correspond to the three subsections that follow. First, the tropospheric response to El Niño events were assessed through quantification of anomalous horizontal heat fluxes composited according to El Niño event magnitude. Second, the tropospheric response to La Niña events were assessed through quantification of anomalous horizontal heat fluxes composited according to La Niña event magnitude. Finally, the symmetric (El Niño – La Niña) and asymmetric (El Niño + La

Niña) components of the anomalous horizontal, tropospheric-mean heat fluxes were quantified to assess the common assumption that El Niño and La Niña result in equal and opposite atmospheric responses.

Tropospheric Response to El Niño

El Niño events are characterized by large SSTAs that terminate rapidly (e.g. Kang and Kug 2002; An and Jin 2004) and can result in failure of the Indian monsoon (Kumar et al. 2006), heavy rainfall within Peru's coastal desert (Larkin and Harrison 2005), and more frequent occurrences of atmospheric rivers on the west coast of North America (Kim and Alexander 2015). Large-scale modes of climate variability, such as PNA or NAO teleconnections, provide an integrated measure of weather over large regions providing a more stable link to the overall physical variability of a system relative to a single, local variable (Hurrell and Deser 2010). Due to the large spatial scales, furthering understanding of the interrelationship between El Niño, PNA, and NAO patterns will enable future studies to advance understanding of subsequent societal impacts including water resource availability and food production (e.g. Hansen et al. 1998; Waluda et al. 2006; Hurrell and Deser 2010; Anderson et al. 2016).

Teleconnections represent simultaneous correlations between temporal fluctuations in meteorological parameters at widely separated points on Earth (Wallace and Gutzler 1981). The PNA and NAO patterns are represented by anomalous circulation dipoles near the climatologic positions of geographically fixed atmospheric centers of action (ACA) such as the Aleutian and Icelandic lows (Wallace and Gutzler 1981; Serreze et al. 1997; Rodionov et al. 2007). Both position and intensity of Aleutian and Icelandic ACAs have been shown to be strongly influenced by the El Niño phenomena, despite great distances separating each region (Trenberth

and Caron 2000). The atmospheric bridge phenomena is the commonly accepted mechanism responsible for these long-distance linkages (Lau et al. 1997), but the relative importance of tropospheric as opposed to stratospheric bridging remains unclear (e.g. Ineson and Scaife 2009; Graf and Zanchettin 2012; Iza et al. 2016). Additionally, the atmospheric response to El Niño forcing is seasonally dependent and proportional to the SSTA magnitude indicating a spectrum of societally relevant impacts primarily focused on changes to water resource availability. Considering the societal of importance of El Niño events in both tropical and extratropical latitudes, information is needed to clarify the tropospheric atmospheric bridge phenomena at global scale for El Niño events of various magnitudes.

Tropospheric Response to La Niña

Given smaller SSTA magnitudes and no reversal of climatology, the atmospheric response to La Niña events has garnered less attention and has frequently been assumed to be equal and opposite (i.e. linear) to that of El Niño events (e.g. Okumura and Deser 2010). However, smaller SSTA magnitudes inherently force a smaller atmospheric response than El Niño events (Kang and Kug 2002), but even so La Niña events are still associated with impactful flooding in Australia, northern South America, and Southeast Asia (Boening et al. 2012) and widespread continental drought over portions of North America, Asia, and Africa (Hoell et al. 2014). Furthermore, patterns of intra-annual variability, such as PNA or NAO, have been shown to be influenced by La Niña events (e.g. Wu and Hsieh 2004) such that a particular phase of the PNA and NAO patterns may be favored during La Niña events (e.g. Hurrell and Deser 2010). However, few investigations have identified the interrelationship between ENSO, PNA, and NAO patterns at sub-seasonal time scales when the phase of PNA and NAO patterns are considered unpredictable (Hurrell and Deser 2010). Therefore, quantifying the anomalous

horizontal redistribution of tropical heat could improve predictability of PNA and NAO patterns and would advance the ongoing discussion on possible effects of ENSO on European climate (Graf and Zanchettin 2012).

Wise et al. (2015) explained that improving predictability of regional climate phenomena depended on a more thorough understanding of impacts associated with multiple, simultaneously occurring teleconnection patterns such as the interrelationship between La Niña, PNA, and NAO patterns. Additionally, it is known that La Niña event magnitude alters the atmospheric response such that larger SSTAs force a larger atmospheric response implying that the connections between Niño 3.4, PNA, and NAO regions during strong and weak La Niña events may differ from that of El Niño. Only a few analyses of integrated water vapor transports have been undertaken to show long distance connections between tropical sources and extratropical sinks (Kim and Alexander 2015) and further sub-seasonal analyses are needed composited for ENSO events of similar magnitudes. Considering the regional implications of PNA and NAO modes of climate variability and their unpredictability, analyses of anomalous heat fluxes during La Niña events of various magnitudes are needed to enhance prediction of PNA and NAO patterns.

Asymmetric Tropospheric Response to ENSO

Asymmetry of SSTA magnitude, duration, and tropical atmospheric response indicate that linear techniques (e.g. empirical orthogonal function, linear regression, warm minus cold composites) commonly used for assessing the atmospheric response to ENSO events may be insufficient (e.g. Okumura and Deser 2010; Feng et al. 2016). A mounting body of evidence indicates an asymmetric component of similar magnitude exists (Wu and Hsieh 2004; Feng et al. 2016) resulting in climatologically relevant implications for surface temperature and precipitation across North America (Zhang et al. 2014). Additionally, Wu and Hsieh (2004)

noted that the PNA (NAO) pattern projected onto the symmetric (non-symmetric) component of the atmospheric response and was consistent with positive phases of the PNA and NAO patterns being excited during El Niño events. However, studies assessing the symmetry of the atmospheric response to ENSO forcing have used seasonal composites such that the month-to-month dependency of PNA and NAO patterns cannot be assessed (e.g. Zhang et al. 2014; Feng et al. 2016). Furthermore, the number of recent studies examining the atmospheric response for variable SSTA (ENSO) magnitudes is small (e.g. Iza et al. 2016), but SSTA magnitude represents a key component of ENSO asymmetry such that further investigation is needed. Therefore, the interrelationship between ENSO and NAO patterns has an important asymmetric component that is climatologically relevant, but not fully understood (Brönnimann 2007) indicating a need for further analyses at sub-seasonal time scales composited based on ENSO event magnitude.

Statement of Need

There has been insufficient attention devoted to anomalous horizontal, tropospheric-mean fluxes of latent and sensible heat during ENSO events that represent anomalous vertical fluxes of heat into the tropical troposphere. Thus, research is needed that can provide the scientific community enhanced understanding of the redistribution of heat throughout the extratropics at monthly resolution associated with both El Niño and La Niña forcing of variable magnitude (Kim and Alexander 2015). Furthermore, the increasing body of evidence suggesting both asymmetric and symmetric components of the atmospheric response to ENSO forcing are climatologically relevant (e.g. Zhang et al. 2014) indicates that the symmetry of extratropical heat redistribution is of considerable interest and requires further investigation. Conceivably, advancements to the mechanistic understanding of the atmospheric redistribution of sensible and

latent heat will enhanced predictability of climate anomalies at Earth's surface (i.e. temperature and precipitation) and thus improve preparedness for impacts to human health and well-being.

Objectives

The overarching objective of this dissertation research was to improve understanding of the extratropical impacts of ENSO events through quantification of anomalous horizontal, tropospheric-mean fluxes of sensible and latent heat using output from state-of-the-art atmospheric reanalysis (ERA-I; Dee et al. 2011). Specific objectives were to a) show anomalous, tropospheric-mean circulations consistent with NAO and PNA patterns during both El Niño and La Niña forcing of various magnitudes; b) investigate the potential to identify spatially continuous areas of anomalous heat fluxes connecting the ENSO region with PNA and/or NAO regions; and c) quantify the symmetric and asymmetric components of objectives a) and b).

Dissertation Structure

This dissertation is presented in the following chapters: in chapter two, "Anomalous Horizontal Heat Fluxes during El Niño Events of Various Magnitude", state-of-the-art atmospheric reanalysis output was used to quantify anomalous horizontal, tropospheric-mean fluxes of latent and sensible heat for all thirteen, three weak, and three strong El Niño events in the period of record (1979-2016) including in-depth analysis of the three strong events. In chapter three, "The Influence of La Niña Events on Tropospheric Fluxes of Sensible and Latent Heat using the ERA-Interim Reanalysis Project", state-of-the-art atmospheric reanalysis output was used to quantify anomalous horizontal, tropospheric-mean fluxes of latent and sensible heat for all twelve, three weak, and three strong La Niña events in the period of record (1979-2016) including in-depth analysis of the three strong events. In chapter four, "Symmetric and

Asymmetric Components of Anomalous Tropospheric-Mean Horizontal Fluxes of Latent and Sensible Heat Associated with ENSO Events of Variable Magnitude", output from the ERA-Interim project was used to quantify symmetric and asymmetric components of the horizontal, tropospheric-mean redistribution of latent and sensible heat for all ENSO events in the period of record as well as for three weak and strong ENSO events. Finally, in chapter five, "Conclusions and Synthesis" a summary of the key findings of this investigation is presented and future research directions are discussed that, if pursued, could lead to improved understanding of climate impacts (e.g. anomalous surface temperature and precipitation patterns) across North America and Europe.

Literature Cited

An, S. I., Jin, F. F. 2004. Nonlinearity and asymmetry of ENSO. *Journal of Climate*, **17**(12): 2399-2412.

Anderson, W., Seager, R., Baethgen, W., Cane, M. 2016. Life cycles of agriculturally relevant ENSO teleconnections in North and South America. *International Journal of Climatology*.

Bellenger, H., Guilyardi, É., Leloup, J., Lengaigne, M., Vialard, J. 2014. ENSO representation in climate models: from CMIP3 to CMIP5. *Climate Dynamics*, **42**(7-8): 1999-2018.

Boening, C., Willis, J. K., Landerer, F. W., Nerem, R. S., Fasullo, J. 2012. The 2011 La Niña: So strong, the oceans fell. *Geophysical Research Letters*, **39**(19).

Brönnimann, S. 2007. Impact of El Niño–Southern Oscillation on European climate. *Reviews of Geophysics*, **45**(3).

Cai, W., Van Rensch, P., Cowan, T., Hendon, H. H. 2012. An asymmetry in the IOD and ENSO teleconnection pathway and its impact on Australian climate. *Journal of Climate*, **25**(18): 6318-6329.

Choi, K. Y., Vecchi, G. A., Wittenberg, A. T. 2013. ENSO transition, duration, and amplitude asymmetries: Role of the nonlinear wind stress coupling in a conceptual model. *Journal of Climate*, **26**(23): 9462-9476.

Dee, D. P., Uppala, S. M., Simmons, A. J., Berrisford, P., Poli, P., Kobayashi, S., Andrae, U., Balmaseda, M. A., Balsamo, G., Bauer, P., Bechtold, P. 2011. The ERA-Interim reanalysis: Configuration and performance of the data assimilation system. *Quarterly Journal of the Royal Meteorological Society*, **137**(656): 553-597.

Dilley, M., Heyman, B. N. 1995. ENSO and disaster: droughts, floods and El Niño/Southern Oscillation warm events. *Disasters*, **19**(3): 181-193.

Feng, J., Chen, W., Li, Y. 2016. Asymmetry of the winter extra-tropical teleconnections in the Northern Hemisphere associated with two types of ENSO. *Climate Dynamics* 1-17.

Graf, H. F., Zanchettin, D. 2012. Central Pacific El Niño, the "subtropical bridge," and Eurasian climate. *Journal of Geophysical Research: Atmospheres*, **117**(D1).

Guan, B., Molotch, N.P., Waliser, D.E., Fetzer, E.J., Neiman, P.J. 2013. The 2010/2011 snow season in California's Sierra Nevada: Role of atmospheric rivers and modes of large-scale variability. *Water Resources Research*, **49**(10): 6731-6743.

Guan, B., Waliser, D.E., Ralph, F.M., Fetzer, E.J., Neiman, P.J. 2016. Hydrometeorological characteristics of rain-on-snow events associated with atmospheric rivers. *Geophysical Research Letters*, **43**(6): 2964-2973.

Hansen, J. W., Hodges, A. W., Jones, J. W. 1998. ENSO influences on agriculture in the southeastern United States. *Journal of Climate*, **11**(3): 404-411.

Harrison, D. E., Chiodi, A. M. 2017. Comments on "Characterizing ENSO Coupled Variability and Its Impact on North American Seasonal Precipitation and Temperature". *Journal of Climate*, **30**(1): 427-436.

Hoell, A., Funk, C. 2014. Indo-Pacific sea surface temperature influences on failed consecutive rainy seasons over eastern Africa. *Climate Dynamics*, **43**(5-6): 1645-1660.

Hubbart, J.A., Link, T.E., Gravelle, J.A. 2015. Forest canopy reduction and snowpack dynamics in a northern Idaho watershed of the continental-maritime region, United States. *Forest Science*, **61**(5): 882-894.

Hurrell, J. W., Deser, C. 2010. North Atlantic climate variability: the role of the North Atlantic Oscillation. *Journal of Marine Systems,* **79**(3): 231-244.

Jacox, M. G., Hazen, E. L., Zaba, K. D., Rudnick, D. L., Edwards, C. A., Moore, A. M., Bograd, S. J. 2016. Impacts of the 2015–2016 El Niño on the California Current System: Early assessment and comparison to past events. *Geophysical Research Letters*, **43**(13): 7072-7080.

Kalnay, E., Kanamitsu, M., Kistler, R., Collins, W., Deaven, D., Gandin, L., Iredell, M., Saha, S., White, G., Woollen, J., Zhu, Y. 1996. The NCEP/NCAR 40-year reanalysis project. *Bulletin of the American Meteorological Society*, **77**(3): 437-471.

Kang, I. S., Kug, J. S. 2002. El Niño and La Niña sea surface temperature anomalies: Asymmetry characteristics associated with their wind stress anomalies. *Journal of Geophysical Research: Atmospheres*, **107**(D19).

Kim, H. M., Alexander, M. A. 2015. ENSO's modulation of water vapor transport over the Pacific–North American region. *Journal of Climate*, **28**(9): 3846-3856.

Kirtman, B. P., Min, D., Infanti, J. M., Kinter III, J. L., Paolino, D. A., Zhang, Q., Van Den Dool, H., Saha, S., Mendez, M. P., Becker, E., Peng, P. 2014. The North American multimodel ensemble: phase-1 seasonal-to-interannual prediction; phase-2 toward developing intraseasonal prediction. *Bulletin of the American Meteorological Society*, **95**(4): 585-601.

Kovats, R. S., Bouma, M. J., Hajat, S., Worrall, E., Haines, A. 2003. El Niño and health. *The Lancet*, **362**(9394): 1481-1489.

Kumar, K. K., Rajagopalan, B., Hoerling, M., Bates, G., Cane, M. 2006. Unraveling the mystery of Indian monsoon failure during El Niño. *Science*, **314**(5796): 115-119.

Larkin, N. K., Harrison, D. E. 2005. Global seasonal temperature and precipitation anomalies during El Niño autumn and winter. *Geophysical Research Letters*, **32**(16).

Larson, S. M., Kirtman, B. P. 2016. Drivers of coupled model ENSO error dynamics and the spring predictability barrier. *Climate Dynamics* 1-14.

Leathers, D. J., Yarnal, B., Palecki, M. A. 1991. The Pacific/North American teleconnection pattern and United States climate. Part I: Regional temperature and precipitation associations. *Journal of Climate*, **4**(5): 517-528.

Liu, Z., Alexander, M., 2007. Atmospheric bridge, oceanic tunnel, and global climatic teleconnections. *Reviews of Geophysics*, **45**(2).

McPhaden, M. J. 1999. Genesis and evolution of the 1997-98 El Niño. *Science*, **283**(5404): 950-954.

McPhaden, M. J., Zebiak, S. E., Glantz, M. H. 2006. ENSO as an integrating concept in earth science. *Science*, **314**(5806): 1740-1745.

McPhaden, M.J. 2015. Playing hide and seek with El Niño. *Nature Climate Change*.

Meehl, G.A., Teng, H. 2007. Multi-model changes in El Niño teleconnections over North America in a future warmer climate. *Climate Dynamics*, **29**(7-8): 779-790.

Minder, J.R. 2010. The sensitivity of mountain snowpack accumulation to climate warming. *Journal of Climate*, **23**(10): 2634-2650.

Müller, W. A., Roeckner, E. 2008. ENSO teleconnections in projections of future climate in ECHAM5/MPI-OM. *Climate dynamics*, **31**(5): 533-549.

Neiman, P.J., Ralph, F.M., Wick, G.A., Kuo, Y.H., Wee, T.K., Ma, Z., Taylor, G.H., Dettinger, M.D. 2008. Diagnosis of an intense atmospheric river impacting the Pacific Northwest: Storm summary and offshore vertical structure observed with COSMIC satellite retrievals. *Monthly Weather Review*, **136**(11): 4398-4420.

Okumura, Y. M., Deser, C. 2010. Asymmetry in the duration of El Niño and La Niña. *Journal of Climate*, **23**(21): 5826-5843.

Peixoto, J. P., Oort, A. H. 1992. Physics of climate.

Ropelewski, C. F., Halpert, M.S. 1986. North American precipitation and temperature patterns associated with the El Niño/Southern Oscillation (ENSO). *Monthly Weather Review*, **114**(12): 2352-2362.

Saha, S., Moorthi, S., Pan, H. L., Wu, X., Wang, J., Nadiga, S., Tripp, P., Kistler, R., Woollen, J., Behringer, D., Liu, H. 2010. The NCEP climate forecast system reanalysis. *Bulletin of the American Meteorological Society*, **91**(8): 1015-1057.

Seager, R., Kushnir, Y., Nakamura, J., Ting, M., Naik, N. 2010. Northern Hemisphere winter snow anomalies: ENSO, NAO and the winter of 2009/10. *Geophysical research letters*, **37**(14).

Simmons, A., Uppala, S., Dee, D., Kobayashi, S. 2007. ERA-Interim: New ECMWF reanalysis products from 1989 onwards. *ECMWF newsletter*, 110: 25-35.

Straus, D.M., Shukla, J. 2002. Does ENSO force the PNA? *Journal of climate*, **15**(17): 2340-2358.

Svoma, B.M. 2011. El Niño–Southern Oscillation and snow level in the western United States. *Journal of Geophysical Research: Atmospheres*, **116**(D24).

Trenberth, K.E. 1997. The definition of El Niño. *Bulletin of the American Meteorological Society*, **78**(12): 2771-2777.

Trenberth, K. E., Branstator, G. W., Karoly, D., Kumar, A., Lau, N.C., Ropelewski, C. 1998. Progress during TOGA in understanding and modeling global teleconnections associated with tropical sea surface temperatures. *Journal of Geophysical Research: Oceans*, **103**(C7): 14291-14324.

Waluda, C. M., Yamashiro, C., Rodhouse, P. G. 2006. Influence of the ENSO cycle on the light-fishery for Dosidicus gigas in the Peru Current: an analysis of remotely sensed data. *Fisheries Research*, **79**(1): 56-63.

Williams, C.J., McNamara, J.P., Chandler, D.G. 2009. Controls on the temporal and spatial variability of soil moisture in a mountainous landscape: the signature of snow and complex terrain. *Hydrology and Earth System Sciences*, **13**(7): 1325-1336.

Wolter, K., Timlin, M.S. 2011. El Niño/Southern Oscillation behaviour since 1871 as diagnosed in an extended multivariate ENSO index (MEI. ext). *International Journal of Climatology*, **31**(7): 1074-1087.

Wu, A., Hsieh, W.W. 2004. The nonlinear Northern Hemisphere winter atmospheric response to ENSO. *Geophysical research letters*, **31**(2).

Zebiak, S. E., Orlove, B., Muñoz, Á. G., Vaughan, C., Hansen, J., Troy, T., Thomson, M. C., Lustig, A., Garvin, S. 2015. Investigating El Niño-Southern Oscillation and society relationships. *Wiley Interdisciplinary Reviews: Climate Change*, **6**(1): 17-34.

Zhang, T., Perlwitz, J., Hoerling, M.P. 2014. What is responsible for the strong observed asymmetry in teleconnections between El Niño and La Niña? *Geophysical Research Letters*, **41**(3): 1019-1025.

Zhu, Y., Newell, R.E. 1998. A proposed algorithm for moisture fluxes from atmospheric rivers. *Monthly Weather Review*, **126**(3): 725-735.

CHAPTER II

ANOMALOUS HORIZONTAL HEAT FLUXES DURING EL NIÑO EVENTS OF VARIOUS MAGNITUDE

In Submission:

Kutta, E. J., Hubbart, J. A., Svoma, B. M., Eichler, T., Lupo, A. 2017. Anomalous Horizontal Heat Fluxes during El Niño Events of Various Magnitude. *International Journal of Climatology*. x:xx.

Introduction

Background

Teleconnections were described by Wallace and Gutzler (1981) as simultaneous correlations between temporal fluctuations in meteorological parameters at widely separated points on earth. Such relationships are particularly apparent for temporal fluctuations with time scales of a week or longer and are most closely associated with geographically fixed standing wave structures such as the Aleutian (Serreze et al. 1997) and Icelandic (Rodionov et al. 2007) lows. Interrelationships between teleconnections have been identified in recent work (e.g. Croci-Maspoli et al. 2007; Graf and Zanchettin 2012; Huang et al. 1998; Iza et al. 2016; Straus and Shukla 2002). Wallace and Gutzler (1981) reviewed five teleconnections and found that the Pacific North American (PNA; e.g. Allen et al. 1940; Dickson and Namias 1976; Namias 1951) and the West Atlantic (WA) patterns were closely related to the North Atlantic Oscillation (NAO) with maximum correlation on the west rather than east side of Greenland. Hurrell and Deser (2010) indicated that one-point correlation maps have been a common method to identify regions correlated with these teleconnections and used 45ºN 165ºW and 65ºN 30ºW reference

points for PNA and NAO patterns respectively. The PNA teleconnection has been described as a pair of north-south dipoles of simultaneous out-of-phase height anomalies across the East Pacific Ocean and North America (Hurrell and Deser 2010) bearing important implications for regional temperature and precipitation predictability within North America (e.g. Wallace and Gutzler 1981; Leathers et al. 1991). The NAO teleconnection also has important implications for regional temperature and precipitation predictability across Europe associated with a singular north-south dipole located in the North Atlantic Ocean (Hurrell and Deser 2010). Regional temperature and precipitation patterns associated with PNA and NAO patterns are modulated by the intensity and position of the Aleutian and Icelandic lows, which have climatologic positions during the boreal winter of 52ºN 175ºE (Serreze et al. 1997) and 62ºN 35ºW (Rodionov et al. 2007). Differences in longitude indicate PNA and NAO patterns were most strongly correlated slightly east of the climatologic low positions. This is consistent with an eastward shift in climate parameters during composite analyses of El Niño events (Müller and Roeckner 2008) indicating an interrelationship between the El Niño-Southern Oscillation (ENSO) and PNA and NAO patterns.

Trenberth and Caron (2000) showed that ENSO strongly influences intensity and position of anomalous centers of action (ACAs) despite long distances from the ENSO region (Niño 3.4; 170ºW to 120ºW; 5ºS to 5ºN). Proposed mechanisms linking sea surface temperature (SST) anomalies to variation in ACA intensity and position include the atmospheric bridge (e.g. Lau et al. 1997), subtropical bridge (Graf and Zanchettin 2012), and alterations to the stratospheric polar vortex (e.g. Ineson and Scaife 2009; Iza et al. 2016). Brönnimann (2007) concluded that the effect of El Niño on both PNA and NAO regions was climatologically relevant but only partially understood. Thus, a need exists to improve understanding of how the PNA and NAO

patterns respond to external forcing such as El Niño or changes in the atmospheric mean. Fulfilling this need is important to better understand impacts associated with climate variability and change (Hurrell and Deser 2010). A possible explanation of the confounding link between ENSO, PNA, and NAO patterns may be that each phenomena reaches both peak amplitude and variance during the boreal winter (Hurrell and Deser 2010; Rodionov et al. 2007; Serreze et al. 1997; Trenberth and Caron 2000). Spatial patterns of both PNA and NAO teleconnections were apparent in the two leading principal components of northern hemisphere sea level pressure (Hurrell and Deser 2010). However, explained variance did not exceed 36% suggesting an interdependency between PNA and NAO teleconnection patterns must exist, but no single index can capture all variability associated with either teleconnection pattern (Hurrell and Deser 2010). Thus, a need exists to show simultaneous spatial anomalies within and connecting ACA's at global scale to better understand the atmospheric bridge phenomena connecting ENSO with PNA and NAO regions (Trenberth and Caron 2000). Furthermore, the atmospheric bridge phenomena is variable based on El Niño event magnitude and seasonality (e.g. Toniazzo and Scaife 2006) such that the strongest atmospheric response should occur with the strongest El Niño event during late winter (Ineson and Scaife 2009). Therefore, this work was undertaken to quantify the anomalous horizontal fluxes of latent and sensible heat corresponding to El Niño events when anomalous upward fluxes of sensible and latent heat were forced into the troposphere from the Pacific Ocean.

Objectives

The primary objective of this work is to quantify spatial patterns of horizontal tropospheric mean heat (i.e. latent and sensible) flux anomalies using composite analyses of El Niño events that occurred between January 1979 and June 2016. Sub-objectives included, a)

assess predominant phase of PNA and NAO patterns (if possible) during November, December and January (NDJ; peak SST anomaly magnitude and variance in Niño 3.4 region [Okumura and Deser 2010]) for composite analyses of weak, strong, and all El Niño events, b) assess spatially continuous pathways connecting ENSO, PNA, and NAO regions during NDJ of each composite analysis, and c) individually analyze each of three strongest El Niño events during NDJ.

Materials and Methods

El Niño Events

The Climate Prediction Center (CPC; e.g. Kirtman et al. 2014) identified the occurrence of all El Niño events since 1950 according to their operational definition of five or more consecutive tri-monthly moving averages of Niño 3.4 region SST anomalies exceeding 0.5ºC (Harrison and Chiodi 2017). For the current work, only events occurring during or after 1979 were included given the temporal limitations of the ERA-Interim project output (ERA-I; Dee et al. 2011). All thirteen El Niño events since 1979 are summarized according to three-month running means of ERSST.v4 SST anomalies (Huang et al. 2015) in the Niño 3.4 region (5ºN-5ºS, 120ºW-170ºW) using centered 30-year base periods updated every five years (Table 1). The most common occurrence of maximum SST anomalies is the NDJ tri-monthly period (bolded). The maximum cool-season (September through February) oceanic Niño index (ONI) values (tri-monthly average of Niño 3.4 index values) were used to categorize each El Niño event into weak, moderate, and strong categories. Composite analyses have been a common method to show atmospheric anomalies associated with ENSO forcing of variable magnitude (e.g. Müller and Roeckner 2008) and season (e.g. Fogt and Bromwich 2006). Weak El Niño events represent the three lowest maximum cool-season ONI values and the strong El Niño events represent the

three largest maximum cool-season ONI values with the remaining El Niño events being categorized as moderate events.

Table 1. Summary of the thirteen El Niño events occurring between 1979 and 2016 including monthly Niño 3.4 Index values, maximum ONI values, each tri-monthly period where the maximum ONI values occurred, and categorization of each El Niño event.

	Niño 3.4 Index Value					
Years	**Nov**	**Dec**	**Jan**	**Max ONI**	**Tri-Monthly Period(s)**	**Category**
1979-80	0.54	0.64	0.65	0.6	**NDJ**, DJF	weak
1982-83	2.03	2.21	2.13	2.1	OND, **NDJ**, DJF	strong
1986-87	1.02	1.06	1.14	1.2	JFM	moderate
1987-88	1.23	1.02	0.91	1.6	JAS, ASO	moderate
1991-92	1.14	1.47	1.65	1.6	DJF	moderate
1994-95	1.04	1.14	0.94	1.0	**NDJ**	moderate
1997-98	2.32	2.23	2.21	2.3	OND, **NDJ**	strong
2002-03	1.26	1.21	0.83	1.2	OND	moderate
2004-05	0.60	0.67	0.78	0.7	SON, **NDJ**, DJF	weak
2006-07	0.91	1.02	0.83	0.9	OND, **NDJ**	moderate
2009-10	1.23	1.35	1.36	1.3	**NDJ**, DJF	moderate
2014-15	0.63	0.61	0.61	0.6	**NDJ**, DJF, FMA	weak
2015-16	2.25	2.24	2.33	2.3	**NDJ**	strong

Nov = November, Dec = December, Jan = January, Max ONI = Maximum Oceanic Niño Index

Reanalysis Data Used

The ERA-Interim reanalysis project (ERA-I) represents a high spatiotemporal resolution state-of-the-art atmospheric reanalysis product produced on a global domain (Dee et al. 2011) by the European Centre for Medium-Range Weather Forecasts (2009; updated monthly) covering the period of record from January 1979 through June 2016. The subset of ERA-I output utilized for the current work included six-hourly model analyses of specific humidity (q), temperature (T), and zonal (u) and meridional (v) components of wind provided on model levels at a nominal spatial resolution of ~0.7º latitude/longitude. ERA-I used eta vertical coordinates characterized by pressure coordinates in the upper atmosphere, hybrid pressure-sigma coordinates at mid to low-levels, and a terrain-following sigma coordinate system at the lowest model levels and at the

model surface (Simmons et al. 2007). Pressure in the eta coordinate system is a function of surface pressure (p_s) and a pair of time-independent spatially invariant coefficients denoted by a and b (Eq. 1) that vary in vertical, but not horizontal dimensions.

$$p_k(\lambda, \varphi, t) = a_k + b_k p_s(\lambda, \varphi, t) \quad \text{(Eq. 1)}$$

Here k is a generalized vertical index for each of the 60 vertical model levels, λ represents longitude, φ represents latitude, t represents time, and p_s represents surface pressure. Spacing between individual model levels represents vertical resolution within the model where greater spacing implies reduced resolution. For the purposes of the current work, the lowest 30 model levels were considered given higher vertical resolution, uncertainties regarding stratosphere-troposphere transport (Skerlak et al. 2014), and the lack of moisture above the 30th model level (Dessler et al. 2014) which is at 201 mb assuming a standard surface pressure of 105 Pa. Density-weighted vertical averages denoted by $\langle \cdot \rangle$ are most accurately estimated on the original model levels (Trenberth 1991) and were evaluated according to equation 2.

$$\langle \cdot \rangle = \int_{p_s}^{ml_{30}} (\cdot) \frac{dp}{g} \quad \text{(Eq. 2)}$$

Here ml_{30} represents the 30th model level, p_s represents surface pressure, dp represents the pressure thickness between model layers, and g represents gravitational constant. The mass-weighted vertically averaged horizontal sensible and latent heat fluxes are $\langle \boldsymbol{v}T \rangle$ and $\langle \boldsymbol{v}q \rangle$ respectively where $\boldsymbol{v} = (u, v)$.

Statistical Analysis and Data Scaling

Monthly averaged output from equation 2 was structured in a multi-dimensional array according to the following structure [latitude, longitude, month of year, year]. Monthly averaged

output for horizontal fluxes of sensible and latent heat were standardized along the yearly dimension such that averaging along the fourth (year) dimension yielded a mean of zero and a standard deviation of one at each grid point. The identification of coherent spatial patterns was assessed by selecting the monthly averages associated with each of the thirteen NDJ periods (n = 13) when El Niño conditions were present. A one sample t-test was performed to evaluate whether the mean was different from zero for either or both components of sensible or latent heat flux. Dashed contours were used to represent p-values that are equal to 0.05, stippling was used to highlight regions within contours. Although this test implicitly assumes independent samples, the focus here was to show coherent spatial patterns that are scientifically significant; we discuss the statistical issues associated with field testing (e.g. von Storch 1999; Wilks 2011) in more detail in 'Comments on Statistical Analyses' (pg. 124).

All horizontal fluxes of sensible heat were scaled by the specific heat of water (4.181 kJ kg^{-1} K^{-1}) under standard atmospheric conditions (20ºC, 101.325 kPa). All horizontal fluxes of latent heat were scaled by the latent heat of vaporization of water (2265 kJ kg^{-1}) at the same standard atmospheric conditions. Scaling was performed to provide horizontal fluxes of sensible and latent heat in the same units (kJ m^{-1} s^{-1}) to allow direct comparison (Shaw and Pauluis 2011). Scaling was also applied to each figure such that the maximum plotted vector magnitude was equal to the maximum value of the corresponding color bar. Reducing vector magnitude to a common value did not alter vector direction and was performed to clarify spatial patterns between anomalous maxima of horizontal heat fluxes.

Results

El Niño Composite

Composite spatial distributions of anomalous tropospheric mean sensible and latent heat fluxes quantified for all thirteen El Niño events during the period of record (1979-2016) are shown in figure 1. For the remainder of this article anomalous cyclonic circulations and anomalous anticyclonic circulations will be referred to as ACC and AAC respectively. North-south dipoles in anomalous circulations were used to assess the response (i.e. predominant phase) of PNA and NAO patterns to variable El Niño forcing, which are summarized at the end of each results section and in the discussion section. Focusing on the northern extratropical Pacific to Atlantic region, the greatest sensible heat flux anomalies (Fig. 1) occurred across the northern Atlantic Ocean associated with an ACC centered near 60ºN 25ºW during November. 60ºN 25ºW was just southeast from the climatologic position of the Icelandic low (62ºN 35ºW) with a broader, less well-defined, AAC characterized by two distinct centers near 40ºN 60ºW and 35ºN 10ºW. During November, an anomalous north-south circulation dipole across the northern Atlantic Ocean was assumed to be associated with predominantly positive NAO conditions (Trigo et al. 2002). Averaged over all thirteen El Niño events, the positive NAO signal diminished during December and results for January suggested an ACC developed in the central Atlantic Ocean with a poorly defined AAC across the northern Atlantic, which suggested a weakly negative NAO pattern. However, coherent spatial patterns indicated enhanced ($p < 0.05$) fluxes were not found within the northern Atlantic Ocean during any month of NDJ analyses composited for all El Niño events. Enhanced coherent spatial patterns ($p < 0.05$) of sensible heat fluxes were apparent across the western Pacific Ocean during November and expanded across the entire Pacific Ocean into Central America during January. The greatest sensible heat flux

anomalies occurred across the northern Pacific Ocean during January associated with an ACC centered near 40ºN 150ºW, which was approximately 3000 km southeast from the climatologic position of the Aleutian low (52ºN 175ºE). Coherent spatial patterns ($p < 0.05$) of poleward latent heat flux was apparent along portions of the southeastern coast of Asia during each month and a compensating enhanced equatorward latent heat flux was apparent across the central Pacific Ocean during January. Collectively, the seasonal evolution (NDJ) of the composite El Niño analyses indicated a positive NAO signal during November, which weakened during December and January as an increasingly positive PNA signal emerged. Coherent spatial patterns ($p < 0.05$) indicated the positive PNA signal strengthened the subtropical jet stream and weakened the polar jet streams across the Pacific Ocean and portions of North and Central America respectively during December and January. Therefore, composite analyses of all El Niño events showed an in-phase relationship between ENSO and NAO patterns during November and between ENSO and PNA during December and January with a reduced poleward heat flux across the north-central Pacific Ocean.

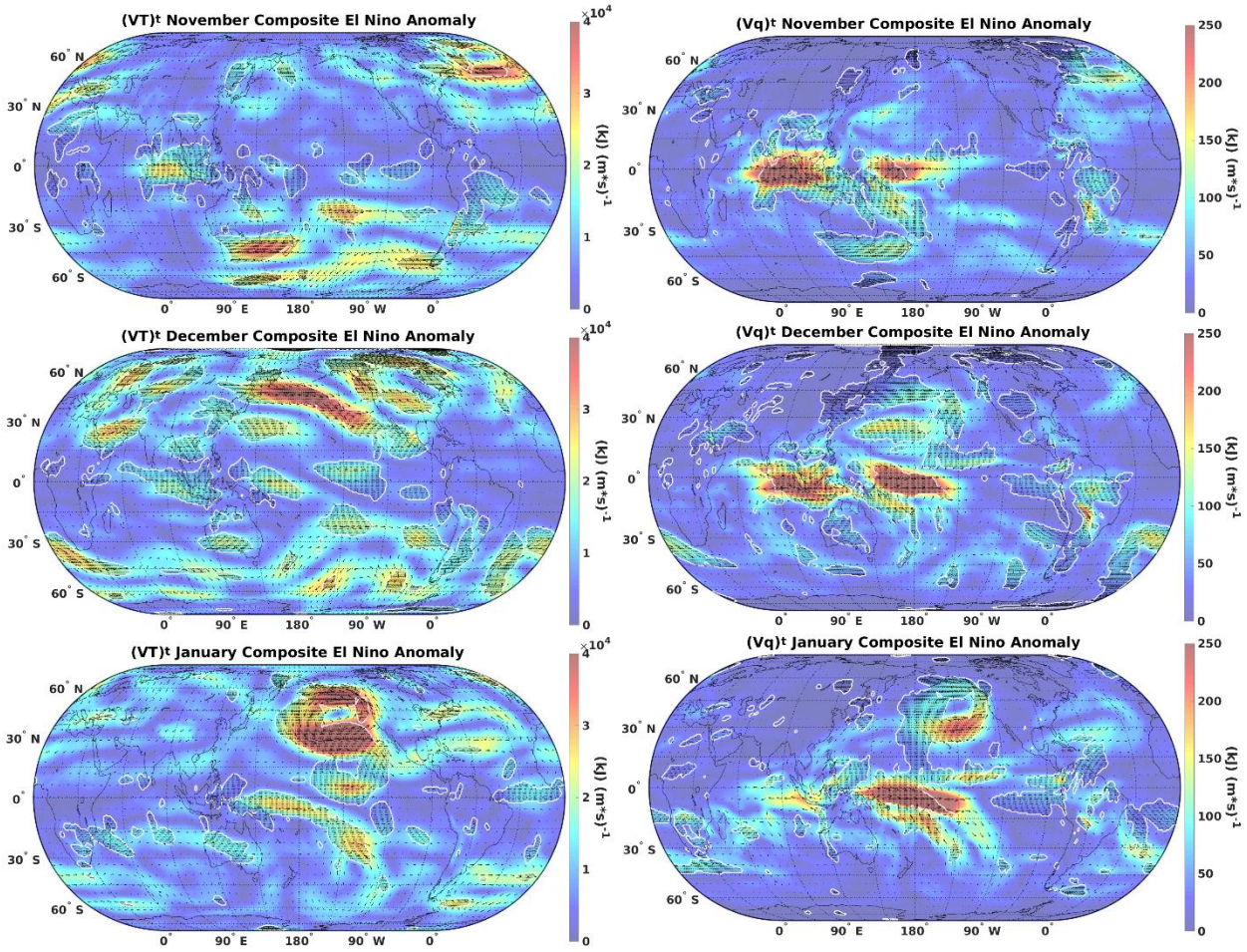

Figure 1. Monthly tropospheric sensible (left) and latent (right) heat flux anomalies for NDJ during composite of all thirteen El Niño events occurring between 1979 and 2016. Color shading represents vector magnitude (kJ m^{-1} s^{-1}), dashed contour and stippling represents significance ($p < 0.05$).

Weak El Niño Composite

Composite analyses of the spatial distribution of anomalous sensible and latent heat fluxes during the three weakest El Niño events (1979/80, 2004/05, and 2014/15; Table 1) are shown in figure 2. During November a wave-train of alternating anomalous circulations (AAC, ACC, AAC, ACC, AAC) was apparent between 150ºE and 30ºW. However, the spatial distribution of these anomalous circulations did not align with canonical PNA or NAO patterns. During December each anomalous circulation in the aforementioned wave-train shifted east

approximately 20-30º of longitude. Additionally, anomalous heat fluxes weakened for four of the five circulation features except the AAC centered near 45ºN 30ºW, which was strongly anomalous (> $6x10^4$ kJ m^{-1} s^{-1}) during December. An elongated ACC was apparent at approximately 20ºN such that a north-south dipole of anomalous circulations was apparent. The dipole pattern across the North Atlantic Ocean was consistent with a negative NAO pattern displaced approximately 20º latitude to the south of the single point correlation for the NAO index (65ºN 30ºW). The North Atlantic dipole, consistent with a negative NAO pattern, persisted through January and shifted approximately 5º latitude to the north. A similarly structured north-south dipole emerged across the northern Pacific Ocean during January such that the mid-point of the two anomalous circulations was approximately 45ºN 165ºW. Coherent spatial patterns ($p < 0.05$) indicated an ACC centered near 35ºN 165ºW during the month of January that enhanced horizontal sensible heat fluxes across the waters adjacent to Hawaii, but an in-phase relationship between ENSO and PNA patterns was not identified. Analyses of tropospheric mean latent heat flux (Fig. 2) indicated similar spatial patterns to that of sensible heat flux analyses, except the north Pacific dipole structure apparent across the northernmost Pacific Ocean. The atmospheric response to weak El Niño forcing across the Atlantic Ocean suggested an out-of-phase relationship between ENSO and NAO during December and January when weak El Niño forcing was present.

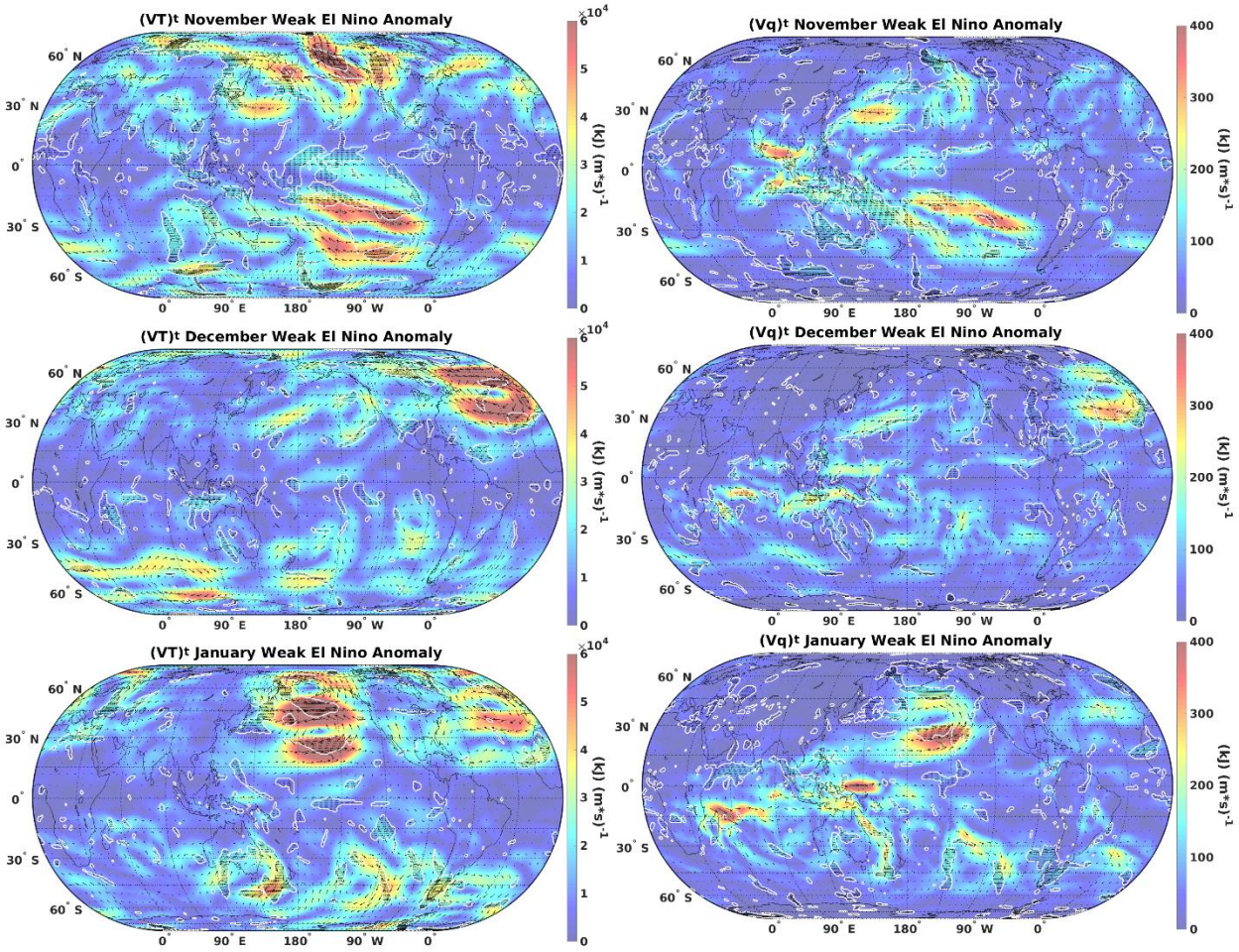

Figure 2. Monthly tropospheric sensible (left) and latent (right) heat flux anomalies for NDJ during composite of three weakest El Niño events (1979/80, 2004/05, 2014/15) occurring between 1979 and 2016. Color shading represents vector magnitude (kJ m^{-1} s^{-1}), dashed contour and stippling represents significance ($p < 0.05$).

Strong El Niño Composite

Composite analyses of the spatial distribution of anomalous sensible and latent heat fluxes during the three strongest El Niño events (1982/83, 1997/98, and 2015/16; Table 1) are shown in figure 3. Across the extratropical Atlantic Ocean analyses of sensible heat flux showed an ACC was apparent near 60ºN 25ºW during November, which was just 5º southeast of the one point correlation coordinates for the NAO pattern (65ºN 30ºW). To the south an AAC elongated approximately west to east near 30ºN such that the spatial distribution of anomalous circulations

suggested a north-south dipole consistent with a predominantly positive NAO pattern during November of strong El Niño forcing. The dipole across the North Atlantic Ocean persisted into December with the cyclonic center near 60ºN 30ºW and two anomalous anticyclonic circulations centered near 40ºN 70ºW and 35ºN 10ºW near the west and east coasts of the Atlantic Ocean respectively. During January the anomalous circulation dipole became ill-defined as the northern ACC elongated at approximately 30ºW longitude such that two distinct centers were apparent near 65ºN 20ºW and 15ºN 20ºW. The eastern coast of the Atlantic Ocean experienced enhanced poleward sensible and latent heat fluxes extending north to near 60ºN during January of strong El Niño forcing.

Across portions of the northern Pacific Ocean and North America the spatial distribution of anomalous circulations became consistent with a positive PNA pattern during December and January (Figures 4 and 5). November was characterized by two ACCs centered near 70ºN 180ºW and 40ºN 130ºW, which shifted southeast through December to be centered near 45ºN 145ºW and 30ºN 90ºW during January. Spatial patterns associated with the ACC centered near the Gulf Coast suggested a weakened polar jet stream (~45ºN) and strengthened subtropical jet stream (~20ºN) across North America during January. Regions of significant ($p < 0.05$) differences associated with this ACC were noted across the plains and Great Lakes of North America, large portions of Central America, and portions of the Gulf of Mexico, Caribbean Sea, and western Atlantic Ocean during Januarys associated with strong El Niño forcing. The two ACCs were shown well in analyses of anomalous tropospheric latent heat fluxes during the month of January with a ribbon of enhanced latent heat fluxes extending across the entire Pacific Ocean near 30ºN. Overall, composite analyses of the three strong El Niño events suggested an in-phase relationship between ENSO, PNA, and NAO patterns. The in-phase relationship varied by month such that

positive NAO conditions were most favored during November and December and positive PNA conditions were most favored during December and January of strong El Niño events.

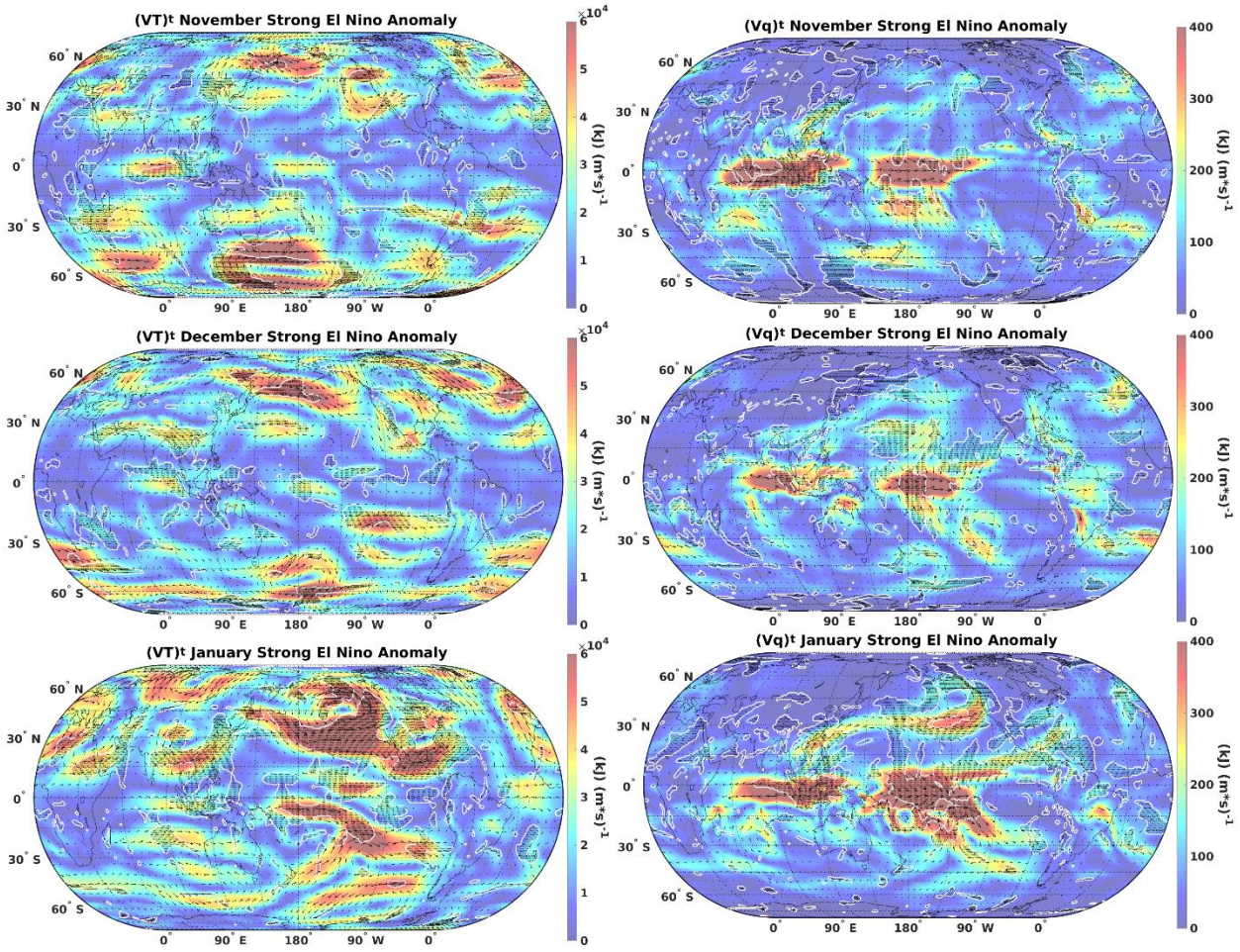

Figure 3. Monthly tropospheric sensible (left) and latent (right) heat flux anomalies for NDJ during composite of three strongest El Niño events (1982/83, 1997/98, 2015/16) occurring between 1979 and 2016. Color shading represents vector magnitude (kJ m^{-1} s^{-1}), dashed contour and stippling represents significance ($p < 0.05$).

Analysis of Three Strongest El Niño Events

The monthly (NDJ) seasonal evolution of sensible and latent heat flux anomalies for each of the three strong El Niño events are shown in Figure 4 and Figure 5 respectively. Since the magnitude of each of the three strongest El Niño events were similar (Table 1), differences in the spatial distributions of anomalous flux patterns or positions of anomalous circulations should be

attributed to differences in the spatial distribution of SST anomalies, natural variability, climate change or alternative modes of climate forcing, that were not addressed in this work. The approximate positions of three ACCs between 120ºE (west) and 60ºW (east) are summarized in Table 2. This region was important for assessing the interrelationship between ENSO and PNA given that it approximately covers the Pacific Ocean and North America, including the Aleutian low (central). The Atlantic Ocean was excluded from this region given that ACCs had large variation in position from month-to-month and event-to-event. The coordinates summarized in Table 2 were subjectively analyzed based on minima in vector magnitude and were subject to +/- 5º error in latitude or longitude. A similar table for anomalous latent heat flux circulations won't be included given ill-defined circulations at high latitude or continental locations given small specific humidity values (Figure 5; e.g. Newman et al. 2012). The seasonal evolution of ACCs across the western Pacific Ocean was spatially variable from month-to-month and event-to-event with an approximate range of ACC centers spanning approximately 50º latitude and 85º longitude. However, substantial tropospheric-mean sensible heat fluxes ($\geq 3.5 \times 10^4$ kJ m^{-1} s^{-1}) were shown crossing all or a portion of the Sea of Okhotsk during all nine months shown indicating a common pathway connecting eastern Asia with the PNA region. The seasonal evolution of ACC centers across central (Aleutian) and eastern (Gulf of Mexico) regions indicated a southeastward shift of ACCs between November and January that was consistent for each strong El Niño event. During January, remarkably consistent ACC positions were apparent across Aleutian and Gulf of Mexico regions with an approximate range of ACC centers spanning just 5º latitude and 15º longitude for the three strongest El Niño events (bolded; Table 2). Such consistency suggested two spatially continuous connections between eastern North America and the NAO region.

Table 2. Summary of positions of anomalous cyclonic circulations of sensible heat fluxes between 120ºE and 60ºW for each strong El Niño event (Table 1). Bolded coordinates indicate positions of persistently anomalous cyclonic circulations for each strong El Niño event.

		Cyclonic Anomalies between 120ºE and 60ºW		
Year	**Month**	**West**	**Central**	**East**
1982/83	Nov	65ºN 155ºE	50ºN 180ºW	40ºN 125ºW
	Dec	65ºN 145ºE	50ºN 155ºW	25ºN 110ºW
	Jan	65ºN 125ºE	**50ºN 150ºW**	**30ºN 90ºW**
1997/98	Nov	65ºN 175ºE	40ºN 140ºW	35ºN 85ºW
	Dec	60ºN 150ºW	35ºN 135ºW	40ºN 75ºW
	Jan	35ºN 175ºW	**45ºN 135ºW**	**25ºN 95ºW**
2015/16	Nov	20ºN 175ºW	65ºN 175ºW	35ºN 90ºW
	Dec	15ºN 170ºE	55ºN 175ºW	40ºN 110ºW
	Jan	55ºN 155ºE	**45ºN 150ºW**	**30ºN 90ºW**

Centers of ACCs across the northern Atlantic Ocean exhibited large month-to-month and event-to-event variability such that assessing a north-south dipole associated with a predominant phase of the NAO pattern was not possible (Figure 4). However, substantially enhanced (> $3.5x10^4$ kJ m^{-1} s^{-1}) tropospheric-mean fluxes of sensible heat were directed onto portions of the western European coast associated with two spatially continuous connections between eastern North America and the NAO region during each month. The first spatially continuous pathway was found at high latitudes (45-75ºN) during NDJ of the 1982-83 El Niño and during November and December of the 2015-16 El Niño, which were assumed to be associated with an enhanced polar jet stream. The second spatially continuous pathway was found at lower latitudes (15-45ºN) during November and December of the 1997-98 El Niño and January of the 2015-16 El Niño, which were assumed to be associated with an enhanced subtropical jet stream. Furthermore, January 1983 and December 2015 were characterized by strongly enhanced sensible heat fluxes (> $1.4x10^5$ kJ m^{-1} s^{-1}) intersecting the British Isles. Analyses of anomalous

tropospheric mean sensible and latent heat fluxes associated with the three strongest El Niño events supported an in-phase relationship between ENSO and PNA patterns. Upstream differences across the western Pacific Ocean resulted in slight variations in position of ACC centers across the PNA region that amplified to create substantially different spatial distributions of ACCs across the NAO region. Therefore, an in-phase relationship between ENSO and NAO patterns was not apparent in Figure 4 or Figure 5, but substantially enhanced tropospheric-mean fluxes of sensible heat were apparent along the western European coast during each NDJ associated with the three strong El Niño events.

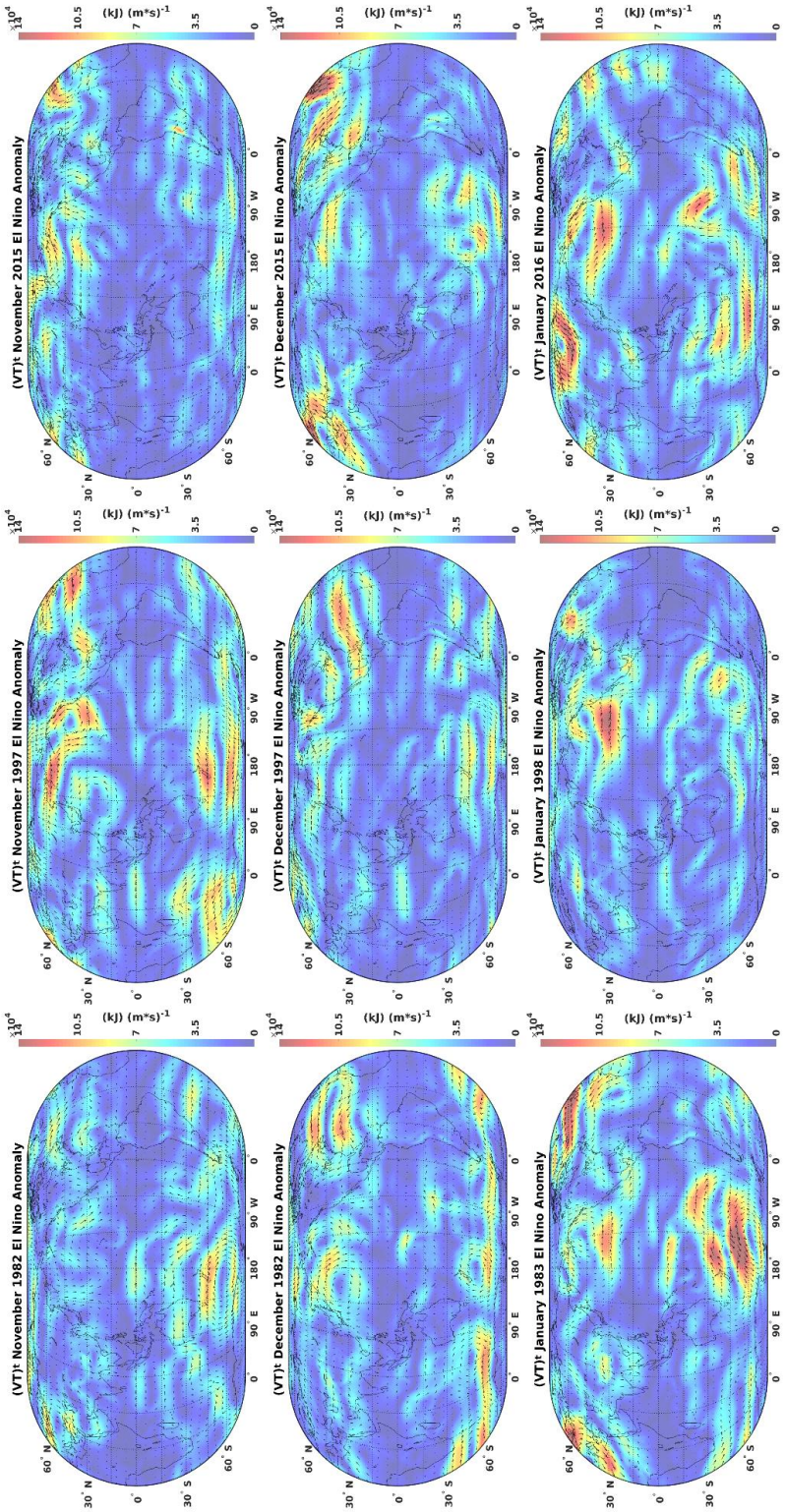

Figure 4. Monthly tropospheric sensible heat flux anomaly time-evolution for NDJ during each of three strongest El Niño events (1982/83, 1997/98, 2015/16; Table 1) occurring between 1979 and 2016. Color shading represents vector magnitude (kJ m^{-1} s^{-1}).

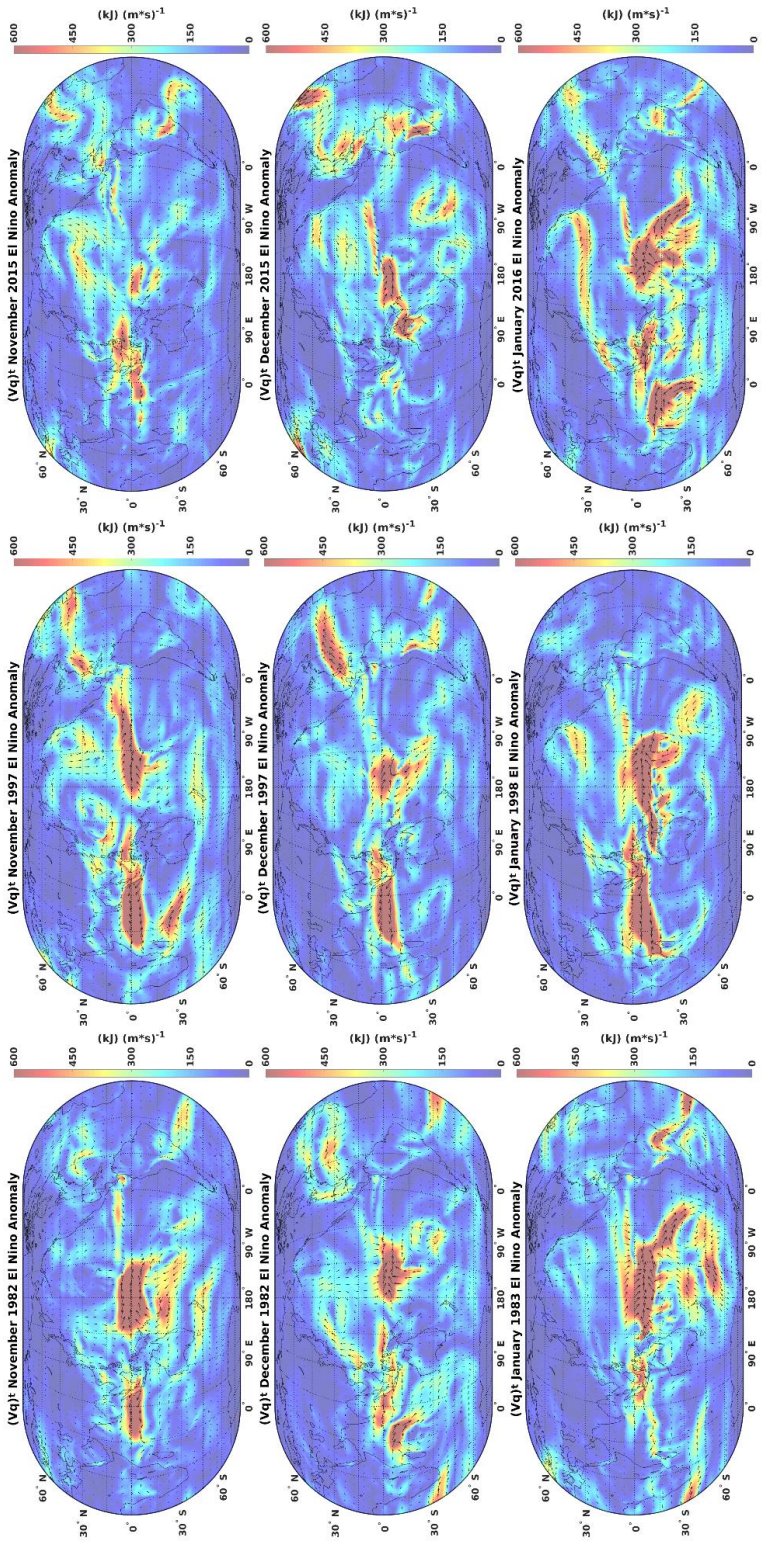

Figure 5. Monthly tropospheric latent heat flux anomaly time-evolution for NDJ during each of three strongest El Niño events (1982/83, 1997/98, 2015/16; Table 1) occurring between 1979 and 2016. Color shading represents vector magnitude (kJ m^{-1} s^{-1}).

Discussion

Composite analyses of thirteen El Niño events that occurred between January 1979 and June 2016 suggested the existence of an in-phase relationship between ENSO, PNA, and NAO patterns of climate variability within the NDJ period. Meehl and Teng (2007) noted that general teleconnection patterns associated with El Niño events included an anomalously deepened Aleutian low, ridging over western North America, and an anomalous cyclonic circulation (ACC) over the southeastern United States (US). Composite analyses of all thirteen El Niño events confirmed these coherent spatial patterns ($p < 0.05$) of tropospheric mean sensible heat flux anomalies across the PNA region consistent with an enhanced subtropical jet stream spanning the width of the Pacific Ocean and a weakened polar jet stream over North America. An enhanced subtropical jet stream across the Pacific Ocean was identified previously by Yang et al. (2002). However, this is the first time anomalous circulations connecting ENSO and PNA patterns have been shown at monthly resolution using tropospheric mean fluxes of sensible heat, which implies potential to quantify the interrelationship between ENSO and PNA patterns from an independent data source. Across the northern extratropical Atlantic Ocean predominantly positive NAO conditions were present (Figure 2) during November, but weakened during December as upstream cyclonic circulation anomalies shifted southeastwards. The anomalous circulation dipole apparent across the NAO region reversed during January, which suggested an out-of-phase relationship between ENSO and NAO patterns during late winter consistent with results of Brönnimann (2007). Therefore, this work was first to show a month-to-month dependency of the in-phase relationship between ENSO, PNA, and NAO teleconnections

implying that interactions between teleconnection patterns cannot be fully captured by seasonally averaged analyses.

Previous literature indicated that changes in El Niño event magnitude triggered changes to distant teleconnections including the PNA (Müller and Roeckner 2008) and NAO (Toniazzo and Scaife 2006) patterns. Results presented in sections 3.3 and 3.4 supported the variable atmospheric response to different El Niño event magnitudes by comparing differences between composite analyses of the three weakest (Figure 3) and strongest (Figure 4) El Niño events. During the weakest El Niño events (Figure 2), the seasonal evolution of anomalous tropospheric heat flux patterns showed a north-south dipole of anomalous circulations centered near 45ºN 165ºW. These coordinates were the same as the single-point correlation for the PNA pattern, but the anomalous circulation centers were located both north and south of single-point correlation (Wallace and Gutzler 1981) such that a predominant PNA phase was not identifiable. As an example, the center of the southern ACC was approximately 1700 km to the southwest of the analogous ACC during the three strongest El Niño events. Such a large southwest shift during weak El Niño forcing moved the ACC away from the PNA region confounding the proposed link between El Niño events and predominantly positive PNA conditions during weak El Niño forcing (e.g. Meehl and Teng 2007; Straus and Shukla 2002; Ropelewski and Halpert 1987). Additionally, large differences were apparent across the northern Atlantic Ocean between composite analyses of the three weakest and strongest El Niño events. The strongest El Niño events produced spatial patterns indicative of positive NAO conditions during November and December before losing the anomalous north-south circulation dipole during January. Alternatively, the weakest El Niño events resulted in an anomalous north-south dipole such that a predominantly negative NAO pattern was apparent during December and January. In addition,

the seasonal evolution of peak anomalies near the NAO region during weak El Niño conditions was lagged by at least one month relative to strong El Niño conditions. Therefore, the magnitude of El Niño events did trigger changes to position, intensity, and seasonality of anomalous circulations associated with PNA and NAO patterns that were also shown to be dependent on seasonality. Changes in El Niño event magnitude influenced the position more than intensity of anomalous circulations within the PNA region, but the influence across the NAO region was manifest both seasonally and by intensity. Also worthy of note were the spatial patterns in anomalous tropospheric latent heat fluxes during strong El Niño conditions, which were consistent with two atmospheric river phenomena. A spatial pattern consistent with an atmospheric river crossing Central America and the Gulf of Mexico into the southeastern US was apparent during December. Additionally, the trans-Pacific connection apparent during January was also consistent with atmospheric rivers impacts the Western US coast given that anomaly vectors across the central Pacific Ocean transitioned from equatorward to poleward near 150ºW. Gimeno et al. (2014) performed a review of atmospheric river literature and established that atmospheric rivers across the East Pacific Ocean and Central America were more commonly referred to as the Maya Express and Pineapple Express, respectively. Wang et al. (1999) detected significant predictability of enhanced winter precipitation across the Gulf Coast and southern plains during El Niño, which could be explained by the presence of an atmospheric river transporting extra eastern Pacific Ocean moisture into the southeastern US.

Analyses of anomalous tropospheric-mean heat fluxes for each of the three strongest El Niño events are provided in Figure 4 and Figure 5. These analyses were particularly relevant given the loss of human life and property attributed to powerful El Niño events (e.g. Changnon 1999; McPhaden 1999). Consistent centers of anomalous cyclonic heat flux patterns were shown

across the northeastern Pacific Ocean and Gulf of Mexico regions (Table 2), which indicated potential to predict the approximate location of these anomalous circulations during January for future El Niño events of similar magnitude. However, weather impacts (e.g. precipitation) along the west coast of North America were substantially different for each strong El Niño event studied (e.g. Wanders et al. 2017; Hoell et al. 2016). Variable impacts along the west coast of North America suggested further work is necessary to investigate the influence of ACCs across the West Pacific Ocean and their potential link to the PNA region during each strong El Niño event. In terms of long-distance teleconnections to the NAO region, results presented in section 3.5 indicated large event-to-event variability of spatial patterns across the North Atlantic Ocean. In general, 1997/98 and 2015/16 El Niño events favored an anomalous circulation dipole near the climatologic position of the Icelandic low suggesting positive NAO conditions, but the 1982/82 El Niño event favored an opposite anomalous circulation dipole across the North Atlantic Ocean consistent with negative NAO conditions. Further work is necessary to confirm the proposed in-phase relationship between ENSO, PNA, and NAO patterns of climate variability on an event-to-event basis. However, the most unique aspect of results presented here indicate common spatial distributions of anomalous circulations and heat flux pathways connecting each region.

Conclusions

An objective of this work was to identify spatial patterns in anomalous tropospheric heat fluxes that connected ENSO, PNA, and NAO regions. Composite analysis of thirteen El Niño events indicated a coherent spatial pattern ($p < 0.05$) of enhanced equatorward fluxes of latent heat that connected PNA and ENSO regions along and just east of the International Date Line during January. A similar region existed for sensible heat flux analyses suggesting the existence

of a spatially continuous pathway connecting PNA with ENSO regions. Enhanced sensible and latent heat fluxes were apparent across the southeastern coast of Asia during each month studied, which were transported eastwards into the PNA region. Composite analyses of the three weak and strong El Niño events indicated that transport across the western Pacific Ocean was more meridional during strong El Niño forcing whereas transport was more zonal during weak El Niño forcing. Individual analysis of each strong El Niño event revealed that the magnitude and direction of sensible heat flux anomalies across the Sea of Okhotsk could help distinguish event-to-event differences across the PNA region. Two spatially continuous tropospheric pathways connecting PNA and NAO regions were proposed, which were high latitude (45-75ºN) and low latitude (15-45ºN) pathways associated with enhancements to the polar and subtropical jet streams respectively. The low-latitude pathway associated with an enhanced subtropical jet stream has been suggested previously by Graf and Zanchettin (2012), but was not shown using analyses of anomalous tropospheric mean heat fluxes. Individual analyses of the three strongest El Niño events showed that the high latitude pathway was present during five of the nine months analyzed and the low latitude pathway present during three of the nine months. The most anomalous sensible heat fluxes along the western European coast were associated with the high latitude pathway and maximum anomalies were intersecting portions of the British Isles.

Heat flux anomalies during composite analyses of all events (n = 13), the three strongest, and three weakest El Niño events were used to assess north-south dipoles of circulation anomalies within characteristic regions of PNA and NAO patterns. Composite analyses of all thirteen El Niño events resulted in an in-phase relationship between ENSO and NAO patterns during November that weakened during December as the in-phase relationship between ENSO and PNA was established, which intensified during January. Composite analyses of the three

strongest and weakest El Niño events indicated that event magnitude primarily influenced anomalous circulation position within the PNA region. Alternatively, El Niño event magnitude primarily influenced seasonality and intensity of anomalous circulations within the NAO region. Results presented for weak El Niño events suggested the ACC centered in the PNA region shifted approximately 1700 km southwest away from the PNA region. Differences across the PNA region amplified further downstream such that an out-of-phase relationship was found between ENSO and NAO, especially during December and January. Therefore, the proposed in-phase relationship was most robust between ENSO and NAO patterns during November and between ENSO and PNA patterns during December and January, but was not robust during weak El Niño forcing. This work improved understanding of the interrelationship between ENSO, PNA, and NAO teleconnections and tropospheric pathways connecting each regional pattern, which are both crucial to understanding impacts to PNA and NAO patterns associated with climate variability and change. In particular, the spatially continuous pathway connecting ENSO and PNA regions near the International Date Line has potential to allow for quantification of the interrelationship between PNA and NAO patterns in near real time.

Acknowledgements

Appreciation is extended to coauthors and external evaluations of the article that greatly improved the quality of the work. This research did not receive any specific grant from funding agencies in the public, commercial, or not-for-profit sectors.

Literature Cited

Allen, R. A., Fletcher, R., Holmboe, J., Namias, J., Willett, H. C. 1940. Report on an experiment in five-day weather forecasting. Massachusetts Institute of Technology and Woods Hole Oceanographic Institution.

Brönnimann, S. 2007. Impact of El Niño–Southern Oscillation on European climate. *Reviews of Geophysics*, **45**(3).

Changnon, S. A. 1999. Impacts of 1997—98 El Niño generated weather in the United States. *Bulletin of the American Meteorological Society*, **80**(9): 1819-1827.

Croci-Maspoli, M., Schwierz, C., Davies, H. C. 2007. Atmospheric blocking: space-time links to the NAO and PNA. *Climate Dynamics*, **29**(7-8): 713-725.

Dee, D. P., Uppala, S. M., Simmons, A. J., Berrisford, P., Poli, P., Kobayashi, S., Andrae, U., Balmaseda, M. A., Balsamo, G., Bauer, P., Bechtold, P. 2011. The ERA-Interim reanalysis: Configuration and performance of the data assimilation system. *Quarterly Journal of the Royal Meteorological Society*, **137**(656): 553-597.

Dessler, A. E., Schoeberl, M. R., Wang, T., Davis, S. M., Rosenlof, K. H., Vernier, J. P. 2014. Variations of stratospheric water vapor over the past three decades. *Journal of Geophysical Research: Atmospheres*, **119**(22).

Dickson, R. R., Namias, J. 1976. North American influences on the circulation and climate of the North Atlantic sector. *Monthly Weather Review*, **104**(10): 1255-1265.

European Centre for Medium-Range Weather Forecasts. 2009, updated monthly. ERA-Interim Project. Research Data Archive at the National Center for Atmospheric Research, Computational and Information Systems Laboratory. https://doi.org/10.5065/D6CR5RD9. Accessed† 10 06 2016.

Fogt, R. L., Bromwich, D. H. 2006. Decadal variability of the ENSO teleconnection to the high-latitude South Pacific governed by coupling with the southern annular mode. *Journal of Climate*, **19**(6): 979-997.

Gimeno, L., Nieto, R., Vázquez, M., Lavers, D. A. 2014. Atmospheric rivers: a mini-review. *Frontiers in Earth Science*, **2**(2).

Graf, H. F., Zanchettin, D. 2012. Central Pacific El Niño, the "subtropical bridge," and Eurasian climate. *Journal of Geophysical Research: Atmospheres*, **117**(D1).

Harrison, D. E., Chiodi, A. M. 2017. Comments on "Characterizing ENSO Coupled Variability and Its Impact on North American Seasonal Precipitation and Temperature". *Journal of Climate*, **30**(1): 427-436.

Hoell, A., Hoerling, M., Eischeid, J., Wolter, K., Dole, R., Perlwitz, J., Xu, T., Cheng, L. 2016. Does El Niño intensity matter for California precipitation? *Geophysical Research Letters*, **43**(2): 819-825.

Huang, J., Higuchi, K., Shabbar, A. 1998. The relationship between the North Atlantic Oscillation and El Niño-Southern Oscillation. *Geophysical Research Letters*, **25**(14): 2707-2710.

Huang, B., Banzon, V. F., Freeman, E., Lawrimore, J., Liu, W., Peterson, T. C., Smith, T. M., Thorne, P. W., Woodruff, S. D., Zhang, H. M. 2015. Extended reconstructed sea surface temperature version 4 (ERSST. v4). Part I: Upgrades and intercomparisons. *Journal of climate*, **28**(3): 911-930.

Hurrell, J. W., Deser, C. 2010. North Atlantic climate variability: the role of the North Atlantic Oscillation. *Journal of Marine Systems*, **79**(3): 231-244.

Ineson, S., Scaife, A. A. 2009. The role of the stratosphere in the European climate response to El Niño. *Nature Geoscience*, **2**(1): 32-36.

Iza, M., Calvo, N., Manzini, E. 2016. The Stratospheric Pathway of La Niña. *Journal of Climate*, **29**(24): 8899-8914.

Kirtman, B. P., Min, D., Infanti, J. M., Kinter III, J. L., Paolino, D. A., Zhang, Q., Van Den Dool, H., Saha, S., Mendez, M. P., Becker, E., Peng, P. 2014. The North American multimodel ensemble: phase-1 seasonal-to-interannual prediction; phase-2 toward developing intraseasonal prediction. *Bulletin of the American Meteorological Society*, **95**(4): 585-601.

Lau, N. C. 1997. Interactions between global SST anomalies and the midlatitude atmospheric circulation. *Bulletin of the American Meteorological Society*, **78**(1): 21-33.

McPhaden, M. J. 1999. Genesis and evolution of the 1997-98 El Niño. *Science*, **283**(5404): 950-954.

Meehl, G. A., Teng, H. 2007. Multi-model changes in El Niño teleconnections over North America in a future warmer climate. *Climate Dynamics*, **29**(7-8): 779-790.

Müller, W. A., Roeckner, E. 2008. ENSO teleconnections in projections of future climate in ECHAM5/MPI-OM. *Climate Dynamics*, **31**(5): 533-549.

Namias, J. 1951. The great Pacific anticyclone of winter 1949–50: a case study in the evolution of climatic anomalies. *Journal of Meteorology*, **8**(4): 251-261.

Newman, M., Kiladis, G. N., Weickmann, K. M., Ralph, F. M., Sardeshmukh, P. D. 2012. Relative contributions of synoptic and low-frequency eddies to time-mean atmospheric moisture transport, including the role of atmospheric rivers. *Journal of Climate*, **25**(21): 7341-7361.

Okumura, Y. M., Deser, C. 2010. Asymmetry in the duration of El Niño and La Niña. *Journal of Climate*, **23**(21): 5826-5843.

Rodionov, S. N., Bond, N. A. and Overland, J. E., 2007. The Aleutian Low, storm tracks, and winter climate variability in the Bering Sea. *Deep Sea Research Part II: Topical Studies in Oceanography*, **54**(23): 2560-2577.

Ropelewski, C.F., Halpert, M.S. 1987. Global and regional scale precipitation patterns associated with the El Niño/Southern Oscillation. *Monthly Weather Review*, **115**(8): 1606-1626.

Serreze, M. C., Carse, F., Barry, R. G., Rogers, J. C. 1997. Icelandic low cyclone activity: Climatological features, linkages with the NAO, and relationships with recent changes in the Northern Hemisphere circulation. *Journal of Climate*, **10**(3): 453-464.

Shaw, T. A., Pauluis, O. 2012. Tropical and subtropical meridional latent heat transports by disturbances to the zonal mean and their role in the general circulation. *Journal of the Atmospheric Sciences*, **69**(6):1872-1889.

Simmons, A., Uppala, S., Dee, D., Kobayashi, S. 2007. ERA-Interim: New ECMWF reanalysis products from 1989 onwards. *ECMWF newsletter*, 110, 25-35.

Skerlak, B., Sprenger, M., Wernli, H. 2014. A global climatology of stratosphere-troposphere exchange using the ERA-Interim data set from 1979 to 2011. *Atmospheric Chemistry and Physics*, **14**(2): 913.

Straus, D. M., Shukla, J. 2002. Does ENSO force the PNA? *Journal of Climate*, **15**(17): 2340-2358.

Toniazzo, T., Scaife, A. A. 2006. The influence of ENSO on winter North Atlantic climate. *Geophysical Research Letters*, **33**(24).

Trenberth, K. E. 1991. Climate diagnostics from global analyses: Conservation of mass in ECMWF analyses. *Journal of Climate*, **4**(7): 707-722.

Trenberth, K. E., Caron, J. M. 2000. The Southern Oscillation revisited: Sea level pressures, surface temperatures, and precipitation. *Journal of Climate*, **13**(24): 4358-4365.

Trigo, R. M., Osborn, T. J., Corte-Real, J. M. 2002. The North Atlantic Oscillation influence on Europe: climate impacts and associated physical mechanisms. *Climate Research*, **20**(1): 9-17.

Von Storch, H., 1999. Misuses of statistical analysis in climate research. *Analysis of Climate Variability*, 11-26.

Wallace, J.M., Gutzler, D.S, 1981. Teleconnections in the geopotential height field during the Northern Hemisphere winter. *Monthly Weather Review*, **109**(4): 784-812.

Wanders, N., Bachas, A., He, X. G., Huang, H., Koppa, A., Mekonnen, Z. T., Pagán, B. R., Peng, L. Q., Vergopolan, N., Wang, K. J., Xiao, M. 2017. Forecasting the hydroclimatic

signature of the 2015-16 El Niño event on the western US. *Journal of Hydrometeorology*, **18**: 177-186.

Wang, H., Ting, M., Ji, M. 1999. Prediction of seasonal mean United States precipitation based on El Niño sea surface temperatures. *Geophysical Research Letters*, **26**(9): 1341-1344.

Wilks, D.S., 2011. Statistical methods in the atmospheric sciences (Vol. 100). Academic press.

Yang, S., Lau, K. M., Kim, K .M. 2002. Variations of the East Asian jet stream and Asian–Pacific–American winter climate anomalies. *Journal of Climate*, **15**(3): 306-325.

CHAPTER III

THE INFLUENCE OF LA NIÑA EVENTS ON TROPOSPHERIC FLUXES OF SENSIBLE AND LATENT HEAT USING THE ERA-INTERIM REANALYIS PROJECT

In Submission:

Kutta, E. J., Hubbart, J. A., Svoma, B. M., Eichler, T., Lupo, A. 2017. The Influence of La Niña Events on Tropospheric Fluxes of Sensible and Latent Heat using the ERA-Interim Reanalysis Project. *Dynamics of Atmospheres and Oceans* x:xx.

Introduction

Background

Five climate subsystems, including the atmosphere, are modulated by both external (e.g. incoming solar radiation) and internal factors (e.g. atmospheric composition) to form Earth's climate system (Peixoto and Oort 1992). Earth's atmosphere is linked with the surface (e.g. hydrosphere, lithosphere, biosphere, cryosphere) through fluxes of mass, energy, and momentum to form a complex, highly non-linear climatic system (Peixoto and Oort 1992). Coupled atmosphere-hydrosphere interactions have garnered particular attention in recent decades given recognition of the El Niño-Southern Oscillation (ENSO) as a dominant source of inter-annual climate variability (e.g. Trenberth et al. 1998). The ENSO phenomenon is quantified through sea surface temperature (SST) anomalies within the Niño 3.4 region (170ºW to 120ºW, 5ºS to 5ºN) that typically reach peak magnitude during December when SST anomaly variance is maximized (Okumura and Deser 2010). The ENSO phenomena has both warm (positive SST anomalies) and cool (negative SST anomalies) phases more commonly referred to as El Niño and La Niña,

respectively. The current operational Climate Prediction Center (CPC; e.g. Kirtman et al. 2014) definition of an El Niño or La Niña event requires at least five consecutive tri-monthly moving averages of SST anomalies within the Niño 3.4 region commonly referred to as the Oceanic Niño Index (ONI; e.g. Yu and Kim 2013). Asymmetry in magnitude and duration of SST anomalies suggest that El Niño events attain larger SST anomalies that terminate rapidly whereas La Niña events have smaller SST anomalies that tend to persist into a second year (e.g. Kang and Kug 2002; An and Jin 2004; Okumura and Deser 2010). Non-linearity in the magnitude and duration of tropical SST anomalies inherent in the ENSO phenomena resulted in a non-linear extratropical atmospheric response that is not fully understood (Wu and Hsieh 2004).

Greater El Niño event magnitude and the reversal of climatology associated with El Niño events (e.g. Kumar et al. 2006; Larkin and Harrison 2005) has drawn more attention than the La Niña phenomena (Okumura and Deser 2010). However, La Niña forcing has been associated with flooding across portions of northern South America, Australia, and Southeast Asia (Boening et al. 2012) and widespread continental drought over portions of North America, Asia, and Africa (e.g. Ropelewski and Halpert 1986; Barlow et al. 2002; Lyon and DeWitt 2012; Hoell et al. 2014). Therefore, La Niña events are societally impactful events and a need exists to better understand the long-distance impacts associated with La Niña events. Most observational studies used linear techniques (e.g. regression, empirical orthogonal function [EOF], or warm minus cold composites) to identify canonical teleconnections assuming that La Niña is a mirror image of El Niño (Okumura and Deser 2010). However, Zhang et al. (2014) detected similarly large symmetric and asymmetric components of wintertime ENSO-related teleconnections over North America (NA) indicating the atmospheric response to La Niña does not mirror that of El Niño. Empirical evidence presented by (Davis 1976; Wallace et al. 1990; Cayan 1992; Trenberth and

Hurrell 1994) indicated observed SST perturbations in mid-latitude oceans temporally lagged the atmospheric anomalies such that extratropical SST perturbations were responses to, rather than causes of, atmospheric changes (Trenberth et al. 1998). This improved conceptual framework helped identify Earth's atmospheric circulation as a 'bridge' linking tropical SST changes in distant, mid-latitude oceans (Trenberth et al. 1998). Simultaneous correlations between temporal fluctuations in meteorological parameters, also known as teleconnection patterns, have become a common method for describing relationships in the variability of large-scale features of the atmospheric circulation (Wallace and Gutzler 1981).

The influence of ENSO on both Pacific-North American (PNA) and North Atlantic Oscillation (NAO) regions was described in a review of literature as climatologically relevant and at least partly understood (Brönnimann 2007). Given an asymmetric atmospheric response to the ENSO phenomena a need exists to improve understanding of the influence La Niña events have on PNA and NAO patterns. The Pacific-North American (PNA) and North Atlantic Oscillation (NAO) patterns have been documented as the most prominent teleconnection patterns across the Pacific and Atlantic Oceans respectively (Hurrell and Deser 2010). The PNA pattern was described as a pair of north-south dipoles of simultaneous out-of-phase height anomalies across the East Pacific Ocean and NA whereas the NAO pattern was described as a similar, but singular north-south dipole across the North Atlantic Ocean (Hurrell and Deser 2010). The Aleutian and Icelandic lows represent atmospheric centers of action (ACA) such that the PNA and NAO patterns describe intra-annual variability in the strength and position of each respective ACA feature (e.g. Serreze et al. 1997; Rodionov et al. 2007). Representative coordinates (one-point correlations) for PNA (45ºN 165ºW) and NAO (65ºN 30ºW) patterns (Hurrell and Deser 2010) were located east of the climatologic position of the Aleutian (52ºN 175ºE; Serreze et al.

1997) and Icelandic (62ºN 35ºW; Rodionov et al. 2007) lows, respectively. Such an eastward shift in the position of the Aleutian and Icelandic lows has been documented in composite analyses of El Niño events (Müller and Roeckner 2008), indicating an interrelationship between ENSO, PNA, and NAO patterns. Wise et al. (2015) explained that improving the reliability of seasonal forecasts depends on improved understanding of impacts associated with multiple, simultaneously occurring teleconnection patterns such as the interrelationship between La Niña, PNA, and NAO patterns.

Analyses of integrated water vapor transports have been extensively used to identify the relationship between atmospheric rivers and heavy precipitation impacting the west coast of North America (e.g. Dettinger et al. 2004; Ralph et al. 2006; Guan et al. 2012, 2013), but only a few studies have analyzed integrated water transports on interannual (ENSO) time scales (Kim and Alexander 2015). Kim and Alexander (2015) showed enhanced integrated water vapor transports into the southwestern United States associated with El Niño events, but indicated that the overall influence of ENSO (including La Niña) on the moisture transport needs to be explored in greater detail. Hurrell and Deser (2010) concluded that the month-to-month changes in phase and amplitude of NAO are unpredictable, but external forcing, such as La Niña, could enhance predictability of NAO patterns. Analyses of integrated water vapor transports are a common method to assess connections from tropical heat sources (ENSO) into the PNA region such that a need exists to spatially expand similar analyses to assess connections across the North Atlantic Ocean. Therefore, this work showed the anomalous horizontal latent and sensible heat fluxes into PNA or NAO regions corresponding to ENSO events when anomalous upward heat fluxes were forced into the tropical troposphere from the Pacific Ocean.

Objectives

The overarching objective of this work was to quantify spatial patterns of horizontal tropospheric mean heat (i.e. latent and sensible) flux anomalies using composite analyses of La Niña events that occurred between January 1979 and June 2016. Sub-objectives included, a) assess the predominant phase of PNA and NAO patterns (if possible) during November, December, and January (NDJ; peak SST anomaly magnitude and variance in Niño 3.4 region) for composite analyses of weak, strong, and all La Niña events, b) assess spatially continuous pathways connecting ENSO, PNA, and NAO regions during NDJ of each composite analysis, c) individually analyze each of the three strongest La Niña events during NDJ.

Materials and Methods

La Niña Events

The occurrence of all La Niña events since 1950 has been documented by the CPC based on tri-monthly moving averages of SST anomalies within the Niño 3.4 region commonly referred to as the Oceanic Niño Index (ONI; Yu and Kim 2013). Harrison and Chiodi (2017) describe the current operational definition of a La Niña event as five or more consecutive ONI values less than or equal to -0.5ºC. For the current work this criteria was relaxed to at least four consecutive ONI values less than or equal to -0.5ºC, because La Niña events often have smaller SST anomalies (An and Jin 2004). Reducing the longevity criteria increased the sample size of all La Niña events occurring since 1979 to twelve, which was comparable to the thirteen El Niño events over the same period of record. January 1979 through June 2016 was the period of record chosen for this work given temporal limitations of the ERA-Interim Project (ERA-I; Dee et al. 2011) and all twelve La Niña events identified have been summarized in Table 3. The most common

occurrence of maximum SST anomalies was the November, December, January (NDJ) tri-monthly period (bolded; Table 3), thus the NDJ period was the focus of this work. Minimum ONI values associated with peak La Niña event intensity during the cool-season (September through February) were used to categorize each La Niña event into weak, moderate, and strong categories. Weak La Niña events were characterized by minimum ONI values between -0.7ºC and -0.8ºC and ONI values less than -0.5ºC for just four consecutive tri-monthly periods. Strong La Niña events were characterized by minimum ONI values between -1.5ºC and -1.8ºC and ONI values less than -0.5ºC for ten or more consecutive tri-monthly periods. The remaining six La Niña events were categorized as moderate La Niña events that had minimum ONI values between -0.8ºC and -1.4ºC and ONI values less than -0.5ºC for seven or more consecutive tri-monthly periods.

Table 3. Summary of all twelve La Niña events occurring between 1979 and 2016 including monthly (NDJ) Niño 3.4 Index values, minimum ONI values, each tri-monthly period where the minimum ONI values occurred, and categorization of each La Niña event.

	Niño 3.4 Index Value					
Years	**Nov**	**Dec**	**Jan**	**Min ONI**	**Tri-Monthly Period(s)**	**Category**
1983-84	-0.89	-0.76	-0.60	-0.8	OND, **NDJ**	weak
1984-85	-0.99	-1.17	-0.99	-1.1	**NDJ**	moderate
1988-89	-1.78	-1.72	-1.76	-1.8	**NDJ**	strong
1995-96	-1.02	-0.97	-0.84	-1.0	OND	moderate
1998-99	-1.20	-1.52	-1.58	-1.4	**NDJ**, DJF	moderate
1999-00	-1.43	-1.60	-1.70	-1.6	**NDJ**, DJF	strong
2000-01	-0.76	-0.84	-0.63	-0.8	OND, **NDJ**	moderate
2005-06	-0.55	-0.78	-0.69	-0.7	**NDJ**, DJF	weak
2007-08	-1.30	-1.30	-1.38	-1.4	DJF	moderate
2008-09	-0.47	-0.82	-0.80	-0.7	**NDJ**, DJF	weak
2010-11	-1.42	-1.41	-1.36	-1.5	SON	strong
2011-12	-1.02	-0.92	-0.67	-1.0	OND	moderate

Nov = November, Dec = December, Jan = January, Min ONI = Minimum Oceanic Niño Index

Reanalysis Data Used

State-of-the-art atmospheric reanalyses are critical for advancing understanding of a suite of hydrometeorological research (Lorenz and Kunstmann 2012). Creation of such reanalyses involves processing large quantities of historic observations using advanced data assimilation methods (e.g. 4D-Var; Dee et al. 2011) to provide physically consistent analyses of a suite of atmospheric quantities. ERA-I was produced at high spatial (~0.7º latitude/longitude) and temporal (6-hourly analyses) resolution over a global domain between January 1979 to the present by the European Centre for Medium-Range Weather Forecasts (ECMWF; Dee et al. 2011). The subset of ERA-I output utilized for the current work were six-hourly model analyses of specific humidity (*q*), temperature (*T*), and zonal (*u*) and meridional (*v*) components of wind provided on model levels between January 1979 and June 2016. ERA-I model levels adhered to the eta vertical coordinate system characterized by terrain-following sigma coordinates at the lowest model levels and the model surface, hybrid pressure-sigma coordinates at mid to low-levels, and pressure coordinates in the upper atmosphere (Simmons et al. 2007). Pressure in the eta coordinate system is a function of surface pressure (p_s) and a pair of time-independent, spatially invariant coefficients denoted by *a* and *b* (Eq. 1) that vary in the vertical, but not horizontal dimensions.

$$p_k(\lambda, \varphi, t) = a_k + b_k p_s(\lambda, \varphi, t) \qquad \text{Eq. 1}$$

Here k is a generalized vertical index for each of the 60 vertical model levels, λ represents longitude, φ represents latitude, t represents time, and p_s represents surface pressure. For the purposes of this work only the lowest 30 model levels were considered given higher vertical resolution, uncertainties regarding stratosphere-troposphere transport (Skerlak et al.

2014), and the lack of moisture above the 30th model level (Dessler et al. 2014) that is at 201 mb assuming a standard surface pressure of 10^5 Pa. Trenberth (1991) explicated that the most accurate density-weighted vertical averages denoted by $\langle\cdot\rangle$ are calculated on the original model levels and were evaluated according to equation 2.

$$\langle\cdot\rangle = \int_{p_s}^{ml_{30}} (\cdot)\frac{dp}{g} \quad \text{Eq. 2}$$

Here ml_{30} represents the 30th model level, p_s represents surface pressure, dp represents the pressure thickness between model layers, and g represents gravitational constant. The mass-weighted vertically averaged horizontal sensible and latent heat fluxes are $\langle \boldsymbol{v}T \rangle$ and $\langle \boldsymbol{v}q \rangle$ respectively where $\boldsymbol{v} = (u, v)$.

Statistical Analysis and Data Scaling

Six-hourly output from equation 2 was averaged monthly and stored in a multi-dimensional array according to the following structure [latitude, longitude, month of year, year]. All monthly averaged output was standardized along the yearly dimension such that the averaging along this dimension resulted in a standard deviation of one and a mean of zero at each grid point. The identification of coherent spatial patterns was assessed by selecting the monthly averages associated with each of the thirteen NDJ periods (n = 13) when El Niño conditions were present. A one sample t-test was performed to evaluate whether the mean was different from zero for either or both components of sensible or latent heat flux. Dashed contours were used to represent p-values that are equal to 0.05, stippling was used to highlight regions within contours. Although this test implicitly assumes independent samples, the focus here was to show coherent spatial patterns that are scientifically significant; we discuss the statistical issues associated with field testing (e.g. von Storch 1999; Wilks 2011) in more detail in 'Comments on Statistical

Analyses' (pg. 124). Scaling was performed after all calculations were made to provide horizontal fluxes of sensible and latent heat in the same units (kJ m^{-1} s^{-1}), allowing for direct comparison (Shaw and Pauluis 2011). All horizontal fluxes of sensible heat were scaled by the specific heat of water (4.181 kJ kg^{-1} K^{-1}) under standard atmospheric conditions (20ºC, 101.325 kPa). All horizontal fluxes of latent heat were scaled by the latent heat of vaporization of water (2265 kJ kg^{-1}) at the same standard atmospheric conditions. Additional scaling was performed to each figure panel such that the maximum plotted vector magnitude was equal to the maximum value of the corresponding color bar. Reducing maximum vector magnitudes to a common value did not alter vector direction and clarified spatial patterns between anomalous maxima of horizontal heat fluxes.

Results

La Niña Composite

Composite spatial distributions of anomalous tropospheric mean sensible and latent heat fluxes quantified for all twelve La Niña events during the period of record (1979-2016) are shown in Figure 6. For the remainder of this article anomalous cyclonic circulations and anomalous anticyclonic circulations will be referred to as ACC and AAC respectively. North-south dipoles in anomalous circulations were used to assess the response (i.e. predominant phase) of PNA and NAO patterns to variable La Niña forcing, which are summarized at the end of each results section and in the discussion section. During November, the greatest sensible heat flux anomalies (~$4x10^4$ kJ m^{-1} s^{-1}; Figure 6) occurred across the Northern Atlantic Ocean associated with an AAC centered near 65ºN 35ºW. Just to the south an elongated ACC extended across the Atlantic basin at approximately 35ºN resulting in an anomalous north-south

circulation dipole consistent with a negative NAO pattern during November. The anomalous dipole feature weakened through December such that a predominant phase of the NAO pattern was not possible during December or January when maximum sensible heat flux anomalies prevailed across the Eastern Pacific Ocean. Two AACs were present during November centered near 35ºN 155ºW and 35ºN 110ºW that were shown to shift eastward during December and January. The western AAC became a strongly anomalous AAC ($> 4x10^4$ kJ m^{-1} s^{-1}) and shifted northeast to be centered near 40ºN 150ºW during January whereas the eastern AAC maintained moderate intensity and shifted southeast to be centered near 25ºN 105ºW. Weaker ACCs were apparent south and north of each respective AAC to form a pair of simultaneous out-of-phase anomalous north-south dipoles consistent with a substantially weakened Aleutian low and predominantly negative PNA pattern (Iza et al. 2016). Of particular note was a coherent spatial pattern ($p < 0.05$) of anomalous sensible heat fluxes connecting the Niño 3.4 region (170ºW to 120ºW, 5ºS to 5ºN) with the single point correlation for the PNA pattern (45ºN 165ºW; Hurrell and Deser 2010) during January. This coherent spatial pattern ($p < 0.05$) connecting ENSO and PNA regions was shown more clearly in analyses of latent heat flux (Figure 6) during both December and January. Overall, analyses indicated a seasonally dependent relationship between ENSO, PNA, and NAO patterns of climate variability with a negative NAO pattern favored during November and increasingly negative PNA pattern favored through December and January. Additionally, a poleward pathway connecting Niño 3.4 and PNA regions was shown to be significant during December and January of La Niña events.

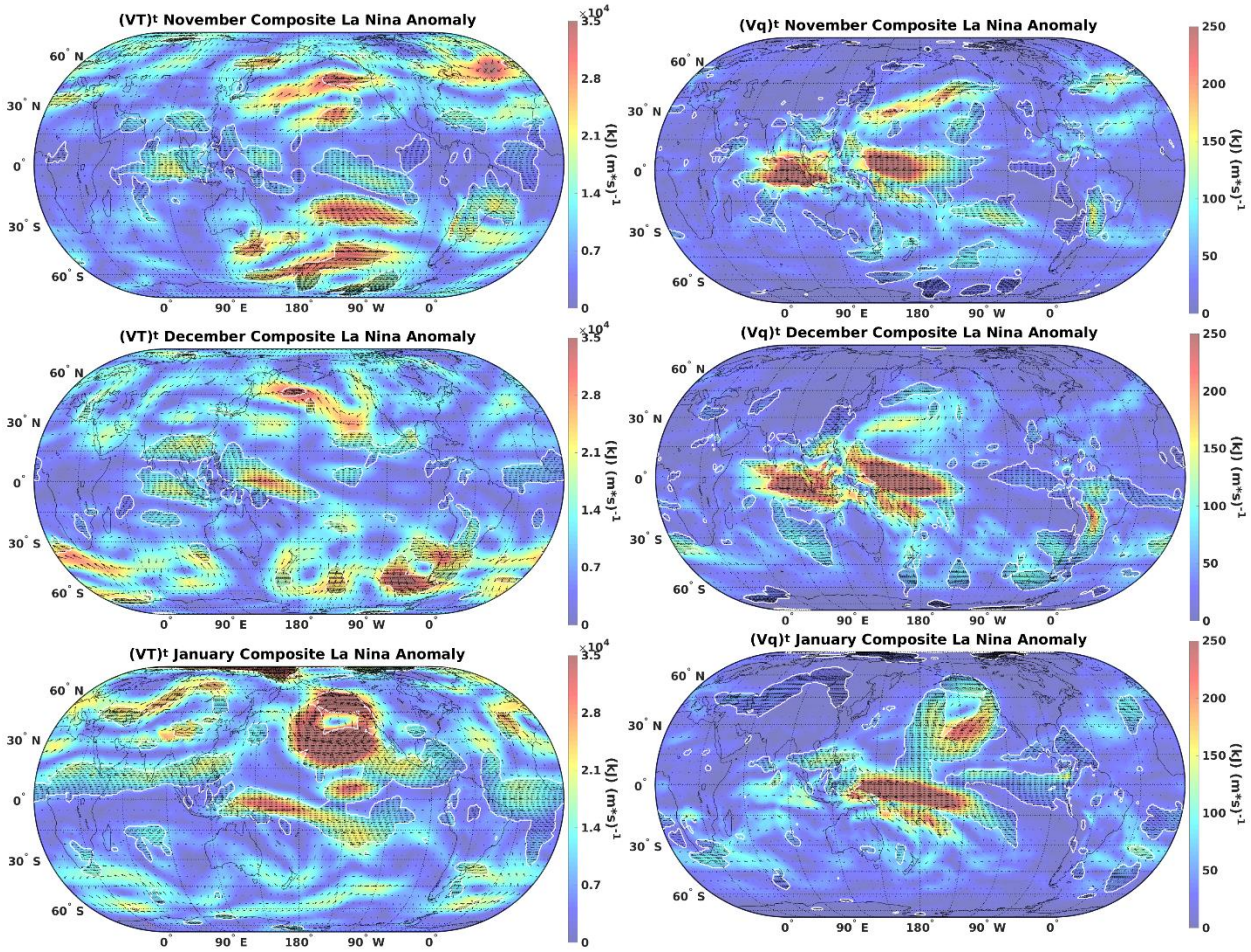

Figure 6. Monthly tropospheric sensible (left) and latent (right) heat flux anomalies for NDJ during composite of all thirteen La Niña events occurring between 1979 and 2016 (Table 3). Color shading represents vector magnitude (kJ m^{-1} s^{-1}), dashed contour and stippling represents significance ($p < 0.05$).

Weak La Niña Composite

Composite analyses of the spatial distribution of anomalous sensible and latent heat fluxes during the three weakest La Niña events (1983/84, 2005/06, 2008/09; Table 3) are shown in Figure 7. In the North Atlantic Ocean an AAC was centered near 60ºN 30ºW and an ACC was centered near 30ºN 40ºW resulting in a north-south dipole consistent with a predominantly negative NAO pattern during November. The configuration of the AAC and ACC dipole shifted south away from the single-point correlation for the NAO pattern (65ºN 30ºW) to be centered

near 50ºN 35ºW and 25ºN 40ºW, respectively during December. Spatial patterns across Western Europe were still consistent with a predominantly negative NAO pattern, but the north-south dipole pattern reversed during January to be consistent with a predominantly positive NAO pattern (Figure 7). During January an ACC was centered near 70ºN 30ºW and an AAC was centered near 40ºN 40ºW, closer to the single-point correlation for the NAO pattern (65ºN 30ºW; Hurrell and Deser 2010). The seasonal evolution of the northern ACC indicated it was centered across the eastern United States (US; ~40ºN 80ºW) during November and shifted northeast during December to be centered near the single-point correlation of the NAO pattern during January (Figure 7). In the North Pacific Ocean an elongated ACC was centered near 40ºN 180ºW during November and a weaker ($< 4x10^4$ kJ m^{-1} s^{-1}) AAC was centered downstream near 35ºN 120ºW, which was not consistent with a predominant phase of the PNA pattern. During December three anomalous circulations were apparent across the Northeastern Pacific Ocean where an ACC was centered near 35ºN 170ºW and two AACs were centered near 65ºN 155ºW and 25ºN 115ºW. This tripole pattern was inconsistent with a predominant PNA phase during December, but during January a pair of simultaneously out-of-phase north-south dipoles consistent with a predominantly negative PNA pattern emerged. The western dipole had AAC and ACC centers near 40ºN 140ºW and 15ºN 150ºW respectively, but the eastern dipole was less defined with an AAC centered in the southwestern US and an elongated ACC extending from Alaska southeastwards to near Florida. During weak La Niña forcing a coherent spatial pattern ($p < 0.05$) connecting ENSO, PNA, and NAO regions was not apparent. However, spatially continuous pathways between the eastern coasts of Asia and NA connected with anomalous circulations across the Northern Atlantic and Pacific Oceans associated with NAO and PNA patterns during November and December. Therefore, results presented in Figure 7 suggested a

seasonal (NDJ) evolution from predominantly negative to positive NAO patterns and the emergence of a predominantly negative PNA pattern during Januarys of weak La Niña forcing.

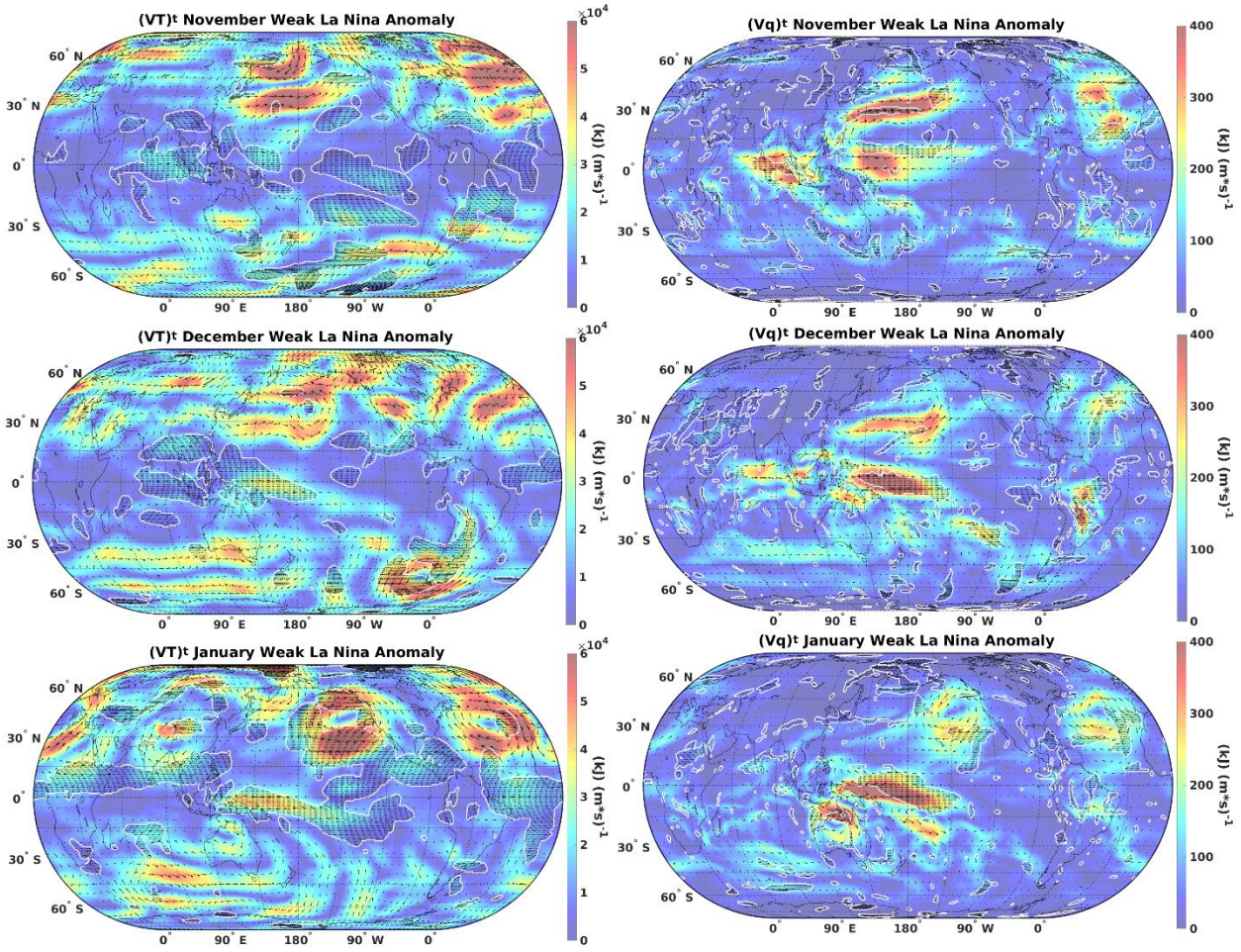

Figure 7. Monthly tropospheric sensible (left) and latent (right) heat flux anomalies for NDJ during composite of three weakest La Niña events (1983/84, 2005/06, 2008/09) occurring between 1979 and 2016. Color shading represents vector magnitude (kJ m^{-1} s^{-1}), dashed contour and stippling represents significance ($p < 0.05$).

Strong La Niña Composite

Composite analyses of anomalous sensible and latent heat fluxes during the three strongest La Niña events (1988/89, 1999/00, and 2010/11; Table 3) are shown in Figure 8. Across the northern extratropical Atlantic Ocean an AAC was centered near 60ºN 30ºW and an ACC was centered near 35ºN 45ºW during November, which is an anomalous circulation dipole

consistent with a predominantly negative phase of the NAO pattern. During December the Northern Atlantic Ocean dipole feature shifted west to have AAC and ACC centers near 60ºN 40ºW and 40ºN 65ºW, respectively. A simultaneous out-of-phase dipole feature analogous to the PNA pattern was apparent across western Europe with ACC and AAC centers near 55ºN 25ºE and 40ºN 50ºE, respectively. Such a configuration of anomalous circulations was consistent with a predominantly negative NAO pattern during Decembers of weak La Niña forcing. The anomalous dipole feature across the Northern Atlantic Ocean shifted eastwards during January to have AAC and ACC centers near 55ºN 5ºW and 35ºN 15ºW respectively, which was consistent with a predominantly negative NAO pattern. Despite changes in the structure and position of each anomalous circulation, a north-south dipole consistent with a predominantly negative NAO pattern persisted through the NDJ period when strong La Niña forcing was present.

Across the northeastern Pacific Ocean a north-south dipole of ACC and AAC features was centered near 55ºN 140ºW and 35ºN 115ºW, respectively. This was generally consistent with the positive phase of the PNA pattern during November, but a pair of simultaneous out-of-phase north-south dipole features were not apparent. Such a spatial pattern was also lacking during December when a strong ($> 6x10^4$ kJ m^{-1} s^{-1}) AAC had two centers across the Northern Pacific Ocean near 60ºN 165ºE and 45ºN 150ºW, but no predominant phase of the PNA pattern was evident. However, a pair of simultaneous out-of-phase north-south dipole features was apparent during January of strong La Niña forcing. The western dipole had AAC and ACC features centered near 40ºN 155ºW and 15ºN 150ºW, respectively and the eastern dipole had ACC and AAC features centered near 60ºN 125ºW and 30ºN 95ºW respectively that was consistent with a predominantly negative PNA pattern. Therefore, strong La Niña events resulted in a single dipole feature resembling a predominantly positive PNA pattern during November

that evolved seasonally into a pair of simultaneous out-of-phase north-south dipole features consistent with a canonical negative PNA pattern during January.

Also of importance to this work were spatially continuous regions of anomalous sensible or latent heat fluxes connecting ENSO, PNA, and NAO regions during strong La Niña events. Analyses of anomalous tropospheric latent heat fluxes showed a spatially continuous pathway connecting the Niño 3.4 region (170ºW to 120ºW, 5ºS to 5ºN) with the single-point correlation for the PNA pattern (45ºN 165ºW) during January, but scientific significance ($p < 0.05$) was inconsistent. Analyses of anomalous tropospheric sensible heat fluxes showed the same pathway connecting ENSO and PNA regions along and just east of the International Date Line and had a continuous area of scientific significance during January. Similar pathways connecting ENSO with NAO or PNA with NAO regions were less clear and no continuous area of significant differences were apparent. Overall, composite analyses of strong La Niña events suggested a persistently negative NAO pattern during the NDJ period whereas a transition from positive to negative phases of the PNA pattern was apparent during the NDJ seasonal evolution.

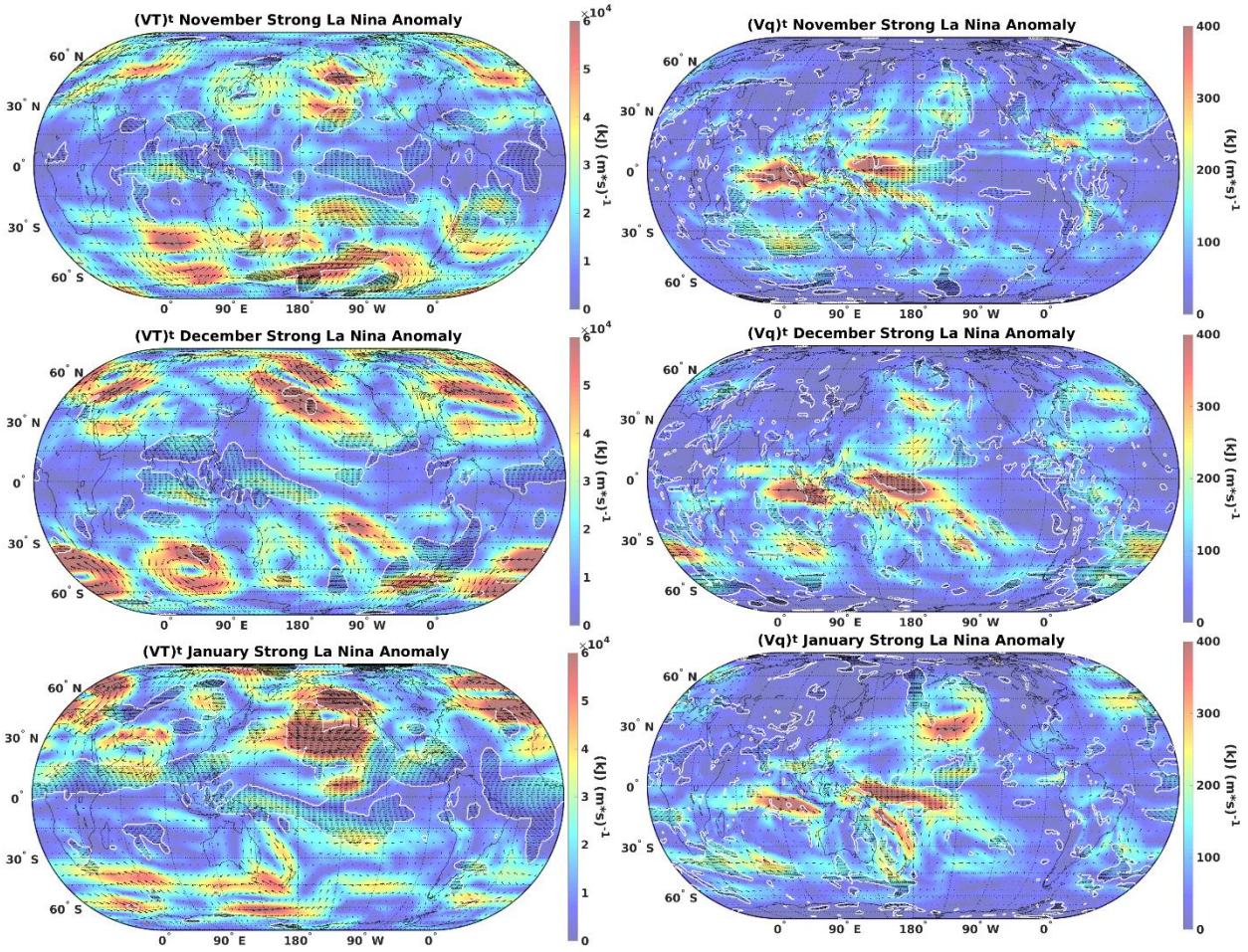

Figure 8. Monthly tropospheric sensible (left) and latent (right) heat flux anomalies for NDJ during composite of three strongest La Niña events (1988/89, 1999/00, 2010/11) occurring between 1979 and 2016. Color shading represents vector magnitude (kJ m^{-1} s^{-1}), dashed contour and stippling represents significance ($p < 0.05$).

Case Study of Three Strongest La Niña Events

The monthly (NDJ) seasonal evolution of sensible and latent heat flux anomalies for each of the three strong La Niña events are included in Figure 9 and Figure 10 respectively to assess the interrelationship between La Niña, PNA, and NAO patterns during individual La Niña events of similar magnitude. Since the magnitude of each of the three strongest La Niña events were similar ($-1.5 \leq ONI \leq -1.8$; Table 3), differences in the spatial distributions of anomalous flux patterns or positions of anomalous circulations should be attributed to differences in the spatial

distribution of SST anomalies, natural variability, climate change or alternative modes of climate forcing, that were not addressed in this work. Differences in the approximate positions of anomalous anticyclonic circulation (AAC) features north of 15ºN for five longitudinal sectors are summarized in Table 4. A similar table for anomalous latent heat flux circulations wasn't included given poorly defined circulations at high latitude or continental locations given small specific humidity values (Figure 10; e.g. Newman et al. 2012). The coordinates summarized in table 2 were subjectively analyzed and were subject to +/- 5º error in latitude or longitude. During November 1999 (Nov99), December 2010 (Dec10), and January 2011 (Jan11) just four distinct AACs were apparent such that two of the longitudinal sectors were merged.

Across the northern Atlantic Ocean AACs near the single-point correlation for the NAO pattern had corresponding ACCs resulting in a north-south dipole consistent with a predominantly negative NAO pattern during five of the nine months examined. The four remaining months had dipole features that were not consistent with a predominant phase of the NAO pattern. Across the northeastern Pacific Ocean AACs were centered within 10 and 25 degrees of latitude and longitude from the single-point correlation for the PNA pattern (45ºN 165ºW) respectively consistent with a weakened Aleutian low. ACCs of lesser magnitude were found to the south of each AAC across the eastern Pacific Ocean during all months examined resulting in a north-south dipole of anomalous circulations. The position of the north-south dipole varied from event-to-event and month-to-month such that a predominant phase of the PNA pattern was difficult to assess, especially given the general lack of a simultaneous out-of-phase dipole across NA for each month examined. However, four of the nine months examined had substantially ($\geq 7x10^4$ kJ m^{-1} s^{-1}) enhanced onshore fluxes of sensible heat along portions of the west coast of the US consistent with a positive PNA pattern. Similar spatial patterns were

apparent for analyses of latent heat flux (Figure 10) such that AACs were predominant across northern Pacific and Atlantic Ocean basins. While position and intensity of the centers of these anomalous anticyclonic circulations varied their presence generally confirmed an in-phase relationship of ENSO, PNA, and NAO patterns during the NDJ period of strong La Niña events.

Table 4. Summary of positions of anomalous anticyclonic sensible heat flux circulations for five hemispheric sectors during each strong La Niña event (Table 3).

		Anomalous Anticyclonic Circulation Centers Poleward of 15ºN				
Year	**Month**	**Asia**	**West Pacific**	**East Pacific**	**North America**	**Atlantic**
1988/89	Nov	55ºN 95ºE	20ºN 160ºE	35ºN 155ºW	30ºN 60ºW	60ºN 10ºW
	Dec	60ºN 110ºE	25ºN 170ºE	45ºN 140ºW	30ºN 90ºW	50ºN 10ºW
	Jan	20ºN 75ºE	40ºN 140ºE	40ºN 155ºW	35ºN 85ºW	50ºN 10ºE
1999/00	Nov	30ºN 30ºE	40ºN 175ºW		40ºN 105ºW	50ºN 20ºW
	Dec	40ºN 55ºE	60ºN 160ºE	40ºN 140ºW	35ºN 70ºW	40ºN 25ºW
	Jan	25ºN 65ºE	65ºN 120ºE	40ºN 165ºW	25ºN 115ºW	50ºN 30ºW
2010/11	Nov	45ºN 50ºE	20ºN 150ºE	45ºN 150ºW	30ºN 115ºW	65ºN 30ºW
	Dec	45ºN 55ºE	50ºN 180ºW		30ºN 110ºW	65ºN 45ºW
	Jan	60ºN 85ºE	70ºN 160ºW	40ºN 140ºW	60ºN 40ºW	

Potential connections between ENSO, PNA, and NAO regions were also assessed by spatially continuous regions of anomalous heat fluxes between the Niño 3.4 region (170ºW to 120ºW, 5ºS to 5ºN) and coordinates of single-point correlations for both PNA (45ºN 165ºW) and NAO (65ºN 30ºW) patterns. Januarys of each strong La Niña event had spatially continuous regions of substantially enhanced sensible (> $3x10^4$ kJ m^{-1} s^{-1}) and latent (> 150 kJ m^{-1} s^{-1}) heat fluxes connecting ENSO and PNA regions. A pathway connecting ENSO and NAO regions was not apparent from these analyses, but a connection between PNA with NAO regions was apparent during strong La Niña forcing. During each month (NDJ) of the 1988/89 La Niña event enhanced westerlies intersected the west coast of NA, traversed the width of NA, and connected with the western edge of the AAC centered across the Northern Atlantic Ocean associated with a weakened Icelandic low. During December and January of the 2010/11 La Niña event a similar

region of enhanced westerlies intersected the west coast of NA, traveled southeast across NA, and connected with the western edge of the ACC spanning the width of the Atlantic Ocean. This suggested two potential pathways connecting PNA and NAO regions: a high latitude pathway associated with an enhanced polar jet stream and a low latitude pathway associated with an enhanced subtropical jet stream. The 1999/2000 La Niña event has aspects of both high and low latitude pathways due to differences in the seasonal evolution of the anomalous circulations that suggested substantial event-to-event and month-to-month variability in potential pathways connecting ENSO, PNA, and NAO regions.

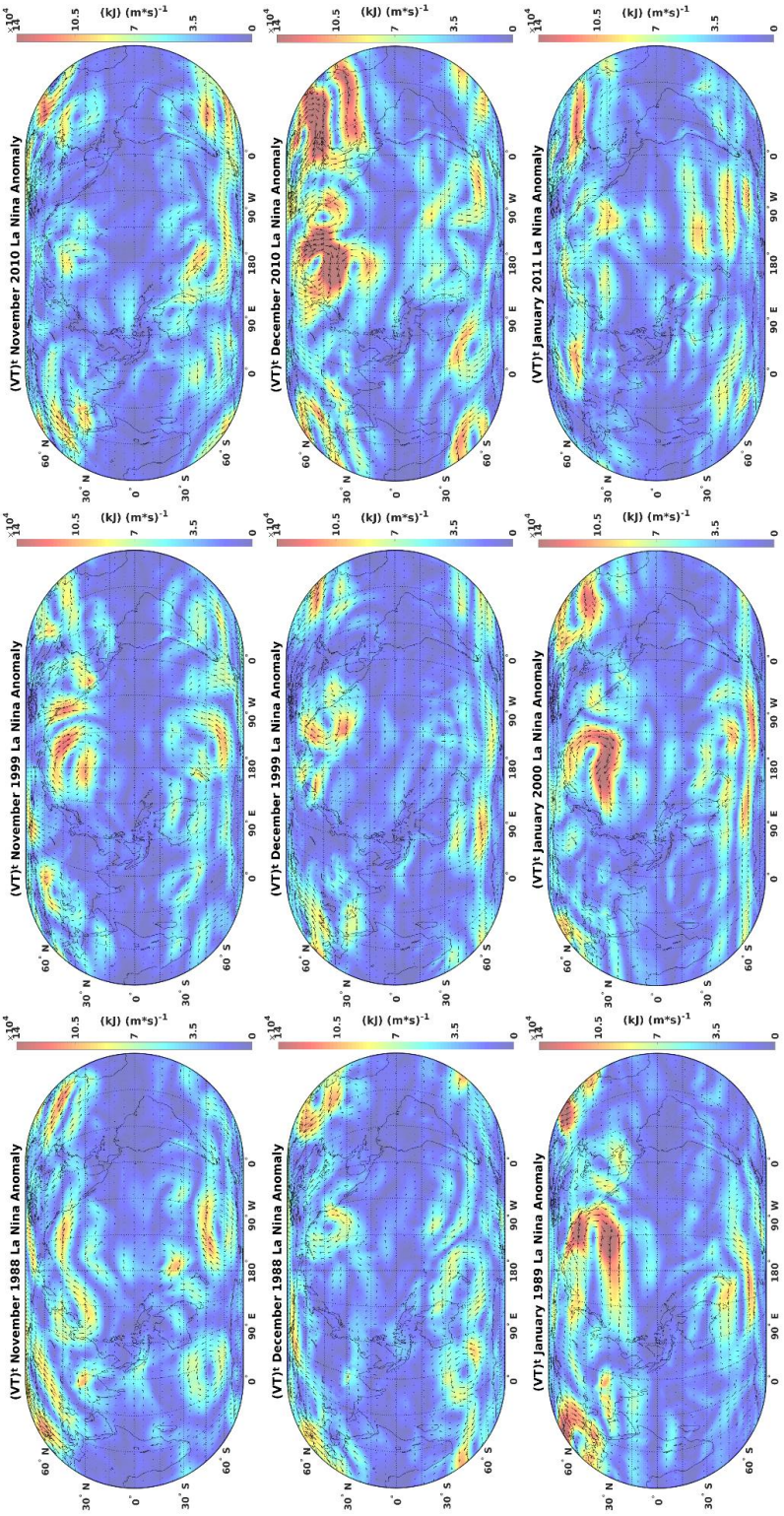

Figure 9. Monthly tropospheric sensible heat flux anomaly time-evaluation for NDJ during each of three strongest La Niña events (1988/89, 1999/00, 2010/11; Table 3) occurring between 1979 and 2016. Color shading represents vector magnitude (kJ m^{-1} s^{-1}).

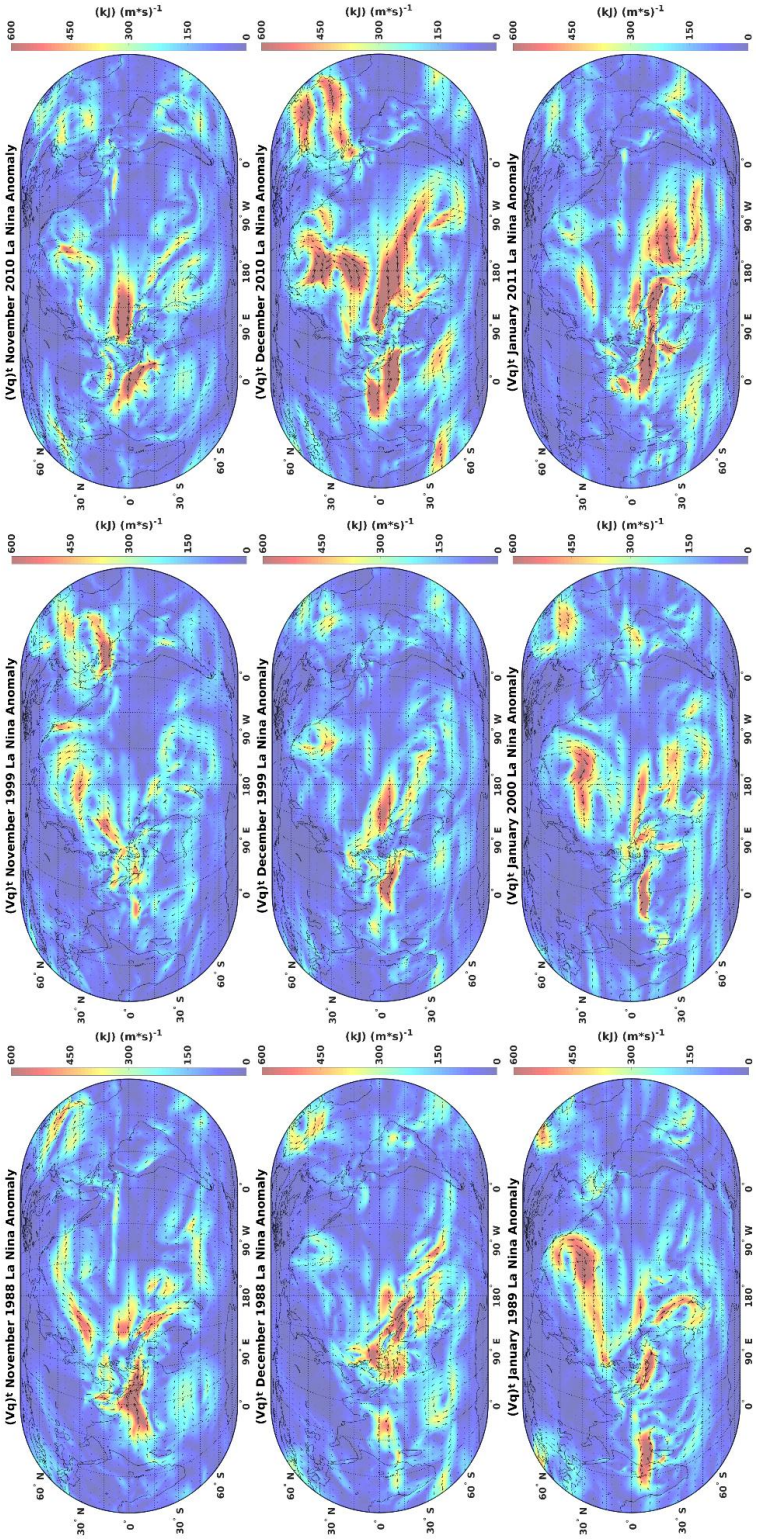

Figure 10. Monthly tropospheric latent heat flux anomaly time-evolution for NDJ during each of three strongest La Niña events (1988/89, 1999/00, 2010/11; Table 3) occurring between 1979 and 2016. Color shading represents vector magnitude (kJ m^{-1} s^{-1}).

Discussion

Composite analyses of twelve recorded La Niña events that occurred between January 1979 and June 2016 suggested the presence of an in-phase relationship between ENSO, PNA, and NAO patterns of climate variability within the NDJ period. Most studies to date have used linear techniques (e.g. regression or EOF) to identify canonical La Niña teleconnections assuming that La Niña is a mirror image of El Niño (Okumura and Deser 2010). Assuming a mirrored response, Meehl and Teng (2007) described general features of the observed La Niña teleconnection pattern as a significantly weakened Aleutian low (Iza et al. 2016), a trough over western NA, and anomalous anticyclonic circulation (AAC) across the southeastern US. Composite analyses of all twelve La Niña events (Figure 6) showed an anomalously weakened Aleutian low during December and a coherent spatial pattern ($p < 0.05$) consistent with a weakened circulation during January centered near 40ºN 150ºW indicating an important and not fully understood sub-seasonal dependency on the interrelationship between ENSO, PNA, and NAO teleconnections. The month-to-month dependency shown indicated seasonal averages that are typically used to assess circulation anomalies (e.g. Kim and Alexander 2015) may be of insufficient temporal resolution to fully understand ENSO's influence on distant teleconnection patterns.

During December a pair of simultaneous out-of-phase north-south anomalous circulation dipoles was consistent with a negative PNA pattern and the pair of anomalous dipoles intensified during January. Implications of a negative PNA pattern during January include a weakened subtropical jet stream and strengthened polar jet stream along the west coast of NA (Figure 6) that could result in drought conditions across the southwest US during La Niña (Hoell et al.

2014). Further downstream, an AAC was centered near 35ºN 110ºW in November and shifted southeast to be centered near 25ºN 105ºW during January that has been associated with drought across the southeastern US (e.g. Mo and Schemm 2008). During an ongoing La Niña event, comparison between the idealized seasonal evolution (Figure 6) and observations averaged over monthly periods would enable decision makers to assess the intensity of individual circulation anomalies that could indicate location of a potential drought across the PNA region. Brönnimann (2007) found a climatologically relevant link between ENSO and NAO regions such that La Niña forcing tends to result in a positive NAO pattern during late winter. However, composite analyses of all La Niña events showed a negative NAO pattern during November that became less clear during December and January (Figure 6). Implications of the pattern shown in Figure 6 include anomalous offshore flow across Western Europe consistent with precipitation deficits (Hoell et al. 2014) and onshore flow across northwestern Africa consistent with precipitation surplus (Nicholson and Selato 2000).

Previous literature indicated changes in ENSO event magnitude triggered changes to distant teleconnections including the PNA (Müller and Roeckner 2008) and NAO (Toniazzo and Scaife 2006) patterns. The current work indicated a predominantly negative NAO pattern during November (Figure 6) of all La Niña events and for the entire NDJ period of strong La Niña events (Figure 8) such that only weak La Niña events resulted in anomalous circulations consistent with a positive NAO during January (Figure 7). Iza et al. (2016) concluded that weak La Niña events were not appropriate to obtain the atmospheric teleconnection of La Niña such that the out-of-phase relationship proposed by Brönnimann (2007) would need to occur after January. Therefore, ENSO event magnitude influenced the NAO teleconnection more than PNA such that La Niña event magnitude is important to accurately anticipate climate impacts across

Western Europe. Across the North Pacific Ocean differences in La Niña event magnitude resulted in larger changes to anomalous circulation position rather than intensity. The spatial distribution of anomalous circulations was consistent with a negative PNA pattern given a strongly anomalous ($> 6x10^4$ kJ m^{-1} s^{-1}) AAC centered in the northeastern Pacific Ocean during January of both strong and weak La Niña events. This indicated an in-phase relationship between ENSO and PNA patterns existed during January regardless of La Niña event magnitude contrary to findings of Iza et al. (2016). However, differences in the centers of each respective anomalous circulation varied such that weak La Niña forcing resulted in anomalous circulations closer to the west coast of NA (Figure 7). The exact position of an AAC in this region has implications for positioning of associated precipitation deficits such that water resource managers along the west coast of NA should monitor the seasonal evolution of this AAC. Furthermore, positioning of this AAC feature influences the pathways connecting each teleconnection region identified in this work.

A spatially continuous and significant ($p < 0.05$) pathway connecting ENSO and PNA regions was found in composite analyses of all twelve La Niña events occurring between 1979 and 2016 (Section 3.1). This pathway was shown during December and January in analyses of latent heat flux and during January in analyses of sensible heat flux (Figure 6), which implied potential to quantify the influence of La Niña forcing on Aleutian low intensity during winter months. A similar pathway connecting ENSO and NAO regions was not obvious for any analyses, but a feature that may be consistent with the subtropical bridge mechanism (Graf and Zanchettin 2012) was shown connecting the Caribbean with the western Mediterranean Sea during November of strong La Niña events (Figure 8). Individual analyses of the three strongest La Niña events (Figure 9 and Figure 10) suggested two potential pathways between PNA and

NAO regions. The 1988/89 La Niña event favored a high-latitude pathway associated with an enhanced polar jet stream. The 2010/11 La Niña event favored a low-latitude pathway associated with an enhanced subtropical jet stream consistent with results of Graf and Zanchettin (2012). Alternatively, analyses of the 1999/2000 La Niña event indicated aspects of each potential pathway were present. Therefore, alternative forcing mechanisms independent of La Niña event magnitude resulted in a high and low-latitude pathways connecting PNA and NAO regions.

Conclusions

An objective of this work was to assess the predominant phase of PNA and NAO teleconnections for composite analyses of La Niña events occurring between 1979 and 2016. Composite analyses of all twelve La Niña events were first to show a month-to-month dependency of the interrelationship between ENSO, PNA, and NAO teleconnections (Figure 6) suggesting seasonally averaged analyses may be of insufficient temporal resolution to fully understand the atmospheric bridging phenomena. During January the Aleutian low weakened associated with a spatial distribution of anomalous circulations consistent with a negative PNA pattern that implied a meaningful weakening (strengthening) subtropical (polar) jet stream along the west coast of NA. Across southeastern NA an AAC consistent with drought in this region was apparent during January with differences in La Niña intensity changing the position of each anomalous circulation. Therefore, water resource managers could benefit from monthly analyses of anomalous circulation location to better anticipate location of potential drought across NA. Irrespective of La Niña event magnitude an in phase relationship between ENSO and NAO patterns was robust during November. Strong La Niña events maintained the in-phase relationship during December and January (Figure 8) whereas weak La Niña events reverted to

an out-of-phase relationship during January (Figure 7). However, anomalous offshore flow from the west coast of Europe was a common feature regardless of La Niña intensity that implied a precipitation deficit (surplus) across Western Europe (northwestern Africa). Therefore, differences in La Niña event magnitude is important for anticipating climate impacts across Western Europe and northern Africa.

Composite analyses of the three strongest La Niña events indicated a consistent in-phase relationship between ENSO and NAO throughout the NDJ period and between ENSO and PNA during December and January. However, individual analyses of each strong La Niña event (Figure 9 and Figure 10) indicated substantial event-to-event and month-to-month variability in the intensity and position of anomalous circulation centers that implied differences in the connection between each teleconnection region. A spatially continuous and significant ($p < 0.05$) pathway connecting the Niño 3.4 and PNA regions along and east of the International Date Line existed (Figure 6) implied potential to quantify the interaction between ENSO and PNA patterns. Spatially continuous pathways connecting PNA and NAO regions were proposed at high and low latitudes based off findings in Figure 9 and Figure 10 that was consistent with enhanced polar and subtropical jet streams, respectively. Therefore, monitoring the temporal evolution of anomalous circulations in tropospheric mean sensible and latent heat flux analyses at monthly resolution improved prediction of climate impacts across NA and Western Europe during future La Niña events, in near real-time. This work improved understanding of the interrelationship between ENSO, PNA, and NAO teleconnections and the potential for tropospheric pathways connecting each regional pattern that a necessary to understand impacts to PNA and NAO patterns associated with climate variability and change. In particular, the spatially continuous pathway connecting ENSO and PNA regions near the International Date Line has potential to

allow for quantification of the interrelationship between PNA and NAO patterns in near real time.

Acknowledgements

Appreciation is extended to coauthors and external evaluations of the article that greatly improved the quality of the work. This research did not receive any specific grant from funding agencies in the public, commercial, or not-for-profit sectors.

Literature Cited

An, S. I., Jin, F. F. 2004. Nonlinearity and asymmetry of ENSO. *Journal of Climate*, **17**(12): 2399-2412.

Barlow, M., Cullen, H., Lyon, B. 2002. Drought in central and southwest Asia: La Niña, the warm pool, and Indian Ocean precipitation. *Journal of Climate*, **15**(7): 697-700.

Boening, C., Willis, J. K., Landerer, F. W., Nerem, R. S., Fasullo, J. 2012. The 2011 La Niña: So strong, the oceans fell. *Geophysical Research Letters*, **39**(19).

Brönnimann, S. 2007. Impact of El Niño–Southern Oscillation on European climate. *Reviews of Geophysics*, **45**(3).

Cayan, D. R. 1992. Latent and sensible heat flux anomalies over the northern oceans: Driving the sea surface temperature. *Journal of Physical Oceanography*, **22**(8): 859-881.

Davis, R. E. 1976. Predictability of sea surface temperature and sea level pressure anomalies over the North Pacific Ocean. *Journal of Physical Oceanography*, **6**(3): 249-266.

Dee, D. P., Uppala, S. M., Simmons, A. J., Berrisford, P., Poli, P., Kobayashi, S., Andrae, U., Balmaseda, M. A., Balsamo, G., Bauer, P., Bechtold, P. 2011. The ERA-Interim reanalysis: Configuration and performance of the data assimilation system. *Quarterly Journal of the Royal Meteorological Society*, **137**(656): 553-597.

Dessler, A. E., Schoeberl, M. R., Wang, T., Davis, S. M., Rosenlof, K. H., Vernier, J.P. 2014. Variations of stratospheric water vapor over the past three decades. *Journal of Geophysical Research: Atmospheres*, **119**(22).

Dettinger, M. D., Cayan, D. R., Meyer, M. K., Jeton, A. E. 2004. Simulated hydrologic responses to climate variations and change in the Merced, Carson, and American River basins, Sierra Nevada, California, 1900–2099. *Climatic Change*, **62**(1-3): 283-317.

European Centre for Medium-Range Weather Forecasts. 2009, updated monthly. ERA-Interim Project. Research Data Archive at the National Center for Atmospheric Research, Computational and Information Systems Laboratory. https://doi.org/10.5065/D6CR5RD9. Accessed† 10 06 2016.

Graf, H. F., Zanchettin, D. 2012. Central Pacific El Niño, the "subtropical bridge," and Eurasian climate. *Journal of Geophysical Research: Atmospheres*, **117**(D1).

Guan, B., Waliser, D. E., Molotch, N. P., Fetzer, E. J., Neiman, P. J. 2012. Does the Madden–Julian oscillation influence wintertime atmospheric rivers and snowpack in the Sierra Nevada? *Monthly Weather Review*, **140**(2): 325-342.

Guan, B., Molotch, N. P., Waliser, D. E., Fetzer, E. J., Neiman, P. J. 2013. The 2010/2011 snow season in California's Sierra Nevada: Role of atmospheric rivers and modes of large-scale variability. *Water Resources Research*, **49**(10).6731-6743.

Harrison, D. E., Chiodi, A. M. 2017. Comments on "Characterizing ENSO Coupled Variability and Its Impact on North American Seasonal Precipitation and Temperature". *Journal of Climate*, **30**(1): 427-436.

Hoell, A., Funk, C., Barlow, M. 2014. The regional forcing of Northern hemisphere drought during recent warm tropical west Pacific Ocean La Niña events. *Climate Dynamics*, **42**(11-12): 3289-3311.

Hurrell, J. W., Deser, C. 2010. North Atlantic climate variability: the role of the North Atlantic Oscillation. *Journal of Marine Systems*, **79**(3): 231-244.

Iza, M., Calvo, N., Manzini, E. 2016. The Stratospheric Pathway of La Niña. *Journal of Climate*, **29**(24): 8899-8914.

Kang, I. S., Kug, J. S. 2002. El Niño and La Niña sea surface temperature anomalies: Asymmetry characteristics associated with their wind stress anomalies. *Journal of Geophysical Research: Atmospheres*, **107**(D19).

Kirtman, B. P., Min, D., Infanti, J. M., Kinter III, J. L., Paolino, D. A., Zhang, Q., Van Den Dool, H., Saha, S., Mendez, M. P., Becker, E., Peng, P. 2014. The North American multimodel ensemble: phase-1 seasonal-to-interannual prediction; phase-2 toward developing intraseasonal prediction. *Bulletin of the American Meteorological Society*, **95**(4): 585-601.

Kumar, K. K., Rajagopalan, B., Hoerling, M., Bates, G., Cane, M. 2006. Unraveling the mystery of Indian monsoon failure during El Niño. *Science*, **314**(5796): 115-119.

Larkin, N. K., Harrison, D. E. 2005. Global seasonal temperature and precipitation anomalies during El Niño autumn and winter. *Geophysical Research Letters*, **32**(16).

Leathers, D. J., Yarnal, B., Palecki, M. A. 1991. The Pacific/North American teleconnection pattern and United States climate. Part I: Regional temperature and precipitation associations. *Journal of Climate*, **4**(5): 517-528.

Lorenz, C., Kunstmann, H. 2012. The hydrological cycle in three state-of-the-art reanalyses: Intercomparison and performance analysis. *Journal of Hydrometeorology*, **13**(5): 1397-1420.

Lyon, B., DeWitt, D.G. 2012. A recent and abrupt decline in the East African long rains. *Geophysical Research Letters*, **39**(2).

Meehl, G. A., Teng, H. 2007. Multi-model changes in El Niño teleconnections over North America in a future warmer climate. *Climate Dynamics*, **29**(7-8): 779-790.

Mo, K. C., Schemm, J. E. 2008. Relationships between ENSO and drought over the southeastern United States. *Geophysical Research Letters*, **35**(15).

Müller, W. A., Roeckner, E. 2008. ENSO teleconnections in projections of future climate in ECHAM5/MPI-OM. *Climate Dynamics*, **31**(5): 533-549.

Newman, M., Kiladis, G. N., Weickmann, K. M., Ralph, F. M., Sardeshmukh, P.D. 2012. Relative contributions of synoptic and low-frequency eddies to time-mean atmospheric moisture transport, including the role of atmospheric rivers. *Journal of Climate*, **25**(21): 7341-7361.

Nicholson, S. E., Selato, J. C. 2000. The influence of La Niña on African rainfall. *International Journal of Climatology*, **20**(14): 1761-1776.

Okumura, Y. M., Deser, C. 2010. Asymmetry in the duration of El Niño and La Niña. *Journal of Climate*, **23**(21): 5826-5843.

Peixoto, J. P., Oort, A. H. 1992. Physics of Climate.

Rodionov, S. N., Bond, N. A., Overland, J. E. 2007. The Aleutian Low, storm tracks, and winter climate variability in the Bering Sea. *Deep Sea Research Part II: Topical Studies in Oceanography*, **54**(23): 2560-2577.

Ropelewski, C. F., Halpert, M. S. 1986. North American precipitation and temperature patterns associated with the El Niño/Southern Oscillation (ENSO). *Monthly Weather Review*, **114**(12): 2352-2362.

Serreze, M. C., Carse, F., Barry, R. G., Rogers, J.C. 1997. Icelandic low cyclone activity: Climatological features, linkages with the NAO, and relationships with recent changes in the Northern Hemisphere circulation. *Journal of Climate*, **10**(3): 453-464.

Shaw, T. A., Pauluis, O. 2012. Tropical and subtropical meridional latent heat transports by disturbances to the zonal mean and their role in the general circulation. *Journal of the Atmospheric Sciences*, **69**(6): 1872-1889.

Simmons, A., Uppala, S., Dee, D., Kobayashi, S. 2007. ERA-Interim: New ECMWF reanalysis products from 1989 onwards. *ECMWF newsletter*, **110**(110): 25-35.

Skerlak, B., Sprenger, M., Wernli, H. 2014. A global climatology of stratosphere-troposphere exchange using the ERA-Interim data set from 1979 to 2011. *Atmospheric Chemistry and Physics*, **14**(2): 913.

Toniazzo, T., Scaife, A. A. 2006. The influence of ENSO on winter North Atlantic climate. *Geophysical Research Letters*, **33**(24).

Trenberth, K. E. 1991. Climate diagnostics from global analyses: Conservation of mass in ECMWF analyses. *Journal of Climate*, **4**(7): 707-722.

Trenberth, K. E., Hurrell, J. W. 1994. Decadal atmosphere-ocean variations in the Pacific. *Climate Dynamics*, **9**(6): 303-319.

Trenberth, K. E., Branstator, G. W., Karoly, D., Kumar, A., Lau, N. C., Ropelewski, C. 1998. Progress during TOGA in understanding and modeling global teleconnections associated with tropical sea surface temperatures. *Journal of Geophysical Research*: *Oceans*, **103**(C7): 14291-14324.

Von Storch, H. 1999. Misuses of statistical analysis in climate research. *Analysis of Climate Variability:* 11-26. Springer Berlin Heidelberg

Wallace, J. M., Gutzler, D. S. 1981. Teleconnections in the geopotential height field during the Northern Hemisphere winter. *Monthly Weather Review*, **109**(4): 784-812.

Wallace, J. M., Smith, C., Jiang, Q. 1990. Spatial patterns of atmosphere-ocean interaction in the northern winter. *Journal of Climate*, **3**(9): 990-998.

Wilks, D.S. 2011. Statistical methods in the atmospheric sciences (Vol. 100). Academic press.

Wise, E. K., Wrzesien, M. L., Dannenberg, M. P., McGinnis, D. L. 2015. Cool-season precipitation patterns associated with teleconnection interactions in the United States. *Journal of Applied Meteorology and Climatology*, **54**(2): 494-505.

Wu, A., Hsieh, W.W. 2004. The nonlinear Northern Hemisphere winter atmospheric response to ENSO. *Geophysical Research Letters*, **31**(2).

Yu, J. Y., Kim, S. T. 2013. Identifying the types of major El Niño events since 1870. *International Journal of Climatology*, **33**(8): 2105-2112.

Zhang, T., Perlwitz, J., Hoerling, M. P. 2014. What is responsible for the strong observed asymmetry in teleconnections between El Niño and La Niña? *Geophysical Research Letters*, **41**(3): 1019-1025.

CHAPTER IV

SYMMETRIC AND ASYMMETRIC COMPONENTS OF ANOMALOUS TROPOSPHERIC-MEAN HORIZONTAL FLUXES OF LATENT AND SENSIBLE HEAT ASSOCIATED WITH ENSO EVENTS OF VARIABLE MAGNITUDE

In Submission:

Kutta, E. J., Hubbart, J. A., Svoma, B. M., Eichler, T., Lupo, A. 2017. Symmetric and Asymmetric Components of Anomalous Tropospheric-Mean Horizontal Fluxes of Latent and Sensible Heat Associated with ENSO Events of Variable Magnitude. *Atmospheric Research* x:xx.

Introduction

Background

On inter-annual time scales, the El Niño-Southern Oscillation (ENSO) represents the most important coupled ocean-atmosphere climate phenomena (Wolter and Timlin 2011). ENSO is characterized by an oscillation of sea surface temperature (SST) anomalies within the tropical Pacific Ocean, most commonly the Niño 3.4 region (5ºN – 5ºS, 170ºW – 120ºW; Harrison and Chiodi 2017). Tropical SST anomalies were previously shown to influence surface fluxes of moisture, heat, and momentum that adjusted the tropical atmospheric circulation forcing large-scale atmospheric Rossby waves in preferred locations that propagated into extratropical latitudes (Trenberth et al. 1998). Thus, anomalous tropospheric heating associated with ENSO forces extratropical impacts through what is commonly referred to as the atmospheric bridge phenomena (e.g. Lau and Nath 1996; Alexander et al. 2002). The atmospheric bridge refers to the atmosphere's ability to link two distant regions of anomalous sea surface temperatures

through fluxes of energy, mass, and momentum (Lau and Nath 1996). Mechanistically, atmospheric bridging can be thought of as anomalous poleward heat fluxes associated with ENSO's tropical heating patterns. These fluxes are necessary to maintain climate equilibrium (e.g. Trenberth and Stepaniak 2003). Therefore, ENSO disturbs the atmospheric circulation through anomalous heat fluxes of the tropical atmosphere resulting in a cascade of seasonally variable extratropical climate impacts that project onto multiple patterns of climate variability (Liu and Alexander 2007).

ENSO's primary extratropical effect is to alter the predictability of mid-latitude climate phenomena such as the North Atlantic Oscillation (NAO) and Pacific North American (PNA) patterns (e.g. Straus and Shukla 2002; Hurrell and Deser 2010). The NAO and PNA patterns originate from mid-latitude dynamics separate from the ENSO phenomena (e.g. Straus and Shukla 2002; Hurrell and Deser 2010) and each represent dominant patterns of Northern Hemisphere mid-latitude climate variability (e.g. Hurrell and Deser 2010; Franzke et al. 2011). Straus and Shukla (2002) explicated that the presence of ENSO forcing skewed the probability density function of positive or negative phases of the PNA pattern such that a linear relationship between ENSO and PNA patterns is commonly observed. A similar, climatologically relevant, link between ENSO and NAO patterns of climate variability has also been proposed by Brönnimann (2007). Hurrell and Deser (2010) described NAO and PNA patterns as north-south dipoles (NSDs) characterized by simultaneously out of phase height anomalies between temperate and high latitude regions. The NAO pattern has a single NSD located over the North Atlantic Ocean and the PNA pattern has a pair of simultaneously out of phase NSDs across the northeastern Pacific Ocean and North America. Representative locations (one-point correlations) for PNA (45ºN 165ºW) and NAO (65ºN 30ºW) patterns (Hurrell and Deser 2010) were located

east of the climatologic position of the Aleutian (52ºN 175ºE; Serreze et al. 1997) and Icelandic patterns (62ºN 35ºW; Rodionov et al. 2007). Both NAO and PNA patterns have regional climate impacts including precipitation and temperature anomalies across North America and Europe (e.g. Leathers et al. 1991; Leathers and Palecki 1992; Rodwell et al. 1999; Seager et al. 2010). Given the important climate impacts associated with each pattern there is a need to better understand the spatial and temporal variability of the influence ENSO forcing has on PNA and NAO patterns.

Both ENSO forcing and the subsequent atmospheric response have been shown to have symmetric and asymmetric components of similar magnitude such that each produced climatologically relevant extratropical impacts (Zhang et al. 2014). The simultaneous existence of both large symmetric and asymmetric components suggests that traditional linear techniques (e.g. regression or empirical orthogonal function analyses) are insufficient to reveal all climatologically relevant impacts associated with the ENSO phenomena (Okumura and Deser 2010). Furthermore, SST anomalies associated with the ENSO phenomena have been characterized by their asymmetric magnitude (e.g. An and Jin 2004) and duration (Okumura and Deser 2010) resulting in symmetric and asymmetric atmospheric responses that are of the same order of magnitude (e.g. Zhang et al. 2014). The most common way to analyze the symmetric and asymmetric atmospheric responses to ENSO forcing is through composite analyses of 500 mb height, surface temperature, and precipitation anomalies (Zhang et al. 2014). However, atmospheric and oceanic media must transport heat poleward to maintain climate equilibrium such that the atmospheric response to ENSO events may be best shown using atmospheric reanalysis products to quantify anomalous atmospheric fluxes of sensible and latent heat (Kim and Alexander 2015). Use of state-of-the-art atmospheric reanalysis output is critical to advance

understanding of a suite of hydrometeorological research topics including the atmospheric response to ENSO forcing (Lorenz and Kunstmann 2012). Large quantities of historic observations from a variety of observation platforms are processed using advanced data assimilation techniques (4D-Var; Dee et al. 2011) to provide the most precise reconstruction of atmospheric parameters over a long period of record. Quantifying symmetric and asymmetric components of anomalous atmospheric heat fluxes using atmospheric reanalysis output will clarify spatial patterns of the atmospheric bridge phenomena to better understand the cascade extratropical climate impacts (ENSO; Alexander et al. 2002).

This cascade of extratropical impacts are driven by anomalous upward fluxes of heat from the Pacific Ocean into the troposphere (Peixoto and Oort 1992), but anomalous horizontal heat fluxes connecting the tropical Pacific Ocean with extratropical latitudes have not been quantified nor has the symmetric or asymmetric components been assessed. Therefore, the overarching objective of this work was to use the ERA-Interim atmospheric reanalysis project (ERA-I; Dee et al. 2011) data output to quantify symmetric and asymmetric components of the atmospheric response to ENSO forcing through horizontal, tropospheric-mean analyses of latent and sensible heat flux anomalies. Sub-objectives included, a) assess symmetry of anomalous fluxes of sensible and latent heat and whether spatial patterns in anomalous fluxes are consistent with PNA and NAO teleconnections, b) assess spatially continuous connections between tropical heat sources and PNA and NAO regions, c) assess the influence of ENSO forcing magnitude on the magnitude and symmetry of the atmospheric response. Quantifying anomalous fluxes of tropospheric heat will identify the favored phase of either PNA or NAO patterns during NDJ months associated with ENSO events of various magnitudes enhancing predictability of climate impacts across North America and Western Europe.

Materials and Methods

ENSO Events

Each El Niño and La Niña event occurring since 1950 has been documented by the Climate Prediction Center (CPC; Kirtman et al. 2014) using the Oceanic Niño Index (ONI; Yu and Kim 2013). The ONI is quantified by calculating SST anomalies within the Niño 3.4 region (170ºW to 120ºW, 5ºS to 5ºN) averaged over three consecutive monthly periods. Harrison and Chiodi (2017) described the current operational definition of an El Niño (La Niña) event as five or more consecutive ONI values greater (less) than or equal to 0.5ºC (-0.5ºC). Using this definition, thirteen El Niño and nine La Niña events were identified over the period of record for the current work (January 1979 through June 2016). However, asymmetries in the SST anomaly magnitude (e.g. An and Jin 2004) and duration are associated with ENSO events such that La Niña events are characterized by smaller SST anomalies that persist for a longer period of time (e.g. Okumura and Deser 2010). This asymmetry suggests that criteria for La Niña events should be relaxed to have a more equal number of El Niño and La Niña events. Relaxing the persistence of negative SST anomalies from five to four consecutive tri-monthly averages identified three additional La Niña events such that samples sizes of El Niño (n = 13) and La Niña (n = 12) events were consistent with an oscillation from one phase to the other. All El Niño and La Niña events that occurred during the period of record were summarized in Tables 1 and 2, respectively. The January 1979 through June 2016 period of record was chosen given temporal limitations of ERA-I and because June 2016 represented the end of the strong 2015-2016 El Niño event.

Table 5. Summary of all thirteen El Niño events and twelve La Niña events occurring between 1979 and 2016 including maximum and minimum ONI values, each tri-monthly period when maximum or minimum ONI values occurred, and categorization of each ENSO event.

El Niño Events			**La Niña Events**		
Years	**Max ONI**	**Category**	**Years**	**Min ONI**	**Category**
1979-80	0.6	**weak**	*1983-84*	-0.8	**weak**
1982-83	2.1	**strong**	*1984-85*	-1.1	moderate
1986-87	1.2	moderate	*1988-89*	-1.8	**strong**
1987-88	1.6	moderate	*1995-96*	-1.0	moderate
1991-92	1.6	moderate	*1998-99*	-1.4	moderate
1994-95	1.0	moderate	*1999-00*	-1.6	**strong**
1997-98	2.3	**strong**	*2000-01*	-0.8	moderate
2002-03	1.2	moderate	*2005-06*	-0.7	**weak**
2004-05	0.7	**weak**	*2007-08*	-1.4	moderate
2006-07	0.9	moderate	*2008-09*	-0.7	**weak**
2009-10	1.3	moderate	*2010-11*	-1.5	**strong**
2014-15	0.6	**weak**	*2011-12*	-1.0	moderate
2015-16	2.3	**strong**			

Max ONI = Maximum Oceanic Niño Index, Min ONI = Minimum Oceanic Niño Index

The atmospheric response to ENSO forcing will be quantified using output from the composited during ENSO events occurring between January 1979 and June 2016. Composite analyses are a common method for showing atmospheric anomalies associated with ENSO forcing of variable magnitudes (e.g. Müller and Roeckner 2008) and season (e.g. Fogt and Bromwich 2006). Therefore, each ENSO event was categorized into weak, moderate, or strong categories based on the magnitude of maximum or minimum SST anomalies (Tables 1 and 2). Weak ENSO events were identified as the three smallest maximum (minimum) SST anomalies, strong ENSO events were identified as the three largest maximum (minimum) SST anomalies, and remaining ENSO events were categorized as moderate El Niño (La Niña) events. The most common occurrence of maximum or minimum tri-monthly mean SST forcing associated with ENSO events during this period of record was the November, December, January (NDJ) period (bolded; Tables 1 and 2). Nine of the thirteen El Niño events and eight of the twelve La Niña

events peaked during NDJ and for this reason NDJ was the tri-monthly period analyzed in this work. Therefore, the NDJ period was chosen for this work given maximum SSTA magnitude and variance during December (Okumura and Deser 2010). All analyses will be performed at the global scale as recommended by Trenberth and Caron (2000), but results and discussion will be focused on the atmospheric response across the northern Pacific and Atlantic Oceans.

Reanalysis Data Used

The ERA-I data set was produced at high spatial (~0.7º latitude/longitude) and temporal (6-hourly analyses) resolution over a global domain by the European Centre for Medium-Range Weather Forecasts (Dee et al. 2011) and has been shown to match with a variety of observations better than other atmospheric reanalyses (Fu et al. 2016). The subset of ERA-I output utilized for the current work included six-hourly model analyses of specific humidity (q), temperature (T), and zonal (u) and meridional (v) components of wind to allow for direct calculation of horizontal fluxes of sensible and latent heat. Data was acquired on original model levels that were defined using an eta vertical coordinate system characterized by pressure coordinates in the upper atmosphere, hybrid pressure-sigma coordinates at mid to low levels, and terrain-following sigma coordinates at the lowest models levels and the model surface (Simmons et al. 2007). Pressure in the eta coordinate system is a function of surface pressure (p_s) and a pair of time-independent spatially invariant coefficients denoted by a and b (Eq. 1) that vary in vertical, but not horizontal dimensions.

$$p_k(\lambda, \varphi, t) = a_k + b_k p_s(\lambda, \varphi, t) \quad \text{(Eq. 1)}$$

Here k is a generalized vertical index for each of the 60 vertical model levels, λ represents longitude, φ represents latitude, t represents time, and p_s represents surface pressure. Only the lowest 30 model levels were considered given greater vertical resolution, uncertainties regarding stratosphere-troposphere transport (Skerlak et al. 2014), and the lack of moisture above the 30th model level (Dessler et al. 2014). Assuming a standard surface pressure of 10^5 Pa the 30th model level is at 201 hPa such that the lowest 30 model levels approximate the tropospheric depth. The most accurate vertical averages are calculated on original model levels using mass-weighted vertical averages (Trenberth 1991) denoted by $\langle\cdot\rangle$ in equation 2.

$$\langle\cdot\rangle = \int_{p_s}^{ml_{30}} (\cdot)\frac{dp}{g} \quad \text{(Eq. 2)}$$

Here ml_{30} represents the 30th model level, p_s represents surface pressure, dp represents the pressure thickness between model layers, and g represents gravitational constant. The mass-weighted vertically averaged horizontal sensible and latent heat fluxes are $\langle \boldsymbol{v}T \rangle$ and $\langle \boldsymbol{v}q \rangle$ respectively where $\boldsymbol{v} = (u, v)$.

Data Analysis, Scaling, and Symmetry

Six-hourly output of each variable (*q, T, u, v;* Section 2.2) was multiplied at each grid point to yield analyses of sensible and latent heat flux on each model level. The mass-weighted vertical average was performed at each grid point and results were averaged at monthly intervals for storage in multi-dimensional arrays according to the following structure [latitude, longitude, month of year, year]. NDJ months associated with ENSO events summarized in tables 1 and 2 were selected for total, strong, and weak composite analyses. Composite analyses for El Niño and La Niña events of various magnitudes were either added or subtracted from each other to

quantify symmetric and asymmetric components, respectively (Zhang et al. 2014). After all aforementioned calculations were made results were scaled to provide horizontal fluxes of sensible and latent heat in the same units (kJ m^{-1} s^{-1}) to allow for direct comparison (Shaw and Pauluis 2011). Horizontal fluxes of sensible heat were scaled by the specific heat of water (4.181 kJ kg^{-1} K^{-1}) under standard atmospheric conditions (20ºC, 101.325 kPa). Horizontal fluxes of latent heat were scaled by the latent heat of vaporization (2265 kJ kg^{-1}) at the same standard atmospheric conditions. Additionally, vectors on each plot were scaled to the maximum value of each color bar to clarify spatial patterns between anomalous maxima of horizontal heat fluxes. This scaling procedure did not change vector trajectories.

The symmetric component of anomalous horizontal, tropospheric-mean fluxes of sensible and latent heat was quantified by subtracting composite analyses of each vector component during La Niña from that of El Niño composites (Zhang et al. 2014). The asymmetric component of anomalous horizontal, tropospheric-mean fluxes of sensible and latent heat was quantified by adding each vector component of composite analyses of El Niño and La Niña (Zhang et al. 2014). Addition or subtraction of composite analyses was performed after all spatial and temporal averages were performed as described above. Therefore, the symmetric component shows the linearity (i.e. mirror image) of anomalies during El Niño and La Niña events whereas the asymmetric component shows the non-linearity (i.e. El Niño is $\geq$ or $\leq$ La Niña) of anomalies. The symmetric component of anomalous sensible heat fluxes (ASHFs) were used to identify north-south dipoles (NSDs) of anomalous mid-latitude circulations consistent with leading patterns of Northern Hemisphere climate variability (e.g. NAO and PNA). The asymmetric component was used to identify differences in position or intensity of ASHFs associated with NAO or PNA patterns. The symmetric component of anomalous latent heat fluxes (ALHFs)

were used to identify connections between PNA and NAO regions with respective tropical heat source regions. The asymmetric component of ALHFs was used to identify differences in position or magnitude of connections between tropical heat sources and either PNA or NAO regions.

Results

Symmetry of Anomalous Heat Fluxes During all ENSO Events

The symmetric and asymmetric components of anomalous sensible heat fluxes[9] (ASHF) during each month of the NDJ period composited over all ENSO events (Table 5) is shown in Figure 11. While symmetric and asymmetric components of ASHF were of the same order of magnitude (10^4 kJ m^{-1} s^{-1}), the maximum anomalies for the symmetric component were larger. The configuration of the symmetric component of ASHF vectors were used to show north-south dipoles[10] (NSD) consistent with PNA or NAO patterns whereas the asymmetric component showed whether ASHF vectors were larger or smaller during El Niño or La Niña events. For example, a NSD shown in the symmetric component across the North Atlantic Ocean consistent with a positive NAO pattern suggests a robust linear relationship between ENSO and NAO patterns existed during both El Niño and La Niña events. If the asymmetric component across the North Atlantic Ocean shows a NSD consistent with a positive (negative) NAO pattern, then the results suggest larger ASHF vectors across the North Atlantic Ocean during El Niño (La Niña) events. Additionally, anomalous circulation dipoles shown in analyses of the asymmetric component not oriented in the north-south direction could indicate horizontal shifts in the NSDs associated with the PNA and NAO patterns.

Across the North Atlantic Ocean the symmetric component of ASHF showed a NSD consistent with the positive phase of the NAO pattern suggesting a robust linear relationship between ENSO and NAO patterns during November (Figure 11). The asymmetric component showed an anomalous circulation dipole oriented east-to-west suggesting the strengthened (weakened) Icelandic low associated with a positive (negative) NAO pattern was centered farther east (west) during Novembers of El Niño (La Niña) events. The symmetric component showed a weakly anomalous ($< 4x10^4$ kJ m^{-1} s^{-1}) NSD centered near 20ºW across the North Atlantic Ocean consistent with a weakly linear relationship between ENSO and NAO patterns during December of all ENSO events. The asymmetric component of ASHF vectors had similar orientation to that of the symmetric component suggesting larger (smaller) anomalies across the North Atlantic Ocean during Decembers of El Niño (La Niña) events. The symmetric component of ASHFs showed another weakly anomalous ($< 4x10^4$ kJ m^{-1} s^{-1}) NSD centered near 35ºW that was consistent with a weakly non-linear relationship between ENSO and NAO patterns during January of ENSO events. The asymmetric component of ASHFs showed a pair of NSD dipoles centered near 65ºW and 15ºW across the North Atlantic Ocean that suggested larger ASHFs across the West (East) Atlantic Ocean during Januarys of El Niño (La Niña) events. Therefore, results presented in Figure 11 indicated a transition from a linear to nonlinear relationship between ENSO and NAO patterns during NDJ of all ENSO events and anomalies were shifted towards (away from) the Western European coast during Novembers of all El Niño (La Niña) events.

The symmetric component across the North Pacific Ocean showed increasing ASHFs consistent with a strengthening linear relationship between ENSO and PNA patterns during December and January of all ENSO events. The symmetric component of ASHF did not indicate

a robust linear relationship between ENSO and PNA patterns during November. The asymmetric component of ASHFs showed a NSD centered near 165ºW and anomaly vectors located in the central Pacific Ocean between 15ºN and 45ºN were of similar magnitude (~$3x10^4$ kJ m^{-1} s^{-1}), but opposite direction indicating La Niña events resulted in larger ASHFs than El Niño events during November. A pair of simultaneously out of phase anomalous NSDs were shown in the symmetric component of ASHFs across the eastern Pacific Ocean and North America consistent with a linear relationship between ENSO and PNA patterns during December and January. The asymmetric component of ASHF was smaller than the symmetric component and the vector direction was the same indicating larger sensible heat flux anomalies during Januarys of El Niño events. Therefore, Figure 11 showed and a robust linear relationship between ENSO and PNA patterns during December and January when the asymmetric component suggested ASHFs were larger during El Niño events.

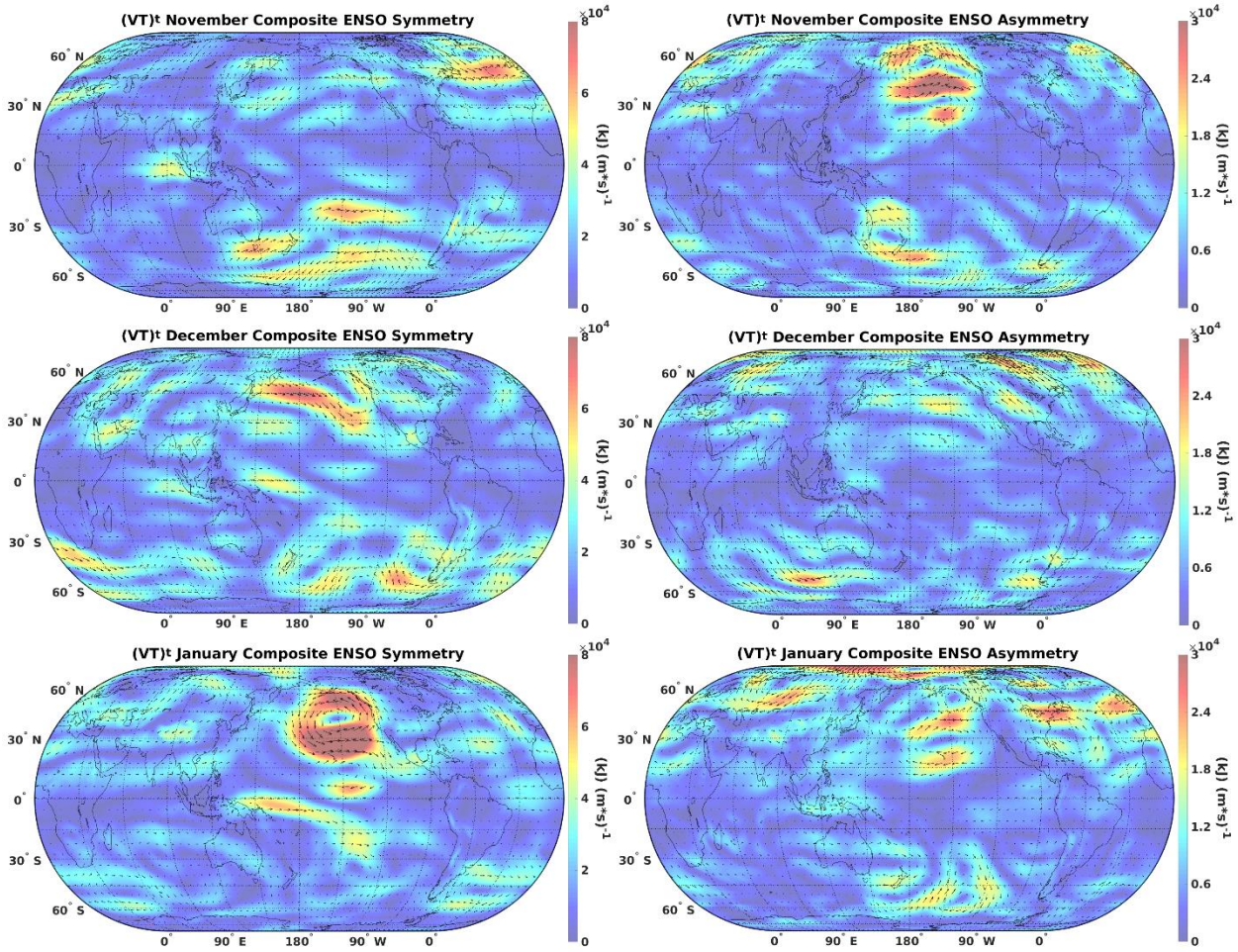

Figure 11. Symmetric (left) and asymmetric (right) components of monthly (NDJ) tropospheric-mean sensible heat flux anomalies during composites of all El Niño and all La Niña (Table 5) events occurring between 1979 and 2016. Color shading represents vector magnitude (kJ m^{-1} s^{-1}).

During the boreal winter tropospheric moisture content is small over high latitude continents, including North America, relative to that over ocean basins such that analyses of anomalous latent heat fluxes[11] (ALHF; Figure 12) were used to identify spatially continuous connections between ENSO, PNA, and NAO regions. The symmetric component showed moderate ALHFs (~4x10^4 kJ m^{-1} s^{-1}) connecting the extratropical Atlantic Ocean with the southeast coast of North America, the NAO region, and the west coast of Europe during November (Figure 12) of all ENSO events. The asymmetric component indicated a further south (north) position of the connection between the east coast of North America and the west coast of

Europe during Novembers of El Niño (La Niña) events. The symmetric component showed increasing ALHFs connecting the East Pacific Ocean with the NAO region during December and January of ENSO events. The asymmetric component showed suggested larger ALHFs across the North Atlantic Ocean during December of El Niño events. The asymmetric component suggested larger ALHFs across the West (East) Atlantic Ocean during Januarys of El Niño (La Niña) events. Therefore, results presented in Figure 12 across the NAO region suggested a symmetric connection between the NAO region and both the east coast of North America and the tropical Atlantic Ocean during November and the East Pacific Ocean during December and January and an asymmetric connection between the east coast of North America during December and January of all ENSO events.

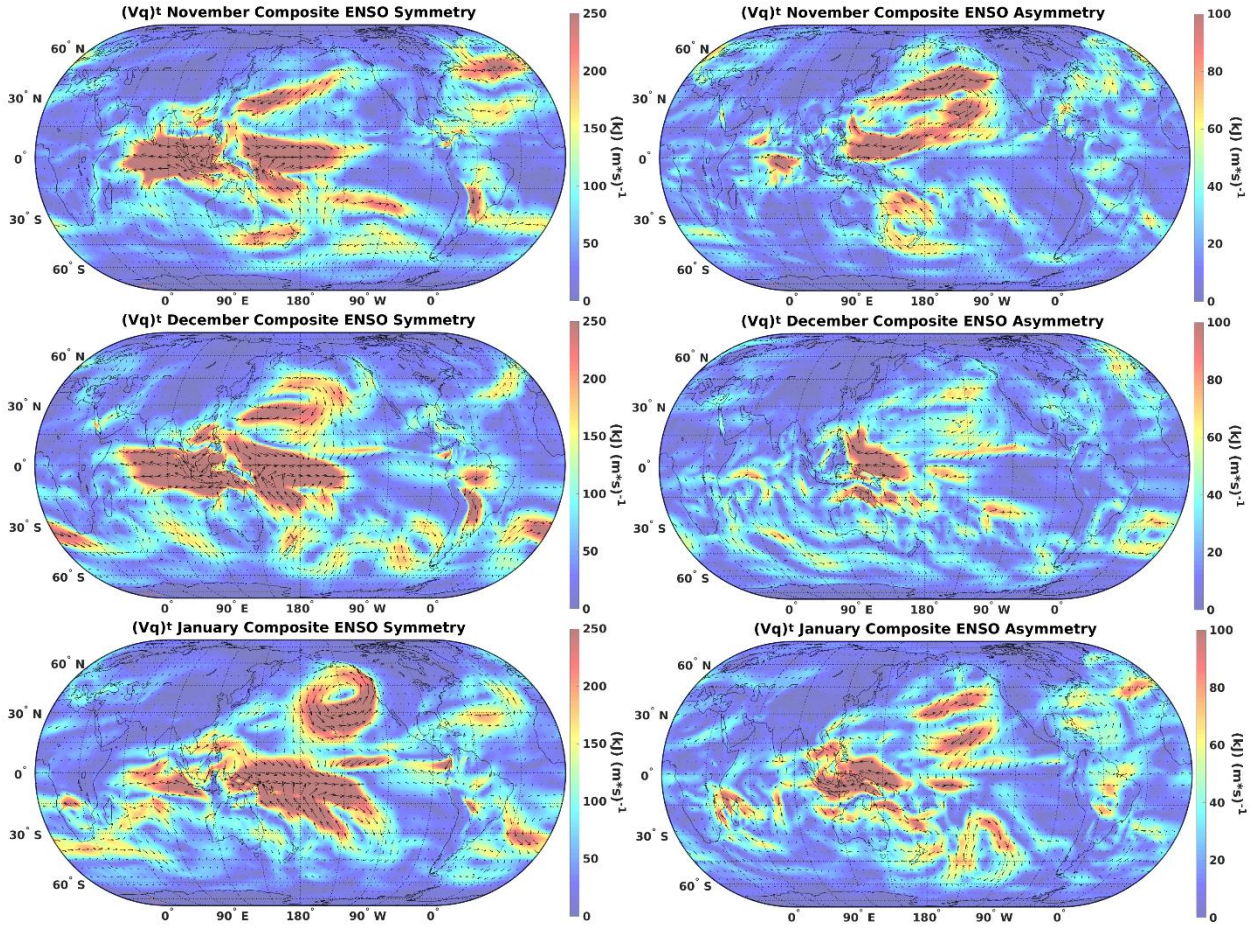

Figure 12. Symmetric (left) and asymmetric (right) components of monthly (NDJ) tropospheric-mean latent heat flux anomalies during composites of all El Niño and all La Niña (Table 5) events occurring between 1979 and 2016. Color shading represents vector magnitude (kJ m^{-1} s^{-1}).

Across the North Pacific Ocean each component of ALHFs presented in Figure 12 showed connections between the PNA region and tropical portions of both the central and West Pacific Ocean during NDJ of all ENSO events (Table 5). The symmetric component of ALHFs was large (> 250 kJ m^{-1} s^{-1}; Figure 12) across the Pacific Ocean and showed equatorward ALHFs strengthening across the north-central Pacific Ocean (0º - 45ºN; 180º - 150ºW) throughout NDJ suggesting linear connection between the PNA region and the Niño 3.4 region. The symmetric component of ALHFs showed poleward ALHFs along the southeast coast of Asia and the west coast of North America during NDJ suggested the equatorward anomalies across the central Pacific Ocean were compensated by poleward anomalies along both coastlines. The asymmetric

component of ALHFs indicated larger poleward ALHFs connecting the tropical West Pacific Ocean with the PNA region during Novembers of La Niña. The asymmetric component of ALHFs suggested an enhanced connection between Niño 3.4 and PNA regions during December and January of La Niña events and between the tropical West Pacific Ocean and the PNA region during December and January of El Niño events. Therefore, the symmetric component of ALHF showed a robust linear connection between the western (central) tropical Pacific Ocean and the PNA region that was enhanced during El Niño (La Niña) events. Alternatively, the asymmetric component showed larger anomalies during November of La Niña and indicated the anomalous circulation was further north (south) during Januarys of El Niño (La Niña).

Symmetry of Anomalous Heat Fluxes during Strong ENSO Forcing

Symmetric and asymmetric components of ASHF were shown in Figure 13 that were composited over the NDJ period of three strong ENSO events (Table 5). Figure 13 showed a NSD centered near 25ºW consistent with a positive NAO pattern suggesting a robust linear relationship between ENSO and NAO patterns during Novembers of strong ENSO events. The symmetric component of ASHFs showed an anomalous NSD centered near 30ºW and 10ºW that were consistent with a robust linear relationship between ENSO and NAO patterns during Decembers and Januarys of strong ENSO events, respectively. The asymmetric component showed a weak ($< 4x10^4$ kJ m^{-1} s^{-1}) NSD centered near 40ºW and suggested the NSD associated with strong La Niña events was centered ~15º longitude west of strong El Niño during November. The asymmetric component showed an east-west oriented anomalous circulation dipole centered near 35ºN during January suggesting strong El Niño (La Niña) anomalies were across the East (West) Atlantic Ocean. A large asymmetric component of ASHFs ($> 7x10^4$ kJ m^{-1} s^{-1}) was shown across the NAO region during January characterized by a NSD centered near 5ºE

and an ACC centered near 35ºN 25ºW. The anomalous NSD was consistent with the symmetric component suggesting ASHFs were shifted ~20º longitude east of the symmetric response during strong El Niño events. Alternatively, a pair of out-of-phase anomalous circulations inconsistent with the symmetric anomalies centered near 25ºW suggested larger anomalies were shifted ~15º west of the symmetric response during strong La Niña events. Therefore, the symmetric component resulted in a robust linear relationship between ENSO and NAO patterns throughout NDJ and the asymmetric component indicated a general eastward (westward) shift of the NSD during strong El Niño (La Niña) events.

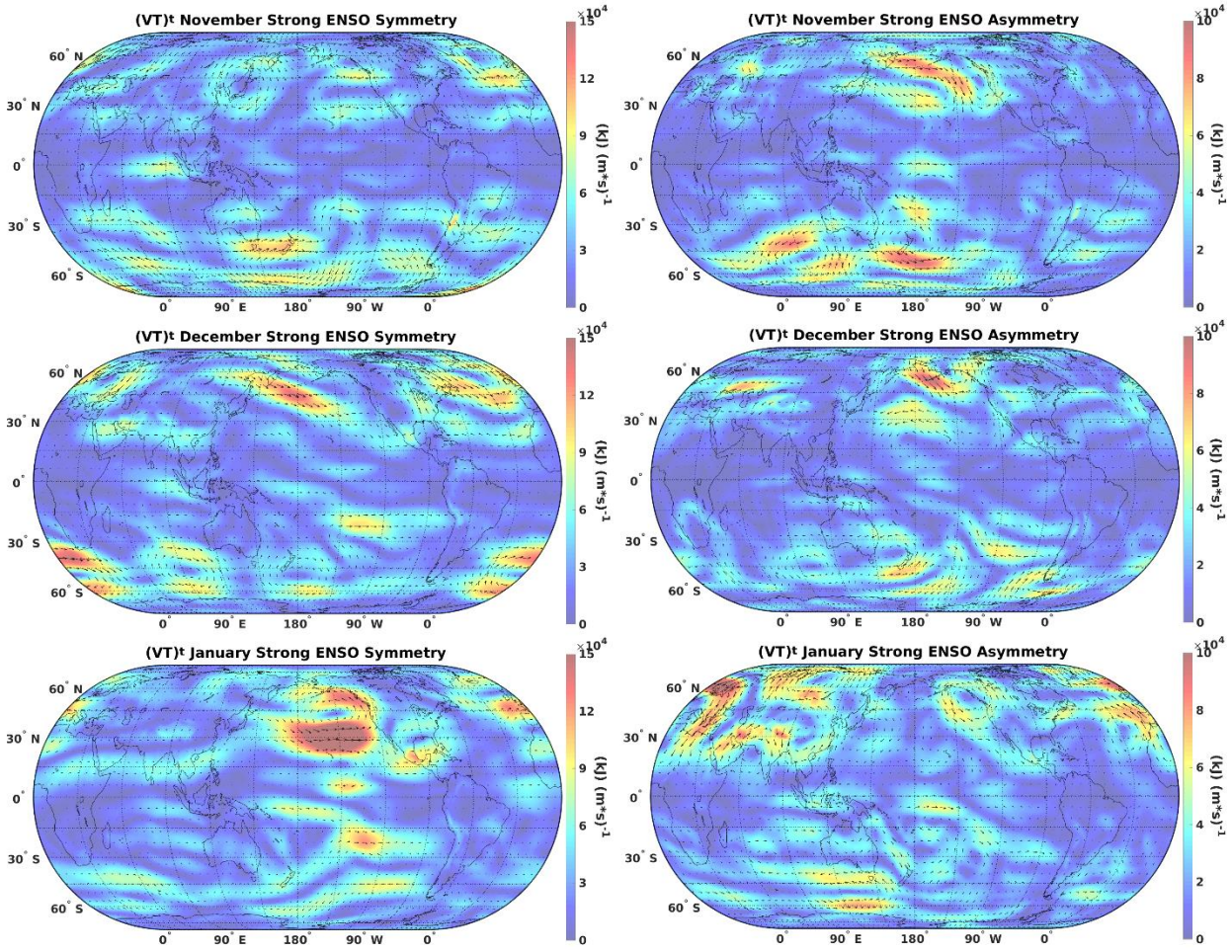

Figure 13. Symmetric (left) and asymmetric (right) components of monthly (NDJ) tropospheric-mean sensible heat flux anomalies during composites of three strong El Niño (1982-83, 1997-98,

2015-16) and La Niña (1988-89, 1999-2000, 2010-11) events occurring between 1979 and 2016. Color shading represents vector magnitude (kJ m^{-1} s^{-1}).

The symmetric component of ASHF showed the monthly (NDJ) evolution of anomalous circulations across the North Pacific Ocean (Figure 13) was consistent with a linear relationship between ENSO and PNA patterns and the asymmetric component generally indicated larger anomalies during strong El Niño than strong La Niña events. A single NSD along the west coast of North America (~125ºW) was not consistent with a predominant phase of the PNA pattern during November. The NSD along the west coast of North America interacted with anomalous circulations across the northwestern Pacific Ocean such that a NSD extended from the east coast of northeastern Asia to the west coast of Central America during December. During January a pair of simultaneous out of phase NSDs were centered near 150ºW and 90ºW suggesting a robust linear relationship between ENSO and PNA patterns during January and to a lesser extent December. The asymmetric component of ASHF showed a NSD centered near 175ºW and an ACC centered near 40ºN 135ºW during November. Both ACC features across the North Pacific Ocean during November indicated strong El Niño enhanced ASHF onto the west coasts of Alaska and the contiguous United States more than strong La Niña events reduced corresponding fluxes. The AAC centered near 40ºN 170ºW was suggested that strong La Niña (El Niño) events resulted in larger (smaller) ASHFs across the north-central Pacific Ocean during November. The asymmetric component was large (> $10x10^4$ kJ m^{-1} s^{-1}) and indicated larger ASHFs connecting the northeast coast of Asia with the west coast of Central America during Decembers of strong La Niña events. Along the west coast of North America the asymmetric and symmetric components of ASHFs indicated enhanced poleward fluxes north of 45ºN and enhanced equatorward fluxes south of 45ºN during strong El Niño events. The asymmetric component showed a pair of simultaneously out of phase NSDs across the eastern Pacific Ocean and North

America indicating larger ASHFs during Januarys of strong El Niño events. Therefore, across the PNA region, the symmetric component suggested a robust linear relationship between ENSO and PNA patterns during January and December whereas the asymmetric component of ASHFs vectors were consistent with the symmetric component indicating generally larger anomalies during strong El Niño rather than strong La Niña events.

Symmetric and asymmetric components of ALHF are shown in Figure 14 and were composited over the NDJ period of the three strong ENSO events (Table 5). The symmetric component of ALHFs showed enhanced poleward latent heat fluxes across southeastern North America and adjacent waters that connected the tropical Atlantic Ocean (0º - 30ºN) and Caribbean Sea with the NAO region and the west coast of Europe centered near ~50ºN during Novembers of strong El Niño events. The asymmetric component was small, but indicated larger ALHFs into the Caribbean Sea from the eastern tropical Pacific Ocean (0º - 15ºN) during November. The symmetric component of ALHF increased across the North Atlantic Ocean during Decembers of strong ENSO event and showed increasing fluxes from the tropical East Pacific Ocean. The asymmetric component suggested a connection between the tropical eastern Pacific Ocean and the west coast of Europe during December of strong ENSO events. The asymmetric component indicated a circulation centered near 25ºN 100ºW indicated that strong El Niño events have larger latent heat fluxes from the eastern Pacific Ocean onto the southeast coast of North America than strong La Niña events. During January the symmetric component indicated an ACC centered across the northern Gulf of Mexico and suggested larger ALHFs (> 250 kJ m^{-1} s^{-1}) from the tropical east Pacific Ocean and the asymmetric component was consistent such that strong El Niño events resulted in larger ALHFs across Central America. The asymmetric component showed a NSD across the far northern Atlantic Ocean indicating the La

Niña anomalies were larger across the northeast Atlantic Ocean (~55ºN) whereas El Niño anomalies were larger across the east-central Atlantic Ocean (~30ºN). Therefore, the symmetric component of ALHF across the North Atlantic Ocean indicated enhanced fluxes from the tropical Atlantic Ocean during November and December or the east-central Pacific Ocean during January and the asymmetric component generally increased during December and January and indicated a connection to the east-central Pacific Ocean.

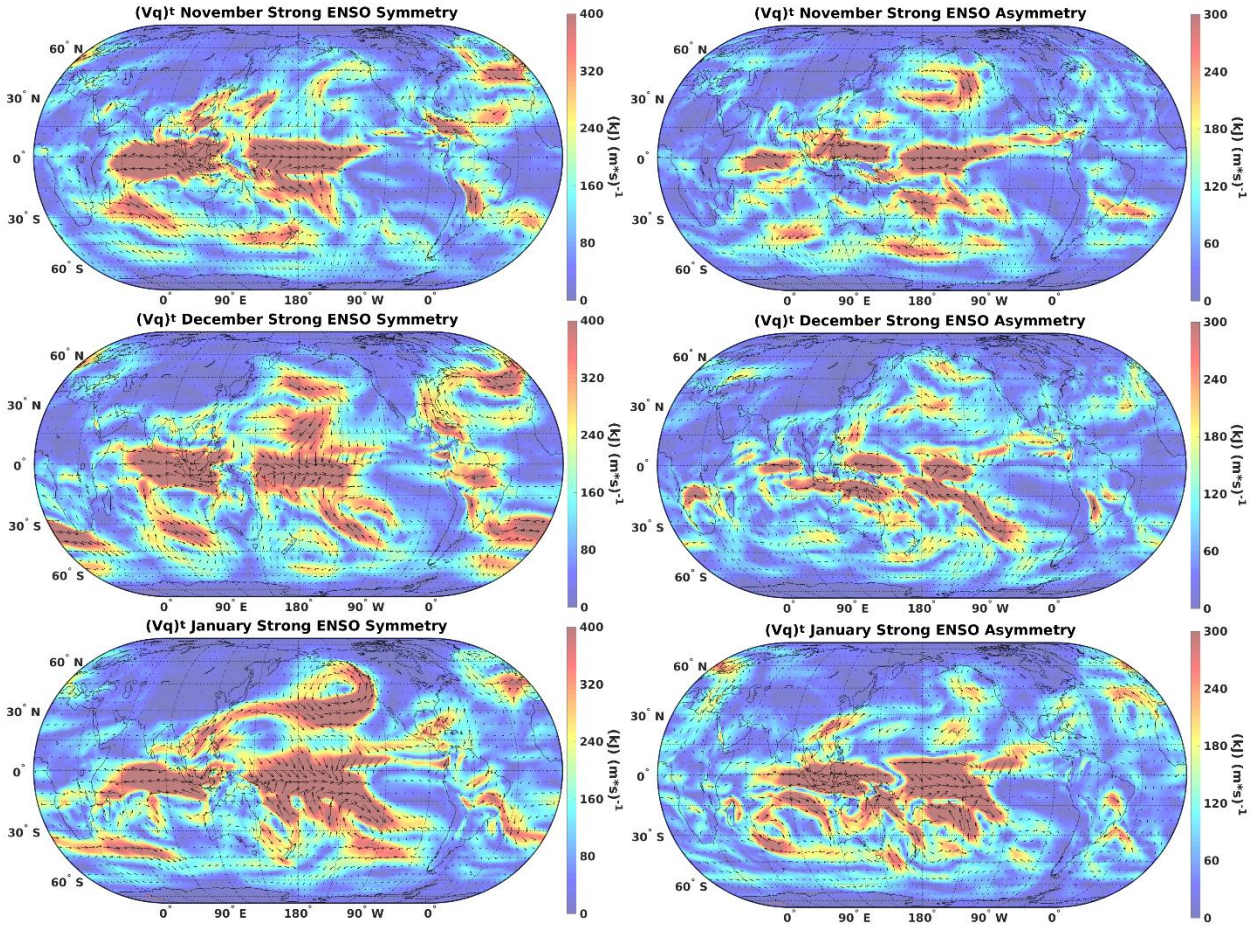

Figure 14. Symmetric (left) and asymmetric (right) components of monthly (NDJ) tropospheric-mean latent heat flux anomalies during composites of three strong El Niño (1982-83, 1997-98, 2015-16) and La Niña (1988-89, 1999-2000, 2010-11) events occurring between 1979 and 2016. Color shading represents vector magnitude (kJ m^{-1} s^{-1}).

Across the North Pacific Ocean the symmetric component of ALHF showed a spatially continuous connection between the western equatorial Pacific Ocean and the PNA region during

strong El Niño events and the asymmetric component generally indicated a larger ALHF during strong El Niño events. During November the symmetric component showed anomalous poleward latent heat fluxes across southeastern Asia throughout NDJ of strong El Niño events. Spatial patterns during December indicated a connection between the southeast coast of Asia and the central Pacific Ocean that was shown to intersect the west coast of North America during Januarys of strong El Niño events. The meridional component of all vectors across the north-central Pacific Ocean (180ºW – 150ºW) showed a connection between the single point correlation of the PNA pattern and the Niño 3.4 region during the NDJ period of strong El Niño events. The asymmetric component indicated larger anomalies during El Niño across the western Pacific Ocean, but larger anomalies during La Niña across the northeast Pacific Ocean during November and January of strong ENSO events. Therefore, results in Figure 14 showed an anomalous equatorward flux of latent heat across the central Pacific Ocean and a connection between Southeast Asia and the PNA region during December and January that was largely symmetric whereas the asymmetric component was largest across Southeast Asia and the Northeast Pacific Ocean.

Symmetry of Anomalous Heat Fluxes during Weak ENSO

The symmetric and asymmetric components of anomalous sensible heat fluxes during weak ENSO events is shown in Figure 15 for composite analyses of three weak ENSO events (Table 5). Results for the symmetric component during November indicated four anomalous NSD patterns across the North Pacific Ocean, North America, and the North Atlantic Ocean. Across the North Pacific Ocean, two simultaneously out of phase anomalous NSDs were located across the northwest (~165ºE) and northeast (145ºW) Pacific Ocean and were located too far west to be associated with a positive PNA pattern. During December anomalous circulations

shifted east such that a north-south oriented tripole pattern near 160ºE in November was centered near 160ºW in January. Results presented in figure 5 did not suggest a relationship between ENSO and PNA patterns. Across the North Atlantic Ocean a NSD was located near 30ºW consistent with a robust linear relationship between ENSO and NAO patterns during Novembers of weak ENSO events. The NSD centered near (~75ºW) during November shifted east to near 30ºW during January suggesting a predominantly negative NAO pattern during January. Therefore, the symmetric component of ASHFs during weak El Niño (La Niña) events suggested a transition from positive to negative (negative to positive) NAO patterns throughout the NDJ period, but were not consistent with a predominant phase of the PNA pattern.

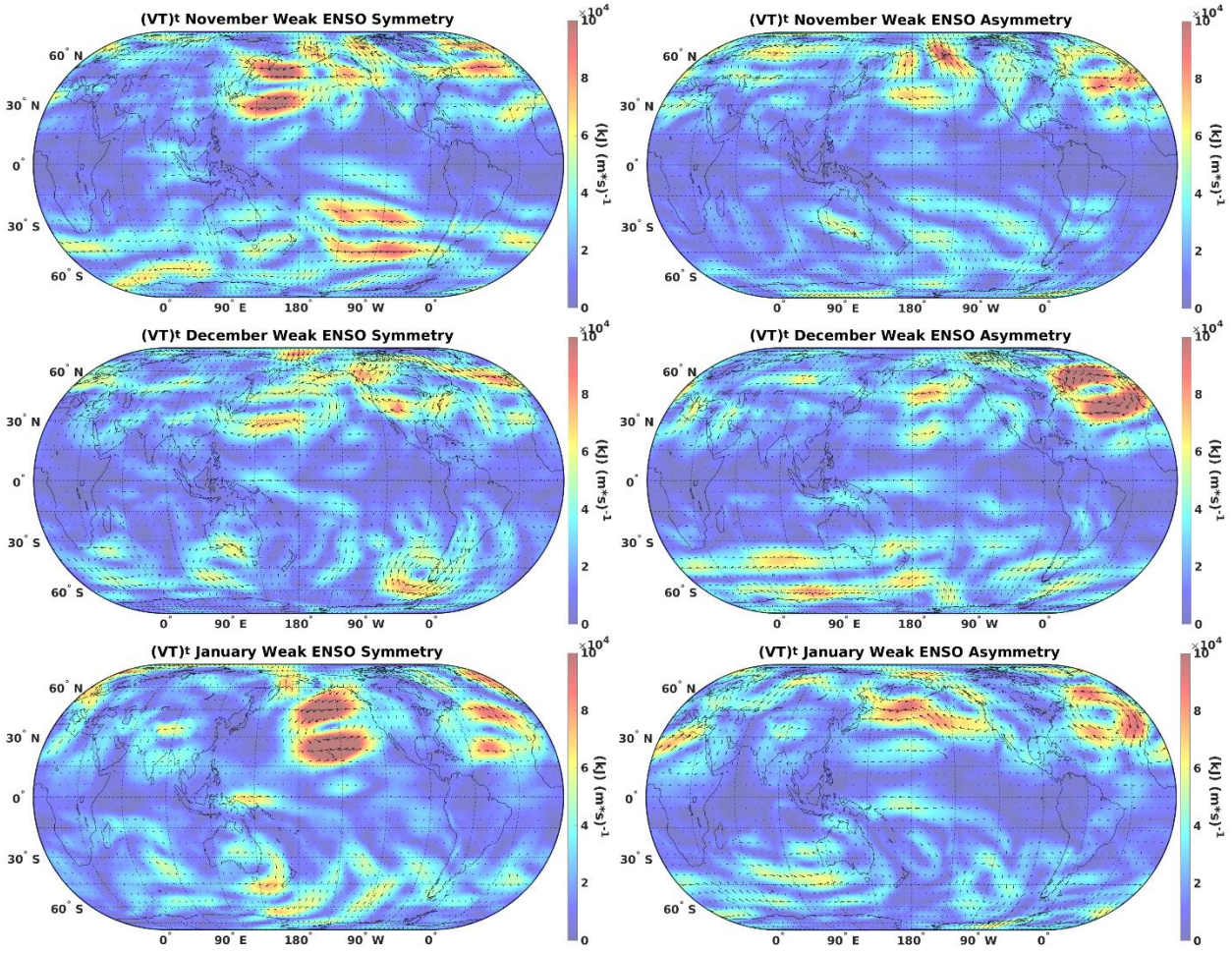

Figure 15. Symmetric (left) and asymmetric (right) components of monthly (NDJ) tropospheric-mean sensible heat flux anomalies during composite of three weak El Niño (1979-80, 2004-05, 2014-15) and La Niña (1983-84, 2005-06, 2008-09) events occurring between 1979 and 2016. Color shading represents vector magnitude (kJ m^{-1} s^{-1}).

The symmetric and asymmetric components of ASHFs during weak ENSO events (Table 5) were approximately the same size indicating both components were climatologically relevant during weak ENSO events (Figure 15). The asymmetric component of ASHFs across the North Atlantic Ocean suggested larger (smaller) ASHFs and a more (less) negative (positive) NAO pattern during Novembers of weak La Niña (El Niño) events. Results showed a NSD of ASHFs across the North Atlantic Ocean shift south during NDJ suggesting larger ASHFs and a transition from negative to positive NAO patterns during weak La Niña events (Figure 15). Across the PNA region the asymmetric component of ASHFs was large (> $7x10^4$ kJ m^{-1} s^{-1}) and was shown

to be important for assessing the relationship between ENSO and PNA patterns. The asymmetric component shows two simultaneously out of phase anomalous circulation dipoles oriented from northwest to southeast suggesting east to west positional differences between the positive (negative) PNA patterns during El Niño (La Niña). The asymmetric component showed NSDs across the northeast Pacific Ocean consistent with larger ASHFs associated with a negative PNA pattern during December of weak La Niña events. The asymmetric component showed a north-south tripole near 180º that suggested larger ASHFs across the central Pacific Ocean during January of weak El Niño events. The AAC across the far North Pacific Ocean had two ACCs centered both west and east of the symmetric component suggesting that anomalous circulations across the Pacific Ocean during Januarys of weak La Niña events were closer to the east coast of Asia and the west coast of North America. Therefore, the asymmetric component suggested ASHFs were larger across the North Atlantic Ocean throughout NDJ during weak La Niña events whereas the asymmetric component across the North Pacific Ocean suggested positional differences in the anomalous circulation patterns during weak ENSO events.

The symmetric and asymmetric components of ALHFs associated with weak ENSO events during NDJ is shown in Figure 16. The spatial patterns of ALHFs were used to identify spatially continuous regions connecting tropical heat sources with anomalous circulations in PNA and NAO regions. The symmetric (asymmetric) component showed smaller (larger) ALHFs into the PNA region from the western tropical Pacific Ocean during November and December of weak El Niño (La Niña) events. The symmetric component showed an ACC centered near 35ºN 150ºW indicating anomalous poleward fluxes across the Northeast (Central) Pacific Ocean connecting the tropical Pacific Ocean with the PNA region during Januarys of weak El Niño (La Niña) events. The asymmetric component showed a west to east anomalous

circulation dipole suggesting larger anomalies associated with weak El Niño (La Niña) across the north central (northeast) Pacific Ocean during January. The symmetric (asymmetric) component across the North Atlantic Ocean showed a NSD consistent with a positive (negative) NAO pattern suggesting a connection between the tropical Atlantic Ocean (east coast of North America) and Western Europe during weak El Niño (La Niña) events. Across the North Atlantic Ocean the asymmetric component was larger than the symmetric component suggesting similar ALHF connections between the north-central Atlantic Ocean and the east coast of North America during December of both weak El Niño and La Niña events. The asymmetric component mirrored the symmetric component across the North Atlantic Ocean suggesting larger ALHFs during Januarys of weak La Niña events. Therefore, the similarly large components of ALHF (Figure 16) suggested anomalous latent heat fluxes from the tropical Pacific and Atlantic Oceans into (out of) the PNA and NAO regions was smaller (larger) during weak El Niño (La Niña) events.

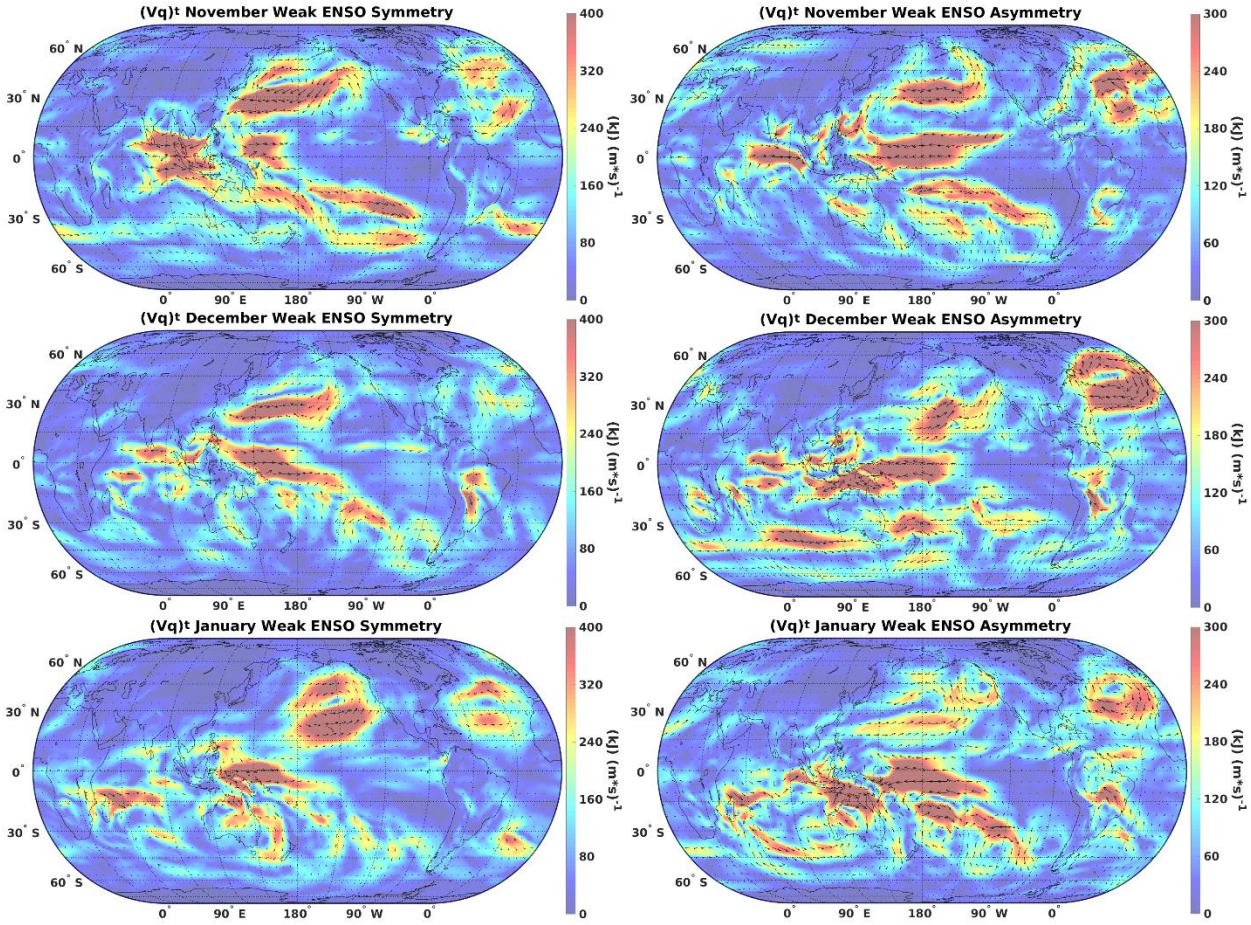

Figure 16. Symmetric (left) and asymmetric (right) components of monthly (NDJ) tropospheric-mean latent heat flux anomalies during composite of three weak El Niño (1979-80, 2004-05, 2014-15) and La Niña (1983-84, 2005-06, 2008-09) events occurring between 1979 and 2016. Color shading represents vector magnitude (kJ m^{-1} s^{-1}).

Discussion

Symmetric and asymmetric components of extratropical ENSO teleconnections are a fundamental feature of recent ENSO events and the less-studied asymmetric component has climatologically relevant impacts to surface temperature and precipitation (Zhang et al. 2014). The current work presents composite analyses of anomalous horizontal fluxes of latent and sensible heat quantified during NDJ when maximum anomalous vertical heat fluxes into the troposphere were forced by ENSO. Anomalous sensible heat fluxes (ASHFs) were quantified from ERA-I output and were used to identify anomalous circulation dipoles consistent with PNA

and NAO teleconnection patterns that are known to be influenced by the ENSO phenomena (e.g. Straus and Shukla 2002; Brönnimann 2007; Hurrell and Deser 2010; Graf and Zanchettin 2012). Results showed a robust linear relationship between ENSO and NAO patterns during November of all ENSO events (Figure 11, Figure 13, and Figure 15). The linear relationship between ENSO and NAO patterns contrasts recent studies that identified an anomalously weakened stratospheric polar vortex associated with El Niño events favoring a non-linear relationship (e.g. Ineson and Scaife 2009; Iza et al. 2016). However, Iza et al. (2016) indicated the stratospheric pathway associated with La Niña events was most frequent during late winter (beyond February 20) associated with strong La Niña forcing. Composite analyses of all twelve and three weak La Niña events (Figure 11 and Figure 15) that occurred between 1979 and 2016 showed spatial patterns consistent with a non-linear relationship during January, but analyses for February and beyond were not included. However, the most robust linear relationship between ENSO and NAO patterns was shown during composite of the three strong La Niña events (Table 5) implying that a similarly robust early season teleconnection may exist through a tropospheric pathway. Additionally, the asymmetric component of ASHFs showed north-south-dipoles (NSDs) of anomalous circulations shifted closer to the west coast of Europe during El Niño events implying greater climate impacts across Western Europe than La Niña events. Therefore, a robust linear relationship between ENSO and NAO patterns was identified in the early winter associated with a tropospheric pathway and the asymmetric component showed non-linear east-west shifts in the anomalous North Atlantic Ocean NSD throughout NDJ.

Across the northeast Pacific Ocean, the symmetric component of ASHFs indicated a robust linear relationship between ENSO and PNA patterns during December and January (Figure 11 and Figure 13) and were also shown to shift due to asymmetry and ENSO event

magnitude. In particular, January showed the spatial distributions of distinct extratropical circulation anomalies modifying the PNA pattern forced by ENSO that were initially posited by Straus and Shukla (2002) implying that methods detailed in the current work effectively identified extratropical anomalies associated with ENSO forcing. The asymmetric component of ASHFs (Figure 11 and Figure 13) showed larger ASHFs across the northeast Pacific Ocean during December and January of El Niño events and indicated an eastward shift of the enhanced Aleutian low nearer to the west coast of North America. The corresponding westward shift corresponding to La Niña indicated east-west shifts of approximately 30º longitude consistent with conclusions of Hoerling et al. (1997) implying altered extratropical storm tracks and tropical heat sources during El Niño and La Niña events. Additionally, this east-west shift was shown to be larger during strong ENSO events (Figure 13) and smaller during weak ENSO events (Figure 15) when weak La Niña anomalies were shown to be larger than weak El Niño during January. Therefore, linear and nonlinear components of ASHFs implied greatest climate impacts across North America were associated with strong El Niño and weak La Niña events implying a need to identify tropical heat source regions.

Analyses of anomalous latent heat fluxes (ALHFs; Figure 12, Figure 14, and Figure 16) were used to identify connections between tropical heat sources and the NAO or PNA regions based on variable ENSO event magnitude. The linear response to ALHFs showed a primarily tropical Atlantic Ocean heat source (Castillo et al. 2014) during November of El Niño events shifted to a primarily East Pacific Ocean heat source during January (Figure 12). This linear response could be consistent with the subtropical bridge mechanism proposed by Graf and Zanchettin (2012) implying cold European winters may increase due to climate change. Enhanced poleward fluxes of latent heat across eastern North America from the tropical Atlantic

and East Pacific Ocean (Figure 14) implied a Maya Express atmospheric river event (Castillo et al. 2014) during December of strong El Niño events. The Maya Express atmospheric river has important implications for precipitation patterns across eastern North America including extreme rainfall events (e.g. Dirmeyer and Kinter 2010). Alternatively, similar linear and nonlinear components of ALHFs suggested equally large impacts to European climate. The connections to tropical heat sources were characterized by a weaker connection to the East Pacific Ocean implying the tropical Atlantic Ocean (Castillo et al. 2014) and Eastern North America were the sources for anomalous latent heat flux into the NAO region during weak ENSO events. Nonlinear components of ALHFs (Figure 12 and Figure 14) indicated larger latent heat fluxes from the Atlantic to Pacific Oceans during La Niña events implying that El Niño events resulted in relatively brief, but intense ALHFs from the Pacific Ocean consistent with the atmospheric river phenomena (Gimeno et al. 2014). Additionally, the nonlinear component indicated larger anomalies across the northeast Atlantic Ocean during Januarys of La Niña events and larger anomalies across the West Atlantic Ocean and Gulf of Mexico regions during Januarys of El Niño events. Therefore, the NAO region was shown to be connected to the east coast of North America and the tropical Atlantic and East Pacific Oceans such that strong ENSO events resulted in the strongest connection between Atlantic and Pacific Oceans and implied a Maya Express atmospheric river during December of strong El Niño events.

Across the northeast Pacific Ocean, the symmetric component of ALHFs indicated a connection between the PNA region and tropical portions of both the west and the central Pacific Ocean and the asymmetric component indicated enhanced poleward fluxes across the west (central) Pacific Ocean during El Niño (La Niña) events. The symmetric component showed equatorward fluxes across the north-central Pacific Ocean (0º - 45ºN; 180º - 150ºW) implying

potential to identify and predict months or weeks when persistent atmospheric anomalies (blocking) associated with extreme North American climate events are possible (Barriopedro et al. 2006). Compensating poleward fluxes were located along the southeast (northwest) coast of Asia (North America) during El Niño events similar to analyses of anomalous integrated water vapor transport (IVT) shown in Kim and Alexander (2015) implying linear, climatologically relevant precipitation patterns in these regions. The asymmetric component across the northeast and tropical West Pacific Ocean was large and it showed that these regions were connected via Southeast Asia during El Niño and the central Pacific Ocean during La Niña, especially during January of strong ENSO events. The symmetric component of ALHFs during January indicated a spatial pattern consistent with a Pineapple Express atmospheric river event indicating enhanced potential for extreme rainfall events across the west coast of North America during strong El Niño events (Gimeno et al. 2014). However, enhanced atmospheric river activity across the west coast of North America was also indicated during Decembers and Januarys of weak La Niña events associated with a large nonlinear component of ALHFs across the northeast Pacific Ocean that has not been previously identified. This asymmetric response indicates that increasing El Niño (La Niña) event magnitude shifted ALHFs closer to (farther from) the west coast of North America implying that the largest positive precipitation anomalies in this region should be anticipated during weak La Niña and strong El Niño events. Therefore, both linear and nonlinear connections between the PNA region and both the tropical western and central Pacific Ocean were identified such that the most anomalous atmospheric river activity was shown during weak La Niña and strong El Niño events.

Conclusions

The primary objective of this work was to quantify the anomalous horizontal latent and sensible heat fluxes corresponding to ENSO events when anomalous upward heat fluxes were forced into the tropical troposphere from the Pacific Ocean. A limited number of studies examining anomalous tropospheric-mean fluxes of sensible or latent heat associated with ENSO exist and neither the seasonal evolution nor its symmetry have been assessed at the global scale. A robust, linear relationship was identified between ENSO and NAO patterns throughout NDJ of strong ENSO events (Figure 13) whereas weak to moderate ENSO events indicated a transition from a linear to nonlinear relationship throughout NDJ (Figure 11 and Figure 15). The asymmetric component indicated a westward (eastward) shift of ASHFs relative to the symmetric component during La Niña (El Niño). A robust, linear relationship was shown between ENSO and PNA patterns during December and January of composite analyses of all ENSO events, especially during strong ENSO events. However, a large asymmetric component existed across the North Pacific Ocean during weak ENSO events such that a positive PNA pattern was identified during weak La Niña events. Therefore, analyses of ASHFs indicated a robust linear relationship between ENSO, PNA, and NAO patterns that was variable based on both month and ENSO magnitude; the asymmetric component generally indicated an eastward (westward) shift of ASHFs during El Niño (La Niña) events such that connections between tropical heat sources and PNA or NAO regions changed.

The symmetric component of ALHFs showed large equatorward fluxes connecting the Niño 3.4 region with the single-point correlation for the PNA patterns (0º - 45ºN: 180º - 150ºW) implying potential to quantify the interrelationship between ENSO and PNA patterns. Compensating poleward ALHFs were shown across the southeast (northwest) coast of Asia

(North America) during El Niño events suggesting enhanced precipitation and the potential for more frequent atmospheric river events across the west coast of North America, especially during Januarys of strong El Niño events. The asymmetric component indicated increasing El Niño (La Niña) event magnitude shifted ALHFs closer to (farther from) the west coast of North America implying the largest precipitation anomalies during strong El Niño and weak La Niña events. The symmetric component across the North Atlantic Ocean indicated ALHFs into the NAO region transitioned from the tropical Atlantic Ocean during November to the tropical East Pacific Ocean during January of El Niño events, especially during Januarys of strong El Niño events. During December of strong El Niño events connections between the tropical Atlantic and East Pacific Oceans were apparent across southeastern North America consistent with a Maya express atmospheric river event. ALHFs during weak ENSO events indicated similarly large linear and nonlinear components such that larger ALHFs were present across the far northeastern Atlantic Ocean during Januarys of weak La Niña and the Gulf of Mexico during Januarys of weak El Niño. Therefore, composite analyses of symmetric and asymmetric components of horizontal, tropospheric-mean fluxes of sensible and latent heat were shown to be effective for identifying NSDs consistent with PNA or NAO patterns and spatially continuous connections between tropical heat source regions and the PNA and NAO regions.

This work advances understanding of the interrelationship between ENSO, PNA, and NAO patterns and the connection to tropical heat sources, which could enhance predictability of atmospheric river events across North America. The symmetric component of the anomalous horizontal heat fluxes was generally larger than the asymmetric component, but both were the same order of magnitude. The asymmetric component was particularly large during weak ENSO events along the west coast of North America and the NAO region that suggested greater impacts

to temperature and precipitation patterns across North America and Western Europe during weak La Niña rather than weak El Niño events. Spatial patterns consistent with atmospheric rivers near the west coast of North America were apparent during Januarys of both strong El Niño and weak La Niña events. Strong El Niño events indicated spatial patterns consistent with a Maya Express atmospheric river across eastern North America during December. Spatial patterns suggested that the asymmetry was a result of differences in the positioning rather than magnitude of anomalous circulation features. Therefore, monitoring the position of anomalous tropospheric mean heat fluxes can be performed at weekly to monthly resolution and will enhance predictability of subsequent surface temperature and precipitation patterns across either PNA or NAO regions.

Acknowledgements

Appreciation is extended to coauthors and external evaluations of the article that greatly improved the quality of the work. This research did not receive any specific grant from funding agencies in the public, commercial, or not-for-profit sectors.

Literature Cited

Alexander, M. A., Bladé, I., Newman, M., Lanzante, J. R., Lau, N. C., Scott, J. D. 2002. The atmospheric bridge: The influence of ENSO teleconnections on air–sea interaction over the global oceans. *Journal of Climate*, **15**(16): 2205-2231.

An, S.I., Jin, F.F. 2004. Nonlinearity and asymmetry of ENSO. *Journal of Climate*, **17**(12): 2399-2412.

Brönnimann, S. 2007. Impact of El Niño–Southern Oscillation on European climate. *Reviews of Geophysics*, **45**(3).

Castillo, R., Nieto, R., Drumond, A., Gimeno, L. 2014. The role of the ENSO cycle in the modulation of moisture transport from major oceanic moisture sources. *Water Resources Research*, **50**(2): 1046-1058.

Dee, D. P., Uppala, S. M., Simmons, A. J., Berrisford, P., Poli, P., Kobayashi, S., Andrae, U., Balmaseda, M. A., Balsamo, G., Bauer, P., Bechtold, P. 2011. The ERA-Interim reanalysis: Configuration and performance of the data assimilation system. *Quarterly Journal of the Royal Meteorological Society*, **137**(656): 553-597.

Dessler, A. E., Schoeberl, M. R., Wang, T., Davis, S. M., Rosenlof, K. H., Vernier, J. P. 2014. Variations of stratospheric water vapor over the past three decades. *Journal of Geophysical Research: Atmospheres*, **119**(22).

Dirmeyer, P. A., Kinter III, J. L. 2010. Floods over the US Midwest: A regional water cycle perspective. *Journal of Hydrometeorology*, **11**(5): 1172-1181.

European Centre for Medium-Range Weather Forecasts. 2009, updated monthly. ERA-Interim Project. Research Data Archive at the National Center for Atmospheric Research, Computational and Information Systems Laboratory. https://doi.org/10.5065/D6CR5RD9. Accessed† 10 06 2016.

Fogt, R. L., Bromwich, D. H. 2006. Decadal variability of the ENSO teleconnection to the high-latitude South Pacific governed by coupling with the southern annular mode. *Journal of Climate*, **19**(6): 979-997.

Franzke, C., Feldstein, S. B., Lee, S. 2011. Synoptic analysis of the Pacific–North American teleconnection pattern. *Quarterly Journal of the Royal Meteorological Society*, **137**(655): 329-346.

Fu, G., Charles, S. P., Timbal, B., Jovanovic, B., Ouyang, F. 2015. Comparison of NCEP-NCAR and ERA-Interim over Australia. *International Journal of Climatology*. **36**(5): 2345-2367.

Gimeno, L., Nieto, R., Vázquez, M., Lavers, D. A. 2014. Atmospheric rivers: a mini-review. *Frontiers in Earth Science*, **2**(2).

Graf, H. F., Zanchettin, D. 2012. Central Pacific El Niño, the "subtropical bridge," and Eurasian climate. *Journal of Geophysical Research: Atmospheres*, **117**(D1).

Harrison, D. E., Chiodi, A. M. 2017. Comments on "Characterizing ENSO Coupled Variability and Its Impact on North American Seasonal Precipitation and Temperature". *Journal of Climate*, **30**(1): 427-436.

Hoerling, M. P., Kumar, A., Zhong, M. 1997. El Niño, La Niña, and the nonlinearity of their teleconnections. *Journal of Climate*, **10**(8): 1769-1786.

Hurrell, J. W., Deser, C. 2010. North Atlantic climate variability: the role of the North Atlantic Oscillation. *Journal of Marine Systems*, **79**(3): 231-244.

Ineson, S., Scaife, A. A. 2009. The role of the stratosphere in the European climate response to El Niño. *Nature Geoscience*, **2**(1): 32-36.

Iza, M., Calvo, N., Manzini, E. 2016. The Stratospheric Pathway of La Niña. *Journal of Climate*, **29**(24): 8899-8914.

Kim, H. M., Alexander, M. A. 2015. ENSO's modulation of water vapor transport over the Pacific–North American region. *Journal of Climate*, **28**(9): 3846-3856.

Kirtman, B. P., Min, D., Infanti, J. M., Kinter III, J. L., Paolino, D. A., Zhang, Q., Van Den Dool, H., Saha, S., Mendez, M. P., Becker, E., Peng, P. 2014. The North American multimodel ensemble: phase-1 seasonal-to-interannual prediction; phase-2 toward developing intraseasonal prediction. *Bulletin of the American Meteorological Society*, **95**(4): 585-601.

Lau, N. C., Nath, M. J. 1996. The role of the "atmospheric bridge" in linking tropical Pacific ENSO events to extratropical SST anomalies. *Journal of Climate*, **9**(9): 2036-2057.

Leathers, D. J., Yarnal, B., Palecki, M. A. 1991. The Pacific/North American teleconnection pattern and United States climate. Part I: Regional temperature and precipitation associations. *Journal of Climate*, **4**(5): 517-528.

Leathers, D. J., Palecki, M. A. 1992. The Pacific/North American teleconnection pattern and United States climate. Part II: temporal characteristics and index specification. *Journal of Climate*, **5**(7): 707-716.

Liu, Z., Alexander, M. 2007. Atmospheric bridge, oceanic tunnel, and global climatic teleconnections. *Reviews of Geophysics*, **45**(2).

Lorenz, C., Kunstmann, H. 2012. The hydrological cycle in three state-of-the-art reanalyses: Intercomparison and performance analysis. *Journal of Hydrometeorology*, **13**(5): 1397-1420.

Müller, W. A., Roeckner, E. 2008. ENSO teleconnections in projections of future climate in ECHAM5/MPI-OM. *Climate Dynamics*, **31**(5): 533-549.

Okumura, Y. M., Deser, C. 2010. Asymmetry in the duration of El Niño and La Niña. *Journal of Climate*, **23**(21): 5826-5843.

Peixoto, J. P., Oort, A. H. 1992. Physics of Climate.

Rodionov, S. N., Bond, N. A., Overland, J. E. 2007. The Aleutian Low, storm tracks, and winter climate variability in the Bering Sea. *Deep Sea Research Part II: Topical Studies in Oceanography*, **54**(23): 2560-2577.

Rodwell, M. J., Rowell, D. P., Folland, C. K. 1999. Oceanic forcing of the wintertime North Atlantic Oscillation and European climate. *Nature*, **398**(6725): 320-323.

Seager, R., Kushnir, Y., Nakamura, J., Ting, M., Naik, N. 2010. Northern Hemisphere winter snow anomalies: ENSO, NAO and the winter of 2009/10. *Geophysical Research Letters*, **37**(14).

Serreze, M. C., Carse, F., Barry, R. G., Rogers, J. C. 1997. Icelandic low cyclone activity: Climatological features, linkages with the NAO, and relationships with recent changes in the Northern Hemisphere circulation. *Journal of Climate*, **10**(3): 453-464.

Shaw, T. A., Pauluis, O. 2012. Tropical and subtropical meridional latent heat transports by disturbances to the zonal mean and their role in the general circulation. *Journal of the Atmospheric Sciences*, **69**(6): 1872-1889.

Simmons, A., Uppala, S., Dee, D., Kobayashi, S. 2007. ERA-Interim: New ECMWF reanalysis products from 1989 onwards. *ECMWF newsletter*, 110, 25-35.

Skerlak, B., Sprenger, M., Wernli, H. 2014. A global climatology of stratosphere-troposphere exchange using the ERA-Interim data set from 1979 to 2011. *Atmospheric Chemistry and Physics*, **14**(2): 913.

Straus, D. M., Shukla, J. 2002. Does ENSO force the PNA? *Journal of climate*, 15(17), pp.2340-2358. DOI: http://dx.doi.org/10.1175/1520-0442(2002)015%3C2340:DEFTP%3E2.0.CO;2

Trenberth, K. E. 1991. Climate diagnostics from global analyses: Conservation of mass in ECMWF analyses. *Journal of Climate*, **4**(7): 707-722.

Trenberth, K. E., Branstator, G. W., Karoly, D., Kumar, A., Lau, N. C., Ropelewski, C. 1998. Progress during TOGA in understanding and modeling global teleconnections associated with tropical sea surface temperatures. *Journal of Geophysical Research: Oceans*, **103**(C7): 14291-14324.

Trenberth, K. E., Caron, J. M. 2000. The Southern Oscillation revisited: Sea level pressures, surface temperatures, and precipitation. *Journal of Climate*, **13**(24): 4358-4365.

Trenberth, K. E., Stepaniak, D. P. 2003. Seamless poleward atmospheric energy transports and implications for the Hadley circulation. *Journal of Climate*, **16**(22): 3706-3722.

Wolter, K., Timlin, M. S. 2011. El Niño/Southern Oscillation behaviour since 1871 as diagnosed in an extended multivariate ENSO index (MEI. ext). *International Journal of Climatology*, **31**(7): 1074-1087.

Yu, J. Y., Kim, S. T. 2013. Identifying the types of major El Niño events since 1870. *International Journal of Climatology*, **33**(8): 2105-2112.

Zhang, T., Perlwitz, J., Hoerling, M. P. 2014. What is responsible for the strong observed asymmetry in teleconnections between El Niño and La Niña? *Geophysical Research Letters*, **41**(3): 1019-1025.

CHAPTER V

CONCLUSIONS AND SYNTHESIS

Background

Studies have repeatedly and conclusively shown that anomalous vertical fluxes of sensible and latent heat couple the ocean-atmosphere climate system forcing a cascade of global climate impacts associated with the El Niño-Southern Oscillation (ENSO) phenomena (e.g. Ropelewski and Halpert 1986; Trenberth et al. 1998). ENSO is a dominant source of inter-annual climate variability (e.g. Wolter and Timlin 2011) leading to a cascade of extratropical impacts that can include substantial societal disruption (Zebiak et al. 2015), severe droughts (e.g. Hoell et al. 2014) and floods (e.g. Kim and Alexander 2015). El Niño has been linked with more frequent atmospheric river events (e.g. Kim and Alexander 2015) resulting in heavy precipitation events, elevated melting levels (Svoma 2011) that reduces the basin average snow water equivalent, and increases the likelihood of rain-on-snow flooding events (Guan et al. 2016). These regional changes to precipitation patterns have important water resource management implications, especially for metropolitan areas that rely on reservoirs filled by seasonal high elevation snow melt (Svoma 2011). Sea surface temperature anomalies (SSTAs) within the Niño 3.4 region (5ºN - 5ºS; 170ºW- 120ºW) are used to quantify the magnitude and direction of anomalous vertical heat fluxes associated with ENSO and attain maximum magnitude and temporal variance during December (Okumura and Deser 2010). The resultant accumulation of atmospheric heat must be redistributed horizontally into temperate climates to maintain global climate equilibrium, which alters the predictability of mid-latitude climate phenomena such as the North Atlantic Oscillation

(NAO) and Pacific North American (PNA) patterns (Straus and Shukla 2002; Hurrell and Deser 2010). The Pacific North American (PNA) and North Atlantic Oscillation (NAO) represent distinct mid-latitude patterns of intra-annual variability (e.g. Hurrell and Deser 2010) that result in substantial climate impacts across North America and Europe, respectively (e.g. Leathers et al. 1991; Seager et al. 2010).

The magnitude and duration of SSTA's associated with El Niño and La Niña events have been shown to be asymmetric (e.g. Kang and Kug 2002; An and Jin 2004; Okumura and Deser 2010; Choi et al. 2013). Therefore, the atmospheric response to each phenomena is not perfectly opposing thus resulting in climatological implications for regionally impacted temperature and precipitation patterns (Zhang et al. 2014). However, and despite understood non-linearity, linear techniques are widely used for studying the atmospheric response to ENSO forcing (Choi et al. 2013; Zhang et al. 2014; Okumura and Deser 2010). Clearly, a need exists to further analyze the symmetry of the atmospheric response to ENSO. Additionally, despite ENSO representing anomalous vertical fluxes of heat into the troposphere, few investigations have been undertaken to quantify the anomalous horizontal fluxes of heat responsible for the cascade of extratropical climate impacts during ENSO events (Kim and Alexander 2015). Therefore, the purpose of this work was to demonstrate that horizontal heat flux anomalies are an effective method to reveal symmetry of the global scale atmospheric response to ENSO forcing, including anomalous circulation patterns consistent with PNA and NAO patterns of intra-annual climate variability.

The general objective of this dissertation research was to improve understanding of the interrelationship between inter-annual (ENSO) and intra-annual (PNA and NAO) patterns of climate variability through analyses of horizontal heat flux anomalies. Specific objectives were to a) show anomalous, tropospheric-mean circulations consistent with NAO and PNA patterns

during ENSO events of various magnitudes; b) investigate the potential to identify spatially continuous areas of anomalous heat fluxes connecting the ENSO region with PNA and/or NAO regions; and c) quantify the symmetric and asymmetric components of objectives a) and b).

Anomalous Horizontal Fluxes during El Niño

This study was among the first to quantify the anomalous horizontal, tropospheric-mean fluxes of sensible and latent heat associated with El Niño events of various magnitudes using output from state-of-the-art atmospheric reanalysis. This study was also among the first to show month-to-month dependency of relationship between El Niño, PNA, and NAO patterns indicating the potential to enhance predictability of regional climate impacts associated with PNA and NAO patterns on monthly to weekly time scales. The magnitude of El Niño events was shown to influence the position more than intensity of the anomalous PNA circulations such that a positive PNA pattern was favored, especially during December and January. Regarding position, the anomalous circulations were nearer to (farther from) the west coast of North America during strong (weak) El Niño events implying larger precipitation and temperature anomalies across the PNA region during strong El Niño events. Alternatively, the magnitude of El Niño events was shown to influence the position and intensity of anomalous NAO circulations implying that El Niño event magnitude is critical for assessing climate impacts associated with El Niño across Western Europe. Weak El Niño events indicated a transition from an in-phase relationship to an out-of-phase relationship between El Niño and NAO patterns during NDJ whereas strong El Niño events indicated a persistent in-phase relationship throughout NDJ implying enhanced predictability during strong El Niño events. Coherent spatial patterns ($p < 0.05$) of anomalous latent heat fluxes indicated a connection between Niño 3.4 and PNA regions implying potential to quantify the interrelationship, which could provide critical information to

decision makers influenced by the PNA pattern. Furthermore, analyses of anomalous latent heat fluxes implied increased frequency of atmospheric river events impacting North America during Decembers and Januarys of strong El Niño events. Therefore, results implied that El Niño events forced anomalous heat flux circulations consistent with enhanced precipitation along the southern west coast of North America (December, January) and the northern coast of the Gulf of Mexico (December) of strong El Niño events. Additionally, results implied that above normal precipitation was implied during Novembers of all El Niño events across Western Europe that persisted throughout NDJ of strong El Niño events, but transitioned to the opposite implications during weak El Niño events. Considering the work used output from a state-of-the-art atmospheric reanalysis over as many El Niño events as possible, this work indicates potential for anomalous horizontal, tropospheric-mean fluxes of sensible and latent heat to improve regional scale forecasts associated with El Niño events of various magnitudes.

Anomalous Horizontal Fluxes during La Niña

To the authors' knowledge, this study was first to show anomalous horizontal fluxes of sensible and latent heat quantified during La Niña events of various magnitudes as well as showing the month-to-month evolution of spatial patterns consistent with PNA and NAO patterns using output from state-of-the-art atmospheric reanalysis. Results indicated that La Niña event magnitude influences position more than intensity of anomalous PNA circulations such that La Niña events favored a negative PNA pattern during December and January. The position of anomalous circulations within the PNA region during weak (strong) La Niña events shifted closer to (farther from) the west coast of North America. However, a large and strongly anomalous ($> 6x10^4$ kJ m^{-1} s^{-1}) anticyclonic circulation was located in the northeast Pacific Ocean during Januarys of both weak and strong La Niña events implying more frequent blocking

events in the North Pacific Ocean. Across the North Atlantic Ocean, strong La Niña events resulted in a persistently negative NAO patterns during NDJ whereas weak La Niña events resulted in a transition from negative to positive NAO patterns during NDJ. The positive phase of the NAO pattern implies high-latitude blocking across the North Atlantic Ocean such that La Niña events could increase frequency or magnitude of high latitude blocking across the North Pacific and Atlantic Oceans. Coherent spatial patterns of anomalous latent heat fluxes indicated a connection between PNA and Niño 3.4 regions implying potential to quantify the interrelationship, which could improve detection and prediction of extreme climate events influenced by the PNA pattern. Results indicate that La Niña events forced anomalous heat flux patterns consistent with cooler than normal temperatures and above normal precipitation across the northern West Coast of North America that shifted northwest (southeast) during strong (weak) La Niña events. Alternatively, above normal precipitation was favored across the Mediterranean Sea region with below normal precipitation favored across northwestern Europe during all Novembers associated with La Niña and throughout NDJ of strong La Niña winters. This work indicates potential for anomalous horizontal, tropospheric-mean fluxes of sensible and latent heat to improve regional scale forecasts associated with La Niña events of various magnitudes.

Symmetry of Anomalous Horizontal Fluxes during ENSO Events

This study was among the first to show symmetric and asymmetric components of anomalous horizontal fluxes of sensible and latent heat quantified during all ENSO events occurring between 1979 and 2016. Additionally, this work was among the first to show a month-to-month evolution of spatial patterns consistent with PNA and NAO patterns using output from state-of-the-art atmospheric reanalysis. Results showed a linear relationships between ENSO and

PNA or ENSO and NAO patterns generally favoring an in-phase relationship during the NDJ period. However, an asymmetric component was also apparent and of similar magnitude such that climatologically relevant differences between the atmospheric response to El Niño and La Niña events existed, especially during weak ENSO events. The asymmetric component suggested anomalies during El Niño events were generally larger than anomalies during La Niña events. The symmetric component increased across the PNA region during NDJ whereas the asymmetric component decreased and the opposite was shown across the NAO region. The asymmetric component indicated anomalous circulations were generally located further west during La Niña events and further east during El Niño events. ENSO event magnitude was shown to have a non-linear influence on positioning of NSDs such that weak (strong) La Niña events and strong (weak) El Niño events shifted the NSDs towards (away from) the west coasts of North America and Europe.

Analyses of anomalous latent heat fluxes identified connections between tropical heat sources and extratropical sink (PNA and NAO) regions. The symmetric (linear) component results showed a primarily tropical Atlantic Ocean heat source transition to a primarily East Pacific Ocean heat source during January. This indicated that December had connections to tropical portions of both Atlantic and Pacific Oceans implying more frequent occurrences of the Maya Express atmospheric river phenomena responsible for extreme precipitation events in the east-central United States (e.g. Dirmeyer and Kinter 2010; Castillo et al. 2014). Alternatively, both symmetric and asymmetric components were equally large across Europe during weak ENSO events such that eastern North America and the tropical Atlantic Ocean were sources for anomalous latent heat fluxes into the NAO region. Across the central Pacific Ocean a linear, equatorward connection between the PNA and Niño 3.4 regions implied potential to identify

months or weeks with enhanced predictability of the PNA pattern due to ENSO-PNA interaction. Compensating poleward fluxes of latent heat were shown along the southeast (northwest) coast of Asia (North America) during El Niño events. During Januarys of strong ENSO events the poleward fluxes of latent heat were shown to connect Southeast Asia and northwestern North America and the portion of that connection between Hawaii and the west coast of North America was consistent with more frequent Pineapple Express atmospheric river events. Therefore, this study showed that both symmetric and asymmetric components of the horizontal redistribution of anomalous tropospheric heat is important for anticipating the magnitude and position of climate anomalies associated with the ENSO phenomena. Implications for atmospheric river events during strong El Niño events could provide water resource managers additional lead time for extreme precipitation events, which also applies to the asymmetric component during weak La Niña events.

Synthesis

Results of the three preceding investigations showed how ENSO phase and SSTA magnitude influenced the position and intensity of climatologic circulations (e.g. Aleutian and Icelandic lows) with implications for regional surface temperature and precipitation patterns across North America and Western Europe. Results indicated El Niño (La Niña) events strengthened (weakened) the Aleutian and Icelandic lows such that anomalous heat fluxes onto the west coasts of North America and Western Europe were southeast (northwest) of climatology. Regional climate implications of results included above (below) normal precipitation south (north) of the respective climatologic winter maximum corresponding with below (above) normal temperatures during El Niño (La Niña) events. Spatial patterns of the symmetric component indicated a linear relationship between ENSO and NAO patterns during

November and between ENSO and PNA patterns during January. Monthly analyses indicated potential to track the temporal evolution of circulation anomalies that could improve temporal predictability of subsequent climate impacts relative to the more common seasonal mean analyses (e.g. Kim and Alexander 2015; Feng et al. 2016). However, recent work contrasting SSTA magnitude and duration between El Niño and La Niña events questioned the assumption of an equal and opposite (i.e. linear) atmospheric response to the two ENSO phases (e.g. Okumura and Deser 2010). During either phase of ENSO, SSTA magnitude was shown to non-linearly influence the west-to-east positioning of anomalous circulations such that strong (weak) El Niño events shifted anomalous circulations closer to (farther from) the west coasts of North American and Western Europe. The opposite was found for La Niña events suggesting more substantial implications to regional precipitation and temperature patterns during weak La Niña and strong El Niño events. Therefore, results of each study highlighted potential benefits of monitoring the horizontal redistribution of tropospheric heat to improve understanding of regional climate variability associated with the ENSO phenomena.

Results and conclusions of this work are critically important for seasonal forecasters seeking supplemental methods to increase predictability of regional climate patterns associated with the ENSO phenomena. The general lack of literature addressing the influence of La Niña events (Hurrell and Deser 2010), the questionable assumption that El Niño and La Niña events result in equal and opposite atmospheric responses (Okumura and Deser 2010), the limits of predictability associated with NWP methods (e.g. Larson and Kirtman 2016), the potential for more frequent strong El Niño and La Niña events due to climate change (Cai et al. 2014; Cai et al. 2015), and recent failures of traditional methods to anticipate strong El Niño events (e.g. McPhaden et al. 2015; Hu and Federov 2017) indicates the need to further analyze historical

ENSO events through observationally based methods including the work presented here. Given the demonstrated potential for analyses of anomalous horizontal heat fluxes (AHHFs) to show spatial patterns consistent with patterns of intra-annual variability (e.g. PNA and NAO) at weekly to monthly time scales indicated the analyses in this work are a valuable addition to traditional techniques. Additionally, strong El Niño events result in global societal disruption (Zebiak et al. 2015) primarily related to changes to regional water resources such that the global analyses presented here could be useful for assessing regional climate patterns outside of the North America and Western European region as well.

Comments on Statistical Analyses

Spatial and temporal autocorrelation combined with small sample sizes suggested that a one-sample t-test may be insufficient to identify statistical significance for this dataset. The sample size of El Niño (n = 13) and La Niña (n = 12) events was limited by the period of record of ERA-Interim and prevented larger sample sizes for analyses of strong and weak ENSO events (n = 3). Atmospheric data often violate the assumption of independence due to temporal dependence leading to underestimation of the variance and inflation of the test statistic resulting in statistical overconfidence (Wilks 2011). Additionally, problems related to spatial autocorrelation occur when results of multiple statistical tests are evaluated simultaneously, such as the spatial patterns over a global domain presented in this work, and is frequently conceptualized as field significance (Livezey and Chen 1983; Wilks 2011). Modern approaches to this problem consider the decomposition of the spatial field into different scales or features, and utilize a formal approach to accommodate the multiple testing problem (e.g., false discovery rates; see Xhen et al. 2002, for an example). However, despite the aforementioned statistical deficiencies, the current work documented scientifically meaningful spatial patterns of

anomalous horizontal heat fluxes during periods of ENSO forcing with important implications for patterns of regional climate variability at sub-seasonal time scales.

Future Work

Each study showed global results during the NDJ period when SSTAs within the Niño 3.4 region typically reach peak magnitude and variance (Okumura and Deser 2010) such that analyses indicated the possibility to monitor temporal evolution of anomalous circulations globally from one month to the next. One natural continuation of this work will be to assess anomalous circulations across the eastern and southern hemispheres. Expanding monthly analyses to an entire year will improve understanding of the temporal evolution of anomalous circulations within PNA or NAO regions, the symmetry of the atmospheric response during each phase of ENSO events of variable magnitudes, and assess the leading and lagging atmospheric response to SSTAs. Such a lead-lag analysis would highlight months and regions with enhanced or reduced predictability based on SSTAs associated with ENSO. The suggestion that weak La Niña events could enhance the frequency of atmospheric rivers along the west coast of North America similar to strong El Niño events was particularly interesting given the lack of literature addressing La Niña events (Hurrell and Deser 2010). This suggestion needs to be investigated further, perhaps using theoretical models, especially given the severe climate impacts associated with strong El Niño events and the general paucity of observational (small sample size) or theoretical modeling studies on La Niña events (assumed to be opposite of El Niño). For example, the weak La Niña event during the 2016-17 winter produced much above normal precipitation across the western United States similar to what was expected during the previous seasons' strong El Niño. However, it remains unclear whether these impacts were a lagged response of the previous strong El Niño or a forced response by the weak La Niña and how much

climate change influenced the precipitation anomalies. Given the increasing amount of ENSO literature addressing variability of SSTA location (e.g. east vs. west-based ENSO), analyses should be performed for composites of eastern and western based ENSO events to improve understanding of the extratropical impacts. The limiting factor for these analyses to be included in this work was the small sample size of El Niño (n = 13) and La Niña events (n = 12) such that subsets of these events could be justified based on either SSTA magnitude or SSTA location. Finally, given that the asymmetric component of the atmospheric response to ENSO forcing has been found to have climatologically relevant impacts, but has been largely neglected until recently indicates that determining which component is greater for a particular location is valuable information (Feng et al. 2016). For example, see Appendix figure 1 below addressing the relative size of symmetric versus asymmetric components of anomalous horizontal heat fluxes during Januarys of weak (top) and strong (bottom) ENSO events. Indeed, the asymmetric component is larger than the symmetric component for a large portion of the land area of the northern hemisphere.

Closing Comments

Understanding of global climate impacts including surface temperature and precipitation patterns during ENSO events has improved in recent years (Zhang et al. 2014) stemming from advances to observation and numerical modeling techniques. However, traditional numerical modeling techniques are ultimately limited by errors in the initial conditions, systematic model errors, and noise-driven errors such that an intrinsic limit to predictability may exist (Larson and Kirtman 2016). Recent modeling failures of a major El Niño event and subsequent extratropical climate impacts (McPhaden et al. 2015; Jacox et al. 2016) indicates the need to further develop

observation-based methods to monitor and predict atmospheric (circulation) anomalies on weekly to monthly time scales to aid both forecasters and decision makers using those forecasts. Output from first-generation atmospheric reanalysis is tremendously useful (22,000+ citations; Kalnay et al. 1996) and is still used in recent literature (Graf and Zanchettin 2012) despite advances to data assimilation schemes (4D-Var; Simmons et al. 2007) that achieve far superior analyses to that of first generation reanalyses (Saha et al. 2010). Therefore, it may be advisable to maximize the use of existing reanalysis output rather than running computationally expensive and inherently flawed numerical modeling experiments. The results of this dissertation research identify a key usage of atmospheric reanalysis output; the quantification of global-scale anomalous horizontal, tropospheric-mean sensible and latent heat fluxes associated with climatologically relevant extratropical patterns during ENSO events. Several potential benefits of this work include increased accuracy of regional forecasts of precipitation and temperature patterns on weekly to monthly time scales implied through analyses of anomalous circulations across the North Pacific (PNA) and Atlantic (NAO) Oceans. The greatest improvements to accuracy will result from real-time monitoring of these anomalous heat fluxes during the evolution of ENSO events. Fittingly, these potential benefits correspond to issues of global proportion associated with a constantly evolving SSTA pattern across the central Pacific Ocean (ENSO). Thus, the current work overwhelmingly supports the use of anomalous horizontal, tropospheric-mean fluxes of sensible and latent heat as a method to identify weeks or months when water resource managers and other decision makers should be alerted to the potential for extreme precipitation or temperature events across North America and Western Europe.

Literature Cited

An, S. I., Jin, F. F. 2004. Nonlinearity and asymmetry of ENSO. *Journal of Climate*, **17**(12): 2399-2412.

Cai, W., Borlace, S., Lengaigne, M., Van Rensch, P., Collins, M., Vecchi, G., Timmermann, A., Santoso, A., McPhaden, M. J., Wu, L., England, M. H. 2014. Increasing frequency of extreme El Niño events due to greenhouse warming. *Nature Climate Change*, **4**(2): 111-116.

Cai, W., Wang, G., Santoso, A., McPhaden, M. J., Wu, L., Jin, F .F., Timmermann, A., Collins, M., Vecchi, G., Lengaigne, M., England, M. H. 2015. Increased frequency of extreme La Niña events under greenhouse warming. *Nature Climate Change*, **5**(2): 132-137.

Castillo, R., Nieto, R., Drumond, A., Gimeno, L. 2014. The role of the ENSO cycle in the modulation of moisture transport from major oceanic moisture sources. *Water Resources Research*, **50**(2): 1046-1058.

Choi, K. Y., Vecchi, G. A., Wittenberg, A. T. 2013. ENSO transition, duration, and amplitude asymmetries: Role of the nonlinear wind stress coupling in a conceptual model. *Journal of Climate*, **26**(23): 9462-9476.

Dirmeyer, P. A., Kinter III, J. L. 2010. Floods over the US Midwest: A regional water cycle perspective. *Journal of Hydrometeorology*, **11**(5): 1172-1181.

Feng, J., Chen, W., Li, Y. 2016. Asymmetry of the winter extra-tropical teleconnections in the Northern Hemisphere associated with two types of ENSO. *Climate Dynamics* 1-17.

Graf, H. F., Zanchettin, D. 2012. Central Pacific El Niño, the "subtropical bridge," and Eurasian climate. *Journal of Geophysical Research: Atmospheres*, **117**(D1).

Hoell, A., Funk, C. 2014. Indo-Pacific sea surface temperature influences on failed consecutive rainy seasons over eastern Africa. *Climate Dynamics*, **43**(5-6): 1645-1660.

Hu, S., Fedorov, A. V. 2017. The extreme El Niño of 2015–2016: the role of westerly and easterly wind bursts, and preconditioning by the failed 2014 event. *Climate Dynamics*: 1-19.

Hurrell, J. W., Deser, C. 2010. North Atlantic climate variability: the role of the North Atlantic Oscillation. *Journal of Marine Systems*, **79**(3): 231-244.

Jacox, M. G., Hazen, E. L., Zaba, K. D., Rudnick, D. L., Edwards, C. A., Moore, A. M., Bograd, S. J. 2016. Impacts of the 2015–2016 El Niño on the California Current System: Early assessment and comparison to past events. *Geophysical Research Letters*, **43**(13): 7072-7080.

Kalnay, E., Kanamitsu, M., Kistler, R., Collins, W., Deaven, D., Gandin, L., Iredell, M., Saha, S., White, G., Woollen, J., Zhu, Y. 1996. The NCEP/NCAR 40-year reanalysis project. *Bulletin of the American Meteorological Society*, **77**(3): 437-471.

Kang, I. S., Kug, J. S. 2002. El Niño and La Niña sea surface temperature anomalies: Asymmetry characteristics associated with their wind stress anomalies. *Journal of Geophysical Research: Atmospheres*, **107**(D19).

Kim, H. M., Alexander, M. A. 2015. ENSO's modulation of water vapor transport over the Pacific–North American region. *Journal of Climate*, **28**(9): 3846-3856.

Larson, S. M., Kirtman, B. P. 2016. Drivers of coupled model ENSO error dynamics and the spring predictability barrier. *Climate Dynamics* 1-14.

Leathers, D. J., Yarnal, B., Palecki, M. A. 1991. The Pacific/North American teleconnection pattern and United States climate. Part I: Regional temperature and precipitation associations. *Journal of Climate*, **4**(5): 517-528.

Livezey, R.E., Chen, W.Y. 1983. Statistical field significance and its determination by Monte Carlo techniques. *Monthly Weather Review*, **111**(1): 46-59.

McPhaden, M.J. 2015. Playing hide and seek with El Niño. *Nature Climate Change*.

Okumura, Y. M., Deser, C. 2010. Asymmetry in the duration of El Niño and La Niña. *Journal of Climate*, **23**(21): 5826-5843.

Ropelewski, C. F., Halpert, M.S. 1986. North American precipitation and temperature patterns associated with the El Niño/Southern Oscillation (ENSO). *Monthly Weather Review*, **114**(12): 2352-2362.

Saha, S., Moorthi, S., Pan, H. L., Wu, X., Wang, J., Nadiga, S., Tripp, P., Kistler, R., Woollen, J., Behringer, D., Liu, H. 2010. The NCEP climate forecast system reanalysis. *Bulletin of the American Meteorological Society*, **91**(8): 1015-1057.

Seager, R., Kushnir, Y., Nakamura, J., Ting, M., Naik, N. 2010. Northern Hemisphere winter snow anomalies: ENSO, NAO and the winter of 2009/10. *Geophysical research letters*, **37**(14).

Simmons, A., Uppala, S., Dee, D., Kobayashi, S. 2007. ERA-Interim: New ECMWF reanalysis products from 1989 onwards. *ECMWF newsletter*, 110: 25-35.

Straus, D.M., Shukla, J. 2002. Does ENSO force the PNA? *Journal of climate*, **15**(17): 2340-2358.

Trenberth, K. E., Branstator, G. W., Karoly, D., Kumar, A., Lau, N.C., Ropelewski, C. 1998. Progress during TOGA in understanding and modeling global teleconnections associated with tropical sea surface temperatures. *Journal of Geophysical Research: Oceans*, **103**(C7): 14291-14324.

Wilks, D.S. 2011. Statistical methods in the atmospheric sciences (Vol. 100). Academic press.

Wolter, K., Timlin, M.S. 2011. El Niño/Southern Oscillation behaviour since 1871 as diagnosed in an extended multivariate ENSO index (MEI. ext). *International Journal of Climatology*, **31**(7): 1074-1087.

Xhen, X., Huang, H.C., Cressie, N. 2002. Nonparametric hypothesis testing for a spatial signal. *Journal of the American Statistical Association*, **97**:1122-1140 (correction: **100**:716-718, 2005).

Zebiak, S.E., Orlove, B., Muñoz, Á. G., Vaughan, C., Hansen, J., Troy, T., Thomson, M. C., Lustig, A., Garvin, S. 2015. Investigating El Niño-Southern Oscillation and society relationships. *Wiley Interdisciplinary Reviews: Climate Change*, **6**(1): 17-34.

Zhang, T., Perlwitz, J., Hoerling, M.P. 2014. What is responsible for the strong observed asymmetry in teleconnections between El Niño and La Niña? *Geophysical Research Letters*, **41**(3): 1019-1025.

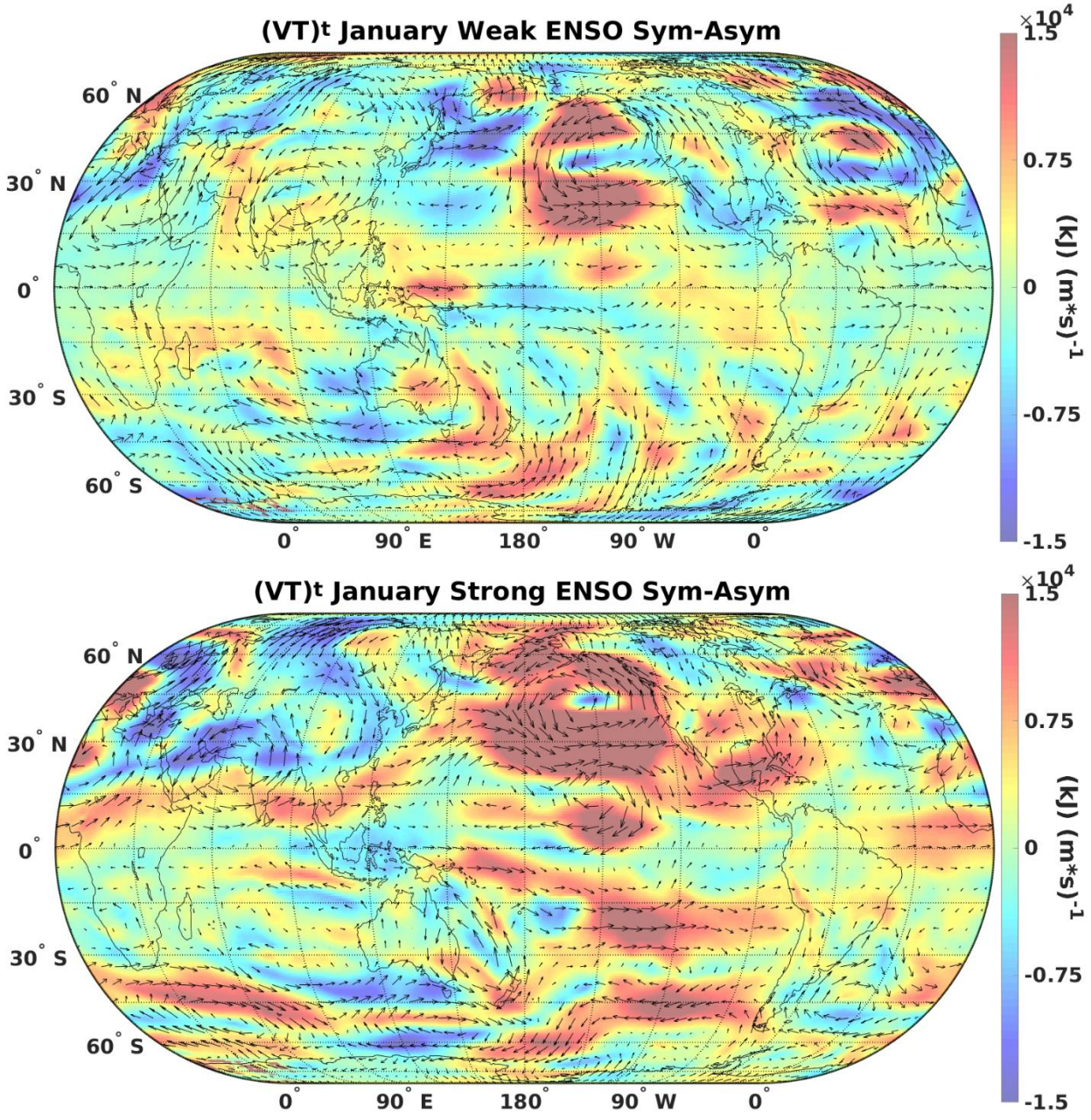

Figure A17. Symmetric minus asymmetric components of anomalous horizontal tropospheric-mean sensible heat fluxes during Januarys of composites of all weak (top) and strong (bottom) ENSO events occurring between 1979 and 2016.

VITA

Evan Kutta grew up in St. Louis, Missouri. He graduated from the University of Missouri in 2012 with a Bachelor of Science emphasizing Atmospheric Science. He graduated from the University of Missouri with a Master's of Science emphasizing Water Resources in 2013. Following completion of his doctoral program, he intends to retreat to the wilderness to contemplate his future and consider how he must give in the same or greater measure as he has received and is still receiving.